ECOLE POLYTECHNIQUE FEDERALE DE LAUSANNE-ICOM

Master Thesis

COLD-BENT GLASS STRUCTURES

Author: Moroni Benjamin

Supervision: Prof. Alain NUSSBAUMER
&
Dr.Christian LOUTER

Assistant: MSc Manuel SANTARSIERO

Lausanne, the 19th of June 2015

Acknowledgements

My gratitude firstly goes to Dr. Christian Louter and Manuel Santarsiero for their support, patience and valuable advices they gave me.

My sincere thanks go to Prof. Alain Nussbaumer and Prof. Jean-Paul Lebet for their valuable comments during the different intermediary presentations.

I'm grateful to Félix-Construction for the assembly of the curtain wall and particularly to Philippe Paraire for his advices, comments and time.

I wish to express my gratitude to Frédérique Dubugnon, Sylvain Demierre, Gérald Rouge and Gilles Guignet who greatly helped me with the experimental work.

Special thanks to Lucien Zeller colleague and valuable friend, for his availability and his good mood.

Summary

In contemporary architecture there is an increasing demand for transparency and curved shape. The Cold-Bending process is an effective and relatively inexpensive way of creating double curved surface glass. This thesis focuses on the shaping of a plate with the application of an out-of-plane displacement at its corner, also called cold-warping.

The behaviour of both, four point-supported glass panels and curtain wall elements, are investigated during the shaping process. Since the phenomenon of buckling instability has been reported during the Cold-Bending process, different researches have investigated that problem. However, any experimental and numerical test have been performed, to my knowledge, on glued-spider point-supported panel and curtain walls. Numerical tests validate by experimental results are used to analyse this instability.

It's shown that the global rigidity of the panel changes during the shaping process. The panel undergoes a continuous change in form during the cold-warping until the instability. Almost right after the $\delta_{instability}$ is reached, the global stability stays constant and so does the global geometry.
From the numerical results, on the four point-supported panel, it has been reported that a linear relation exists between $\delta_{instability}$ and the thickness of the glass. However, that relation is specific to each different size of square or rectangle panels. Indeed, it seems that the complete relation should be: $\delta_{instability}$=C*t [mm], with C=f(L,L/B) [-].
Results from both numerical and experimental tests have shown that an instability occurs for each type of supports (punctual or linear), in one or the other direction U3. Thus, two types of instability, which appears in function of the *edges boundaries condition and imperfections*, have been reported.
The *classical instability* is characterized by a supported diagonal that buckle to a stiffer form, preventing significant changes in its shape, and by the forced diagonal that consequently develop a severe curvature. Thus, the centre surface, right after the instability, start moving in the opposite direction of δ. The major change of the shape deforms the edges from a straight shape to a curved one, and ripple appears along the supported diagonal.
The *second instability mode* is characterized by the sudden "Jump-Out" of the centre surface right after $\delta_{instability}$ is reached, in the same direction than δ. The non-buckling of the supported diagonal alters the shape of the forced diagonal by a *"Belt-Effect"*. The edges are then, curved in the opposite direction as in a classical instability.
Thus, there are three type of deformation mode with different stress pattern for each.
Finally, numerical investigations have shown that two-sides supported panels were the best solution for the cold-warping process. Indeed, reaction forces and the stress inside the panel decrease, whereas $\delta_{instability}$ becomes higher.

Table of contents

Abbreviations and symbols

Abbreviations

FTG	Fully Tempered Glass
HSG	Heat Strengthened Glass
IGU	Insulated Glass Unit
Ld_Point	The point where the imposed out-of-plane displacement is applied
LVDT	Linear variable differential transformer
FE	Finite element
Free	The support is free to move in the XY plane
Free-X	The support is free to move only in the X direction
Fix	The support is fixed in the X, Y, and Z direction

Symbols

A	Surface
B	Width
C	Centre point of the panel
E	Young Modulus
F	Point Load
G	Shear Modulus
L	Length
M	Moment
S	Strain, Stress
Smax	Maximum principal stresses
t	Thickness
$\alpha_{\sigma,\ max} = \sigma_{max} / \sigma_{norm}$	Ratio between the actual non-linear stress values and the nominal uniform stress
δ	Applied cold-warping displacement, in one corner, in the U3 direction
$\delta_{instability}$	Applied cold warping displacement to get the instability
ε	Strain
ν	Poisson's ratio
σ	Stress
σ_{max}	Tensile ultimate stress of a glued assembly, non-linear stress
$\sigma_{nom}=F/A$	Nominal Stress in the glue

1. Introduction

1.1. Introduction to the topic

The constant development of the architecture and the increasing number of architectural offices has led to a new trend. Architectural contests are nowadays the key of the celebrities and success and fanciful building are the sinews of war to win those competitions.

Moreover, complex-building shapes have emerged in parallel with new numerical tools (advanced 3D software (e.g. Grasshopper)). Consequently the demand in freeform design, also called fluid design, which is chiefly characterized by curved surface, is steadily increasing.

No need to say that the rapid upcoming of evolved numerical modelling tools have to be contrasted by the building industry. In order to follow the progress the industry has to front the new challenges offered by the complex design.

Figure 1 Freeform demand [3]

The value of a building mainly depends on the space, the structure, the light and its exterior, the façade. As the demand in natural light is high, due to the comfort to the users and the good energy balance it provided, façades in modern architecture are mainly composed by glass.

Thus, in the quest of transparency and fluid forms, special attention needs to be paid to the curved glass surfaces.

The “Hot Bending” method to curve the flat glass panel into the desired form has long been used. This method consists in heating, the glass, up to the weakening point (i.e. 600 [°C]), and then the glass is pushed (commonly by the gravity) into a mould. Once the glass reaches the desired form, the product is cooled down in a controlled manner. The final product is a tension free curved glass, which can have a very strong curvature. However, some drawbacks have to be instilling to the Hot Bending. First of all, complex curved façades are composed by panels, which have not the same curvature, so that for each different curvature a new mould has to be produced. That’s

why delivery time is bigger and the cost is even higher. As curved panels are done into the manufactory, transport costs are more expensive in order to carry different panels with different curvatures (less practical than for flat panel). The CO_2 assessment is even worse, as this method requires heating the panels. Finally, the optical properties affect the quality of the hot bend product. Indeed, due to the heating process, the thickness is affected, which leads to major optical distortion.

To conclude, Hot Bend technique perfectly fits for small project with strong curvature, but large-scale projects need other techniques.

This alternative method is the so-called “Cold-Bending” technique.

The Cold-Bending method can be seen as an alternative to the Hot Bending one. In Cold-Bending flat glass panels are brought to the desired geometry by means of external forces. Those forces hold the curved glass panel into the desired form. Indeed, the elastic deformation allows the glass to be mechanically formed in a cold state.
Therefore, a cold bent glass is not a product but rather a construction method.

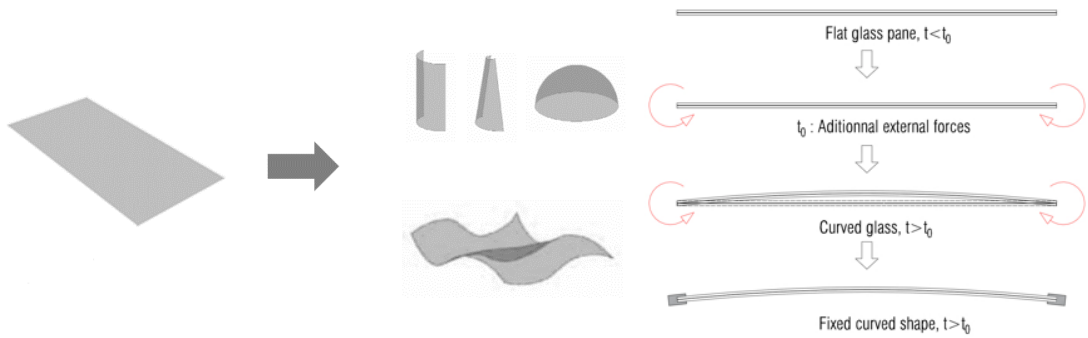

Figure 2 From a flat glass panel to the specific curved glass, [3]

All the additional costs due to mould or transportation shouldn’t be considered by this method. The CO_2 assessment do not suffers from the bending process and the optical quality is not influenced by the change in thickness.

The Cold-Bending is an efficient powerful tool of complex aesthetical design in modern architecture. Nevertheless as the flat panel is deformed elastically, Cold-Bending induces stress inside the panel and so the curvature is limited.

Due to the tempering process it is possible to cold bend thermally strengthened glass without introducing tension stresses at the surface of the panel. However, particular attention should be paid to that induced permanent stress, especially for laminated glass panels and IGU.

Cold-Bending method can be achieved by two techniques; the first one is the Cold-Bending by assembly and the other way is to cold bend by laminating (explain in [3]). The present study concerns the first method, “Cold-Bending by assembly”.

1.2. Problem definition

An instability phenomenon has been reported during the cold-warping process, by Eekhout and Staaks[19]. The cold-warping correspond to the Cold-Bending process, the shaping of the plate is done with the application of a vertical out-of-plane load at one of its corners. During the cold-warping process the deformation configuration is defined by two distinct modes. Change in the geometry is observed after the instability point.

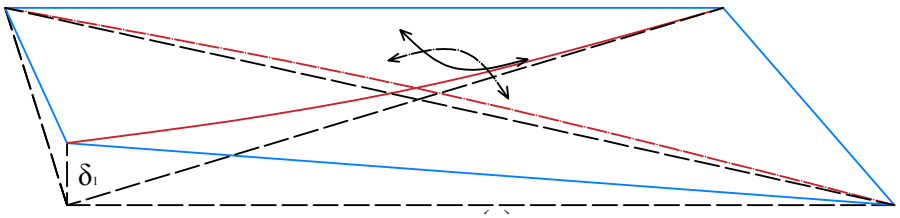

Figure 3 Deformation pattern before the instability, hyperbolic paraboloid shape

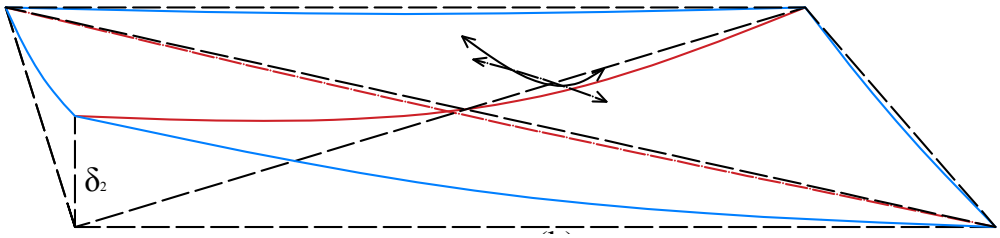

Figure 4 Deformation pattern after the instability $\delta_1 < \delta_{instability} < \delta_2$

The first mode can be defined by a hyperbolic paraboloid; the edges remain straight and the diagonals are curved.
The instability occurs when the imposed displacement δ reaches a certain value; $\delta_{instability}$. Afterward the edges become curved and one diagonal become stiffer preventing significant change in its shape and consequently the vertical deflection is confined to the other diagonal. The change in geometry of the stiffer diagonal appears in the form of ripples [10]. Undesired optical distortions are then observed.

Figure 5 visual distortions due to the ripples

The visual distortions as well as the geometry changes, due to the instability, cause a negative balance of the cold-warping shaping.

1.3. Objectives

The purpose of this thesis is to explore and investigate the instability occurring of cold-warped panels. As in the industry engineers cannot waste their time to study the behaviour of cold-warped panels, this study aims first to give simple table, to design quickly cold-warped façade.

Firstly, numerical and experimental tests are performed in parallel to design the test setup. Secondly, the validity of the results is based on the correlation of both tests.

The instability of the panel, described by a snap-through buckling [8], implies negative consequences. That’s why different solutions will be investigated in order to limit this phenomenon.

1.4. Research outlines

In order to provide useful results the research focuses on regular glass geometry. As the most common geometry is the quadrilateral one, the study is dedicate to square and rectangular panels.

Only the monolithic panels are investigated. For the short-term laminated glass can be approximate by monolithic panel [1], thus to made the correlation possible, panels with huge thickness are considered during the study.

The long-term behaviour of laminated panel and viscoelastic material reach beyond the scoped of the study and will not be considered.

The glass exhibits a quasi-perfect elastic behaviour up to the fragile fracture and thanks to the Float Glass process the glass is isotropic. These properties would justify a physically linear relation (Elastic study), [5]. The type of analysis is thereby restricted to a pure geometrical nonlinear analysis.

Different types of glass with different strengths exist (e.g. Annealed Glass, Heat Strengthened Glass or Fully Tempered Glass) with the same elastic properties. So that the study does not focus on a particular type of glass, nonetheless users of the design table would be able to specify the type of glass used.

Support conditions have a huge impact on the behaviour of cold-warped panels [3] [10]. Thereby the study focuses on the cold-warping of four point-supported glass, which can be executed as glued spider fitting, and on linear supported glass (frame-support). As Cold-Bending includes additional stress inside the panel, bolted spider fitting is not treated (Stress accumulation near the drilled hole which is the weak part of the panel due to small cracks).

1.5. Methodology

The study is divided into four parts; the first one consists on the numerical and experimental study of a cold-warped point supported panel. Both tests are performed on 4 x 1’000 x 2’000 [mm] panels with four point-fitted supports. The objective of those tests is to calibrate the numerical model and to validate it (stress and deformation).

The second part consists on the numerical and experimental study of 1’000x2’000 [mm] curtain wall element. The calibration and the validation of the numerical model is the goal of this part.

Part three and four consist on the numerical investigation of cold-warped, four point-supported glass and frame-supported element. The results of those tests provided benchmarks, which should be used to design quickly cold-warped façade.

Furthermore, as the Epoxy behaviour used for the point-fitted support is not well defined, several tests are performed in order to know σ_{nom}, E and ν.

Finally, to validate the numerical work LVDT, Strain Gauges and digital image correlation system are used in the experimental part of the study.

Both experimental and numerical tests were done simultaneously during the master thesis.

2. Cold-warping of point-supported panel

In this part the cold-warping of a specific panel is investigated. The plate is in the vertical position, as it would be for a cold-warped glass façade.

Tests are performed on monolithic glass plates, that's why the speed loading is not considered. The viscoelastic behaviour of the resin is not taken into account; in fact the Appendix III shows that the stiffness of the resin doesn't affect the behaviour of the panel during the shaping process.

2.1. Specimens definitions

2.1.1. Panel description

The experimental work is done on 4 x 1'000 x 2'000[mm] panels. This geometry has the particularity to have the same L/B ratio as the most commonly used façade panels (1'500 x 3'000[mm]).

A total of four HSG panels (1'000 x 2'000[mm]) and one FTG panel (1'000 x 2'000[mm]) were made available by the ICOM. Also different square panels were available, but they were annealed and so unusable for Cold-Bending purpose.

The FTG panel has already been used for another experiment and some scratches were visible on it. That's the reason why tests on point-supported panel are performed on HSG.

A preliminary study is done on an aluminium (EN AW-5005 (AlMg1) H14/24) plate of the same size. Glass and aluminium have, almost, the same elastic properties (E and ν), and according to Appendix X the behaviour during the shaping process is really dependent on ν. Thus, the tests were initially conducted on the aluminium plate, in order to rise if the test setup was suitable or not, without risks of brittle failure in a sharped pattern.

2.1.2. Support description

As already said, the experiment is performed on a HSG plate. The strength of the glass is approximately 50[MPa] and might be a limit to the cold-warping experiment. Indeed the cold-warping is not a product but a construction method. Cold-warping flat panels result in an additional stress, it therefore seems that the use of HSG must be done at the expense of a bolted connection.
In fact the small contact surface of the bolted connection implies high local stresses, in addition to that, the drilled hole in the glass (required for that type of connection) causes small crack, which severely reduces the strength of the panel.
Therefore, the choice of the connection had been oriented toward a glued spider fitting.

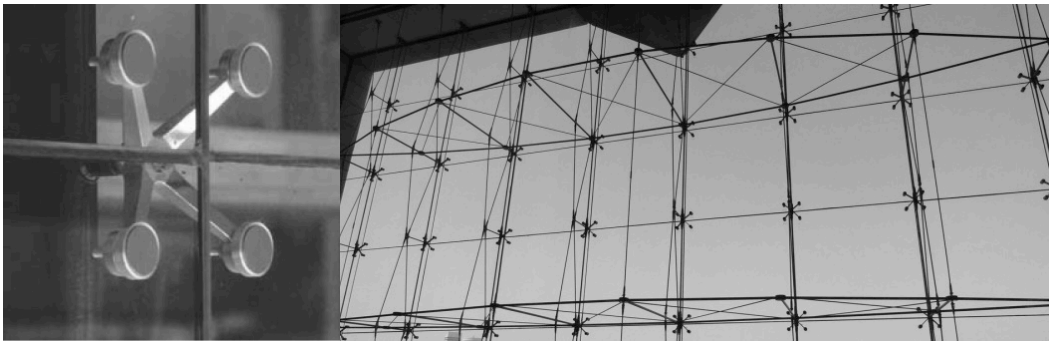

Figure 6 Glued spider fitting (left), and glass façade supported by spider connection (right) [c]

Glued point-fitting have the advantage on bolted point fitting connection to not decrease the strength of the glass on the one hand, moreover, the contact surface is bigger and less important is the stress concentration.

The use of SADEV R10006 TSSA connection has been chosen in order to achieve this type of connection.

Figure 7 Sadev R1006 TSSA point-fitted connection

Out-of-plane loads are carried out by the spider fitting by mean of compression and tension, depending of the direction of the load. Whereas in-plane load are undertake by shear stress. For both load the adhesive, in between the glass and the support, have to carry the stress, which might be considerable.

Thus, based on Appendix IX an epoxy resin (Araldite 2000) has been used for this experiment.

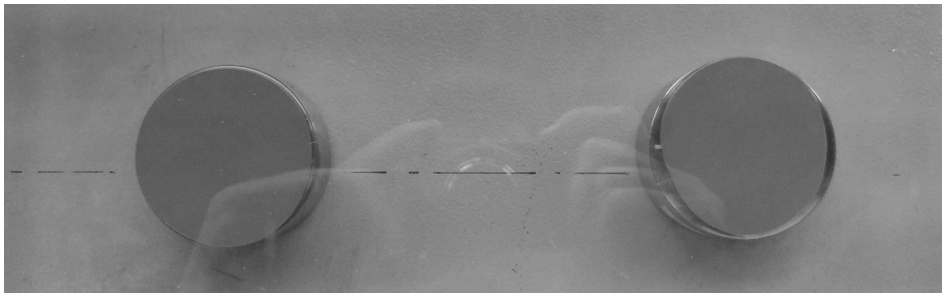

Figure 8 Araldite2000 glued support

2.1.3. Boundary conditions

Point-fitting connections are well known in the façade domain. Thus, in order to allow in-plane expansion of the glass a typical arrangement of the support is provided, see Figure 9.

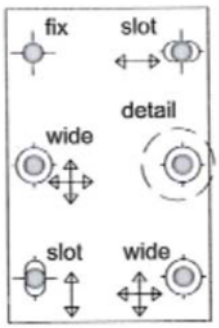

Figure 9 In-plane typical boundary conditions [4]

In order to have an experiment close to the reality, boundary conditions in respect to Figure 9 have been used.

Figure 10 Boundary condition for the cold-warping experiment (from behind).

The displacement in the Z-direction (U3) is restrained for all the support. Moreover, in order to achieve cold-warping test, only one support of the panel is pushed in the Z-direction; this point is the so-called Loaded Point in Figure 10.
The SADEV R1006 TSSA got a ball joint (see Figure 7), so that each support is free to rotate.

2.2. Numerical Modelling

In order to predict the behaviour of the panel, under an out-of-plane displacement, a numerical model has been done. Results of the modelling will be the basis of the experimental test expectation (stress variation, displacement, reaction forces…).

The finite element analysis was performed with Abaqus/CAE 6.12-3 software.

The analysis type of the modelling is a non-linear one. Indeed the out-of-plane imposed displacement makes the plate subjected to severe deflections. Hence stresses redistribute from bending to membrane. This transition occurs when deflections are approximately equal to plate thickness. Linear analysis would overestimate the stress in the plate. The analysis is then geometrically non-linear.

The viscoelastic behaviour of the epoxy resin and the plastic behaviour of the stainless steel support are not taken into account on this study; only the elastic behaviour is used. As the glass is a fully elastic material until the point of fracture, the analysis is then geometrically non-linear and material linear.

2.2.1. Solid Model

Initially a solid model was built. As the cold-warping induces severe out-of-plane displacement compare to the thickness of the plate, special attention should be paid to the shell modelling.

Moreover, in order to have a global model that takes into account the influence of the supports and especially the rigidity of the Araldite, solid model seems to fit the best, in spite of the longer computational time.

2.2.1.1. Global Model

The idea of the modelling is to reproduce, the most faithfully, the panel as it is in reality. However, the most faithfully doesn't mean that the model have to include all the elements of the reality. In order to reduce the complexity of the model some simplifications should, and have to, be made.

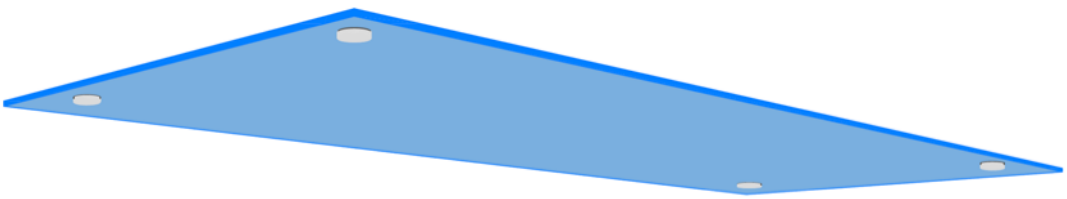

Figure 11 point-fitted glued supports on a monolithic panel

In our case the complexity of the model is the modelling of the different supports. To have a consistent mesh the support is extrude from the panel. Different partitions of

the cells allow the input of different elastic properties to the support part (i.e. aluminium and resin material properties).

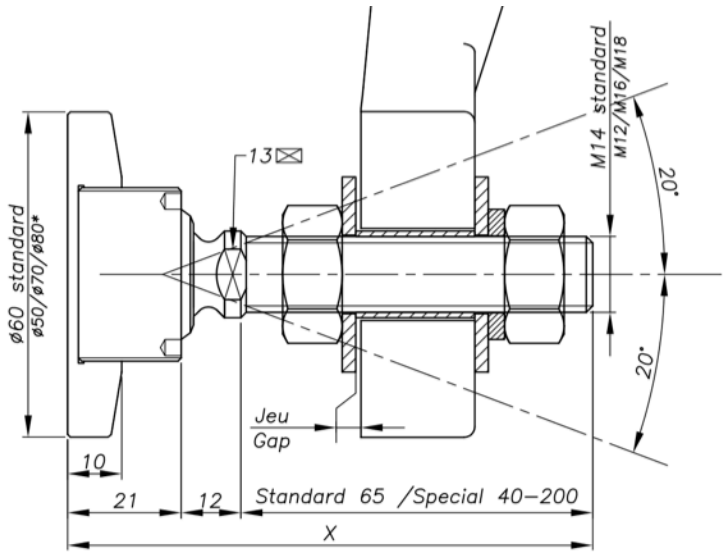

Figure 12 Detail of the glued support, [b]

However, the detail Figure 12 could be simplified as following. The fixing plate (60 [mm] diameter) is modelling by a flat circular plate of the same radius without the screw thread. It's admitted that the real assembly would have the same rigidity as the flat plate.

Moreover, the ball joint of the assembly is modelling by a multipoint constraint, the master point is the centre of gravity of the ball joint, whereas the slave point is a part of the top surface of the flat circular plate, as showed in Figure 13.

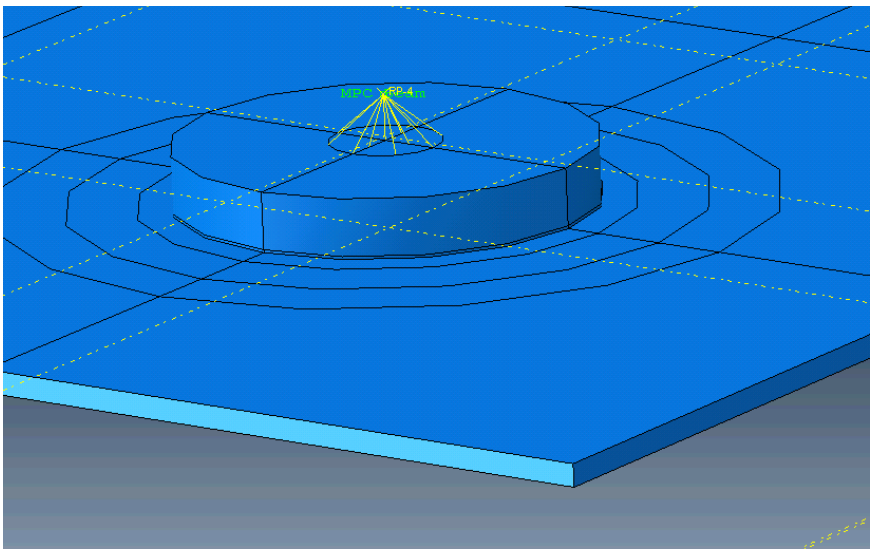

Figure 13 Modelling of the support

The most important part is to respect the boundary conditions exposed in Figure 10. Thus, the master point of the multipoint constraint, for each support, is the attachment point of the boundary condition. Only translational displacements are restrained, to represent the action of the ball joint the rotational constraint is free to rotate.

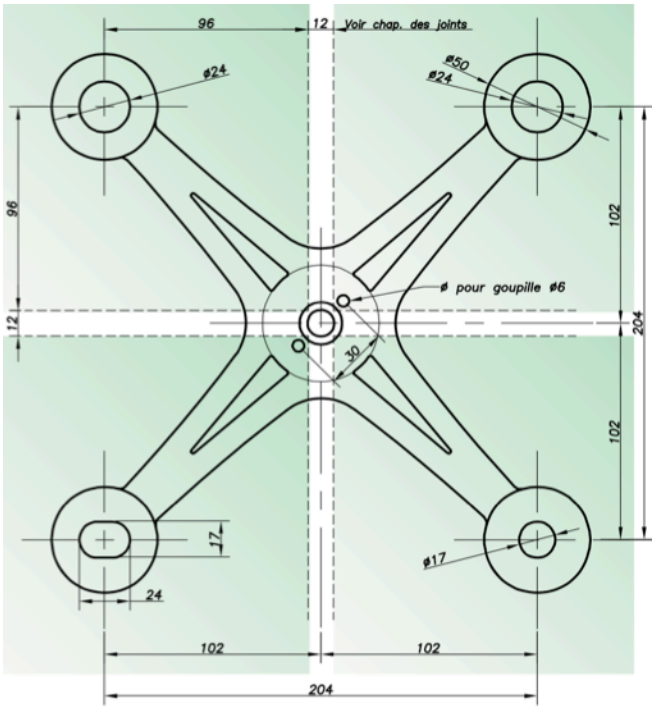

Figure 14 Spider fixing system, specific “centre and clamp” distance [b]

The same “clamp distance” is used in our experiment, that’s to say 96 [mm] between the centre of the support and the edges.

2.2.1.2. Element type

Some differences in the solid elements libraries are available in Abaqus. Hexahedral elements have been used for the main part of the model. They provide a solution of equivalent accuracy than triangular and tetrahedral elements at less cost. Hexahedra have a better convergence rate than triangles and tetrahedral, and sensitivity to the mesh orientation in regular meshes is not an issue.

Nonetheless hexahedra are more sensitive to initial element shape.

Moreover, Abaqus makes available first- and second-order elements. Second order requires bigger computational time. However, second-order elements capture stress concentrations more effectively and are very effective in bending-dominated problems. They are then the best option for cold –warping problem.

Thus, the element is a continuum stress/displacement (C) three-dimensional (3D) with twenty nodes (second-order hexahedral element), also called C3D20.

Reduced-integration elements use a lower-order integration to form the element stiffness. Mass matrix and distributed loadings use full integration. Reduced integration decrease the running time, in our case element type C3D20 has 27 integration points, while C3D20R has only 8 (2x2x2); therefore, element assembly is roughly 3.5 times more costly for C3D20 than for C3D20R.

Hence, reduced-integration elements property is used, and the final elements are C3D20R.

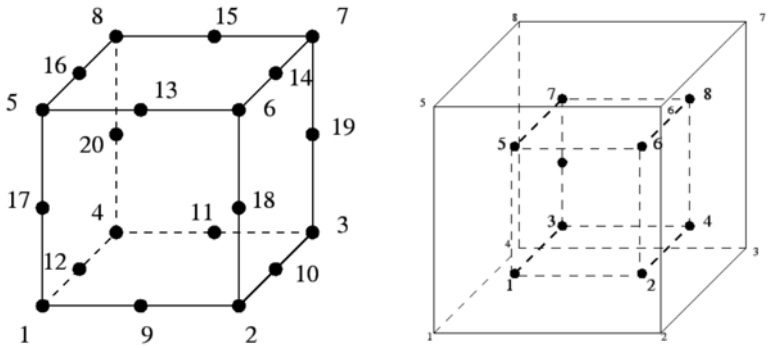

Figure 15 20-node brick element (left), 2x2x2 integrations point scheme in hexahedral elements (right),[a]

The C3D20R element is a general-purpose quadratic brick element, with reduced integration, using it should give accurate result for the instability problem.

2.2.1.3. Mesh study

The mesh design is divided into two main parts; the main part is the glass one and the second one is the area around each support.

The glass part is a simple hexahedral part. As the geometry is rectangle, the mesh is regular without distortion in this area.

The support part is trickier. A particular parametric radial mesh is built in order to capture the stress concentration.

Convergence test was employed to define the appropriate mesh density, see Appendix I Mesh Study.

To compare the stress in the panel to the numerical results, a special refine mesh has been done. The global seed used is very fine (10 [mm]) as well as the mesh in the support area.

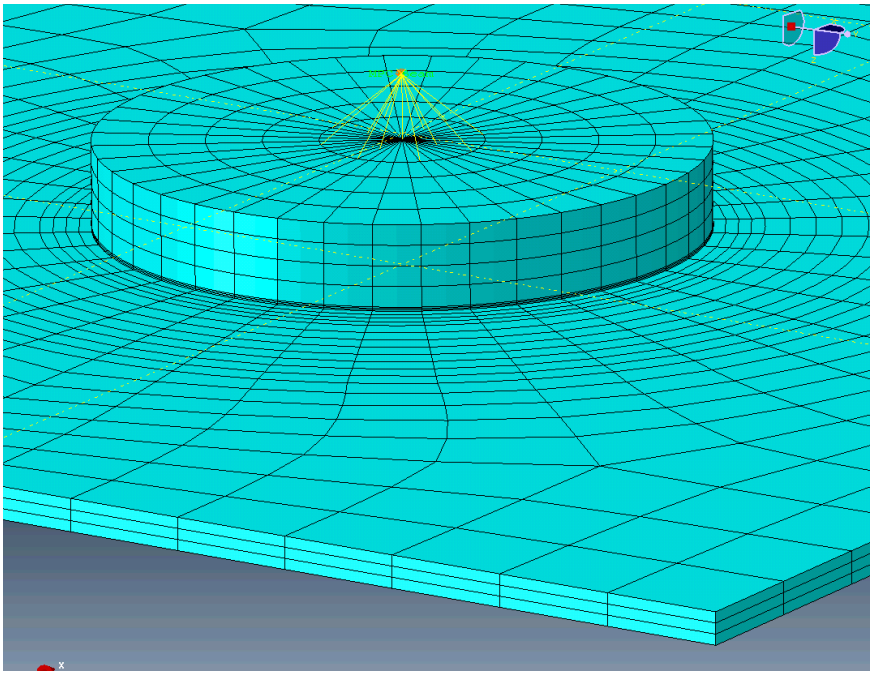

Figure 16 Mesh of the solid model

Finally, the structured mesh has been created by dividing the thickness in three elements.

2.2.1.4. Applied load and displacement

As already said the panel is in the vertical direction (XY plane in Figure 10). The initial deflection of the thin panel due to the gravity is almost zero (it would be different if the panel was in the horizontal direction).

The load case takes into account the self-weight of the panel and an external pressure in the Z-direction (right angle to the glass plane).

This pressure is applied in order to enhance the rate of convergence of the numerical computations. In fact, the numerical solution may locally converge to a meta-stable symmetric configuration beyond the bifurcation point, which is globally highly unstable [8].

To avoid such possibility a uniformly total pressure of 0.1 [N], which is almost nothing, has been find by iteration.

The applied displacement to get the cold-warping is applied to the right bottom corner (see Figure 10). The displacement is applied at Ld_Point, in the boundary condition module in Abaqus.

A total number, of one hundred load steps, uniformly distributed, is used in order to have consistent results.

2.2.2. Results of the numerical model with solid elements

2.2.2.1. Instability phenomena

The used terminology is defined Figure 17.

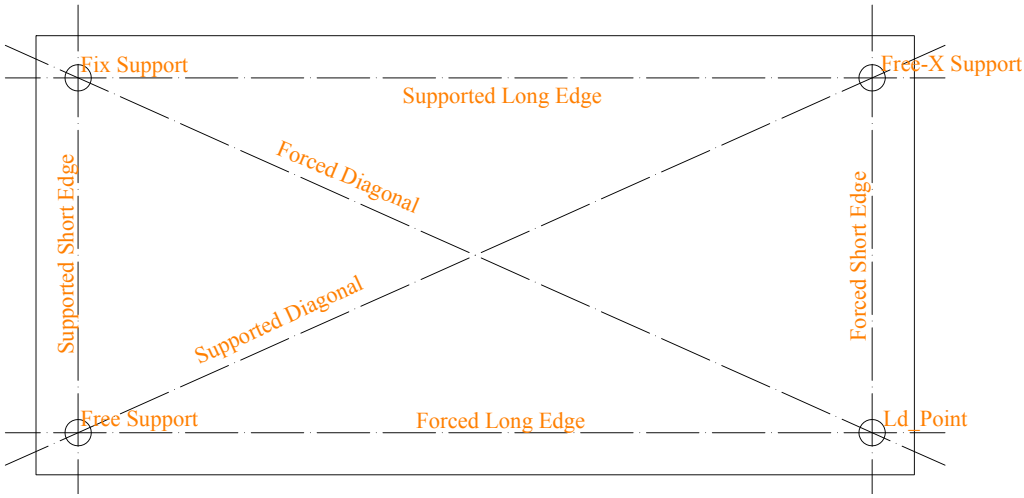

Figure 17 Terminology from behind the panel

It has been reported in [3] and [19] that a global instability occurs during the cold-warping. The instability is generalized to the whole panel as the entire geometry change.

Hence the onset of the global instability phenomenon may be easily detected by measuring the relative displacements of the loaded corner (Ld_Point) with respect to the centre of the plate (C).

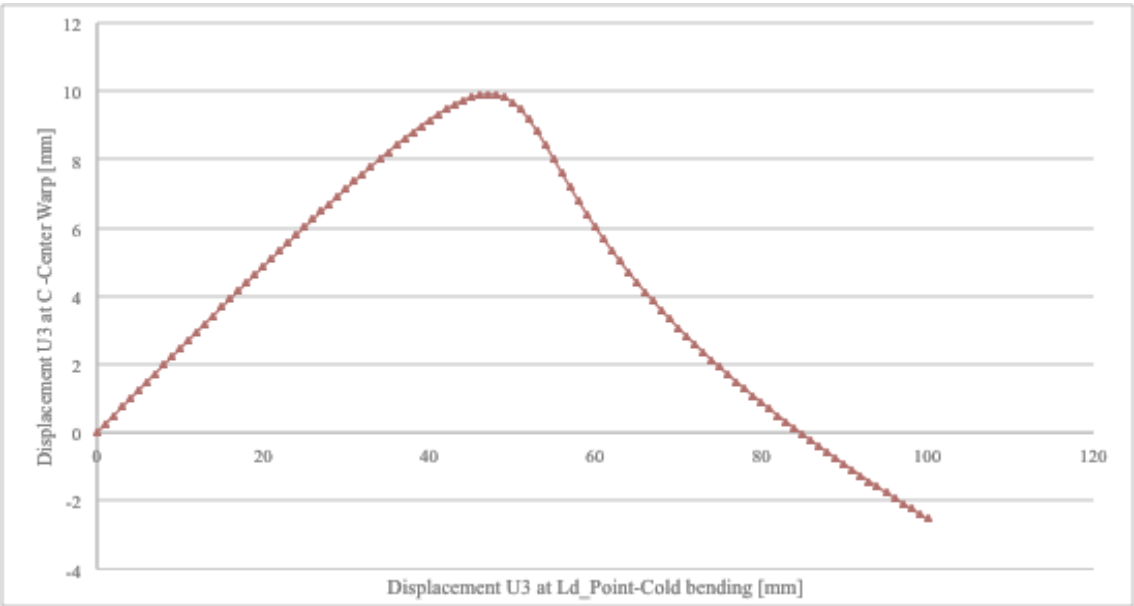

Chart 1 Displacement of the centre of the plate in relation with the imposed displacement

The phenomenon of instability reported by different papers is well characterized by the Chart 1. In fact one can see that a change occurs when the vertical displacement at Ld_Point exceed 47 [mm]. After this value the point C starts moving in the opposite direction of the imposed displacement.

This change in the deformation mode can be better understood by plotting the deformation pattern U3 (Z-direction).

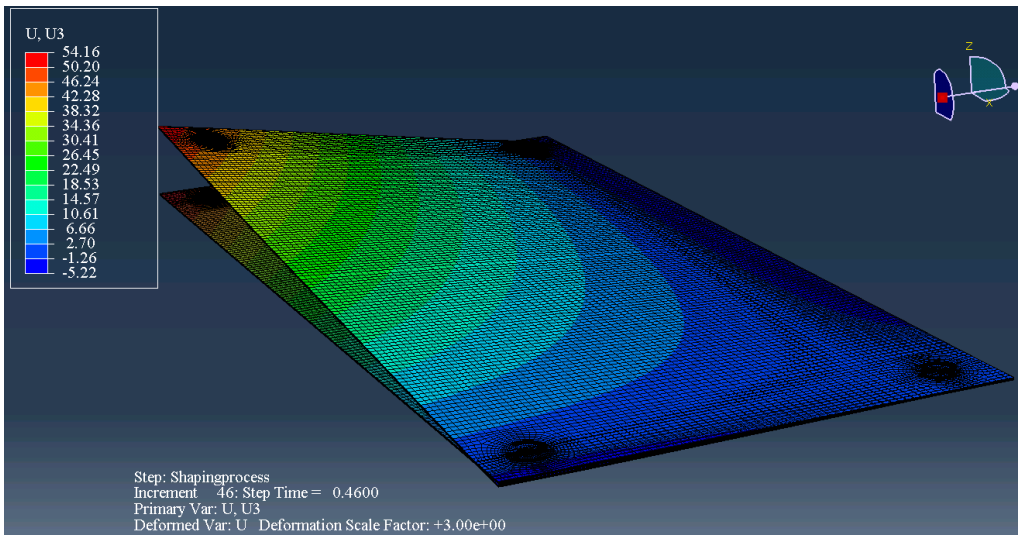

Figure 18 Deformation pattern before the instability, $\delta_{applied}$=46 [mm])

The first deformation pattern is close to the Kirchhoff-Love theory (explain in §2.2.3.2 and in Figure 26). The edges stay straight and the surface is “camber” to the outside.

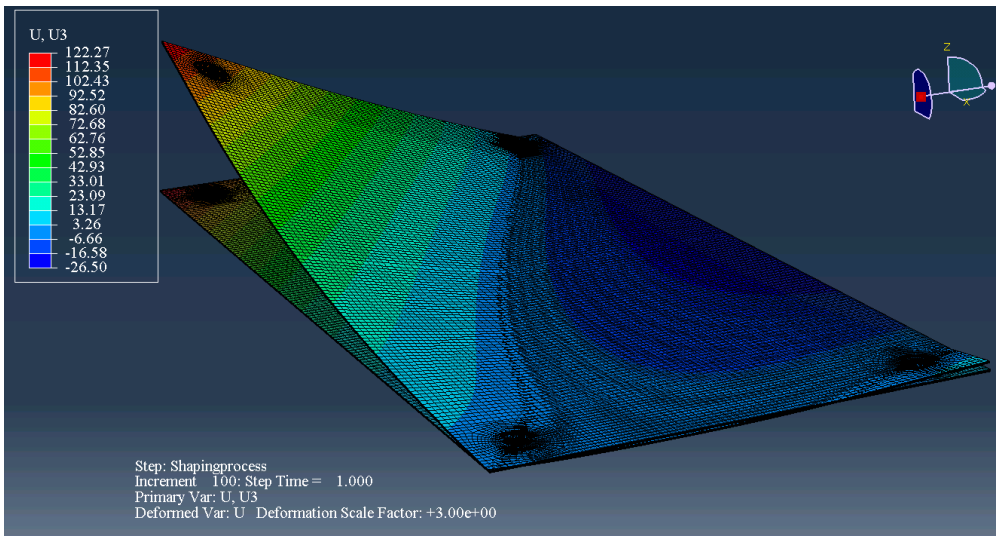

Figure 19 Deformation pattern after the instability, $\delta_{applied}$=100[mm])

After the instability the whole surface snaps open to the inside. The curvature of the forced diagonal becomes huge contrary to the supported diagonal, which is close to

zero. All the edges are then curved, in particular the forced edges, which have a severe curvature.
The change in form can be seen as the buckling of the supported diagonal.

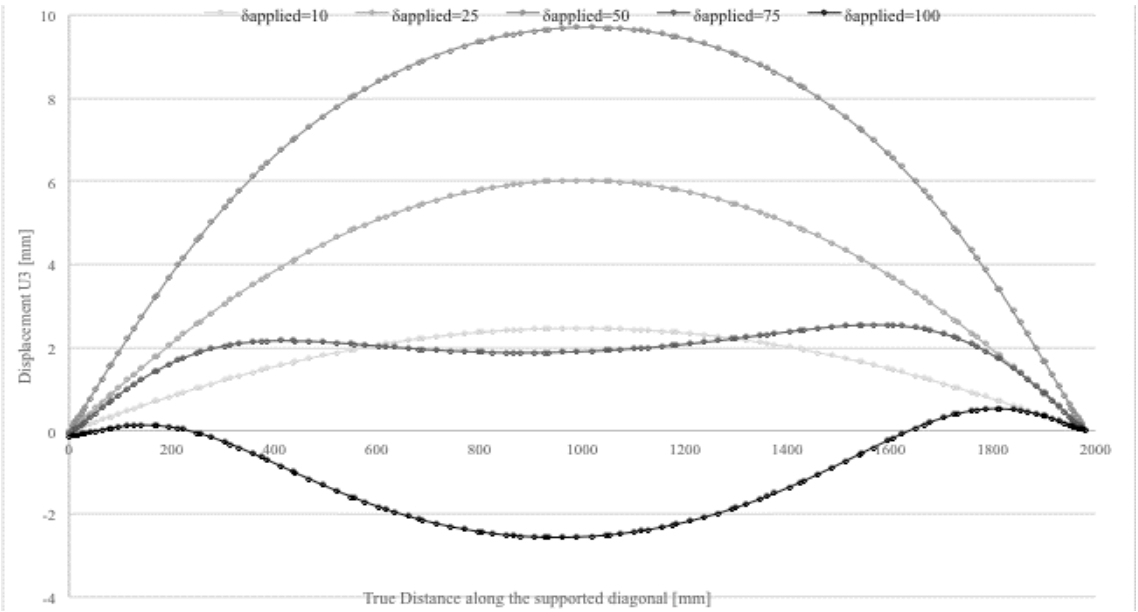

Chart 2 Displacement U3 along the supported diagonal during the shaping process

The supported diagonal become stiffer and tends to get back to its initial position. The buckling of the supported diagonal results in ripple distortion along it, also called Cold-Bending distortion.

Finally to get a global equilibrium the vertical deflection is confined to the forced diagonal, see Chart 3.

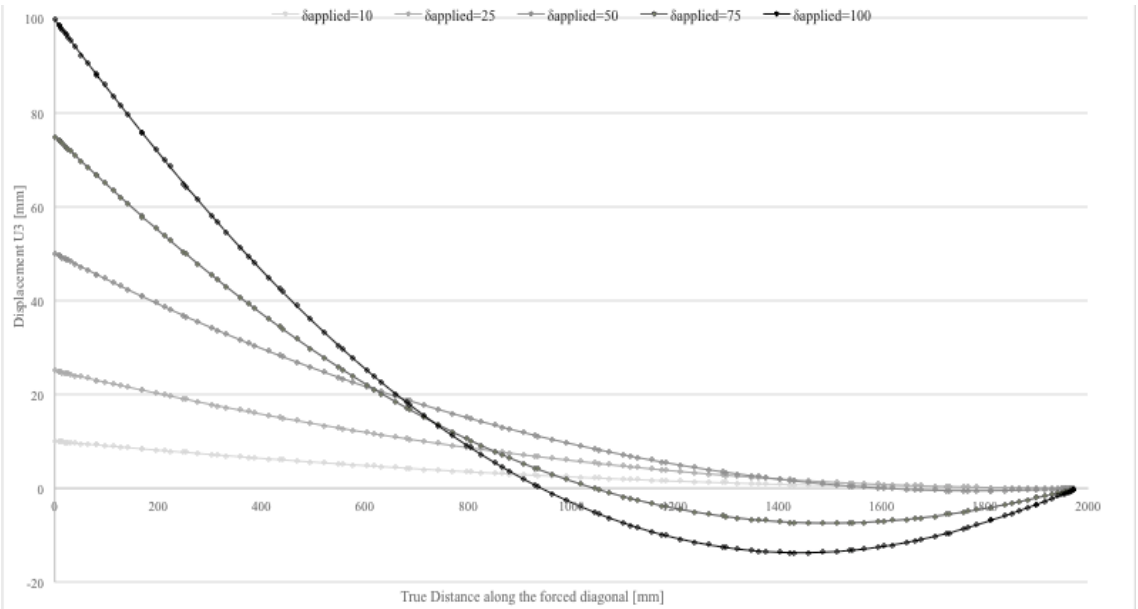

Chart 3 Displacement U3 along the forced diagonal during the shaping process

The displacement of the forced diagonal becomes negative near the Fix support in order to reach a higher curvature.

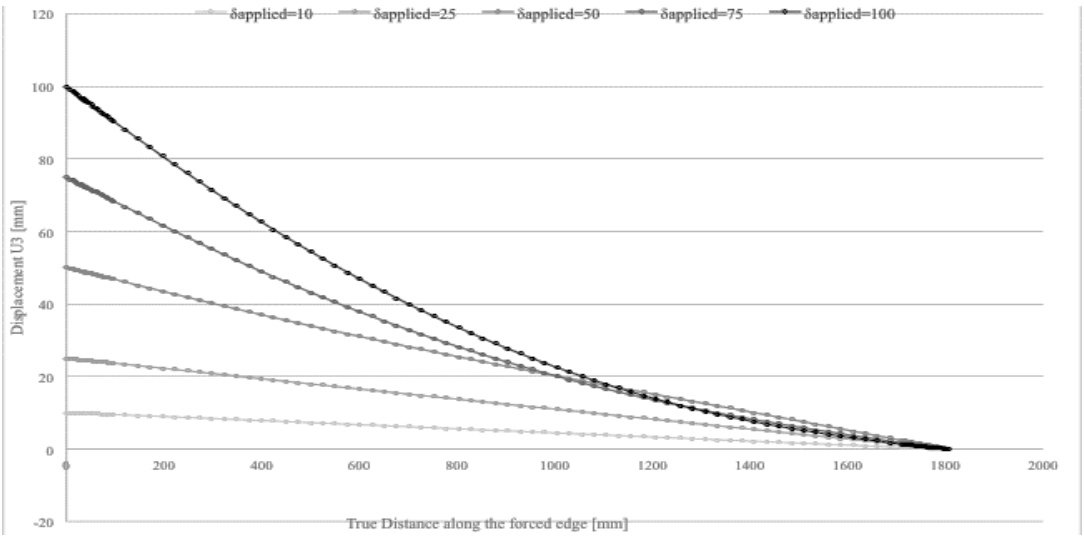

Chart 4 Displacement U3 along the forced long edge during the shaping process

The forced edge, which is almost straight in the first deformation mode, becomes curved after the instability. Therefore, the shape diverge from the hyperbolic paraboloid initial one, and the Kirchhoff-Love theory is not valid anymore.

2.2.2.2. Stress built-up

The stress is also affected by the change in form of the panel. Indeed the forced diagonal develops a severe curvature, which result in a membrane compressive stress at the intrados of the central part of panel, Figure 20 and Figure 21.
The stress built-up during the shaping process can be described in two steps. The first step is before the instability (δ=46 [mm]) and the second one is after (δ=100 [mm]).
The maximum in plane stress is plot for each step, and is ideal to localize the stress concentration and the stress variation during the shaping process.
The stress is display in [MPa] in the following screenshot of Abaqus.

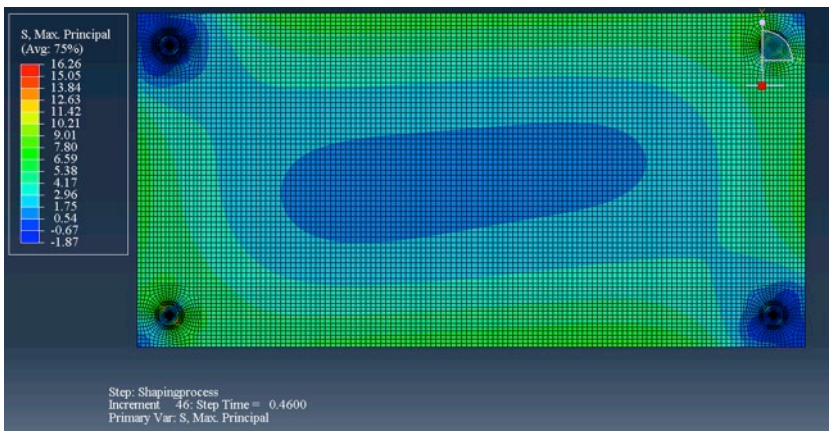

Figure 20 Maximum principal stresses before the instability (front view; δ=46 [mm])

As expected, for a lightly warped panel, the developed stress is quite small. The global maximal stress is around 10[MPa] whereas the local maximum stress is around 16[MPa]. However, at the centre the stress is close to zero since the geometry is anticlastic (the forced diagonal is convex whereas the supported one is concave, with approximately the same radius of curvature for each diagonal).

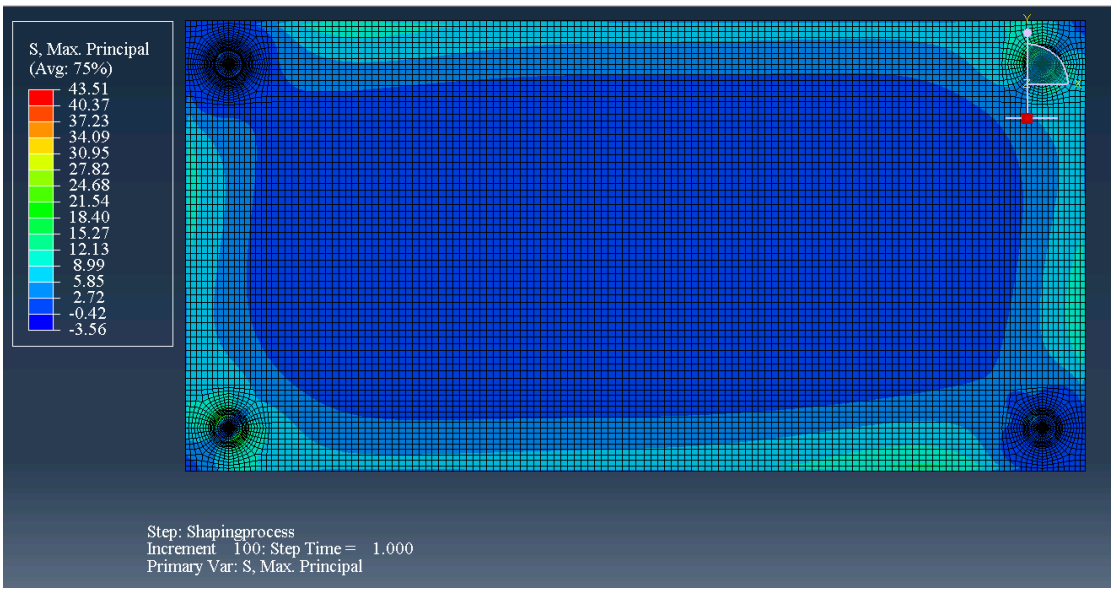

Figure 21 Maximum principal stresses after the instability (front view; δ=100 [mm])

The developed in-plane compressive membrane stress is almost spread all-over the intrados surface for an out-of-plane imposed displacement of 100[mm]. The in-plane compressive membrane is explained by the severe curvature of the forced diagonal, which becomes dominant in the geometry. A simple analogy to a bended beam explains the compression at the intrados.

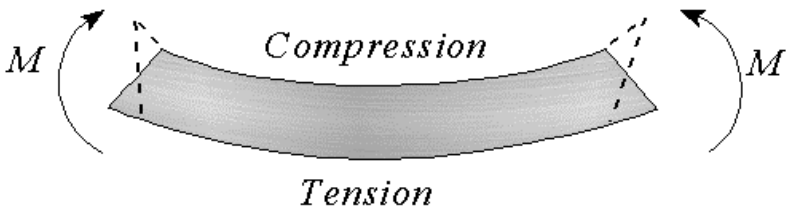

Figure 22 Beam analogy

The compressive in plane stress developed a maximal compressive stress around -3[MPa], which is almost nothing. However, some tensile in-plane stresses are recorded in the support area and the edges, the tensile stress is bigger in term of absolute value.

A tensile membrane stress appears at the extrados of the cold-warped panel when the instability is reached; see Figure 23 and Figure 24.

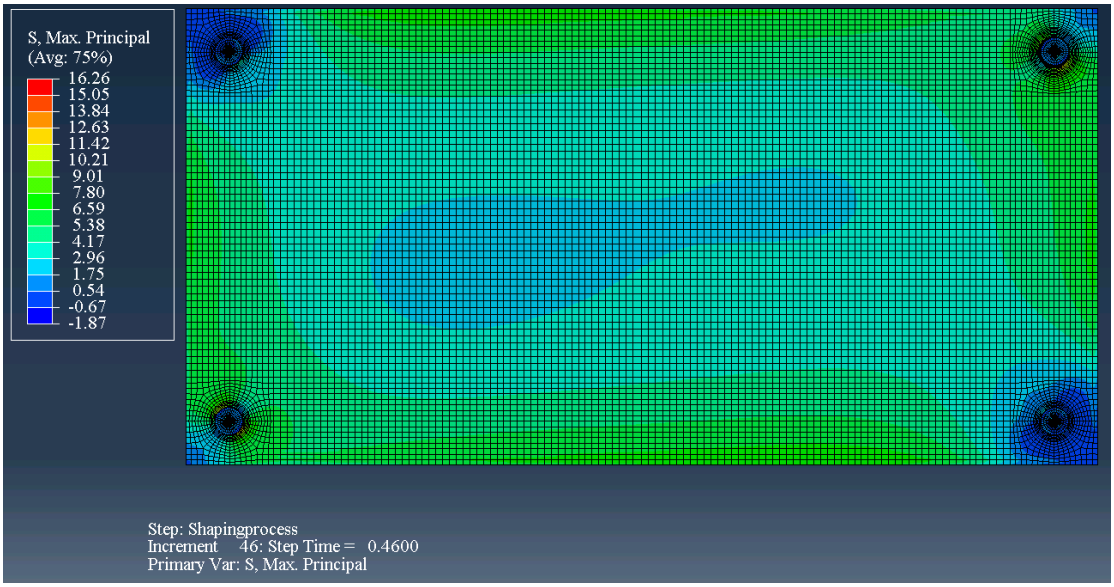

Figure 23 Maximum principal stresses before the instability (behind view; δ=46 [mm])

The in-plane stress is close to zero in the central part of the panel, for the same reasons as for the intrados part.

If one continues with the beam's analogy, then one can predict the stress pattern at the extrados.

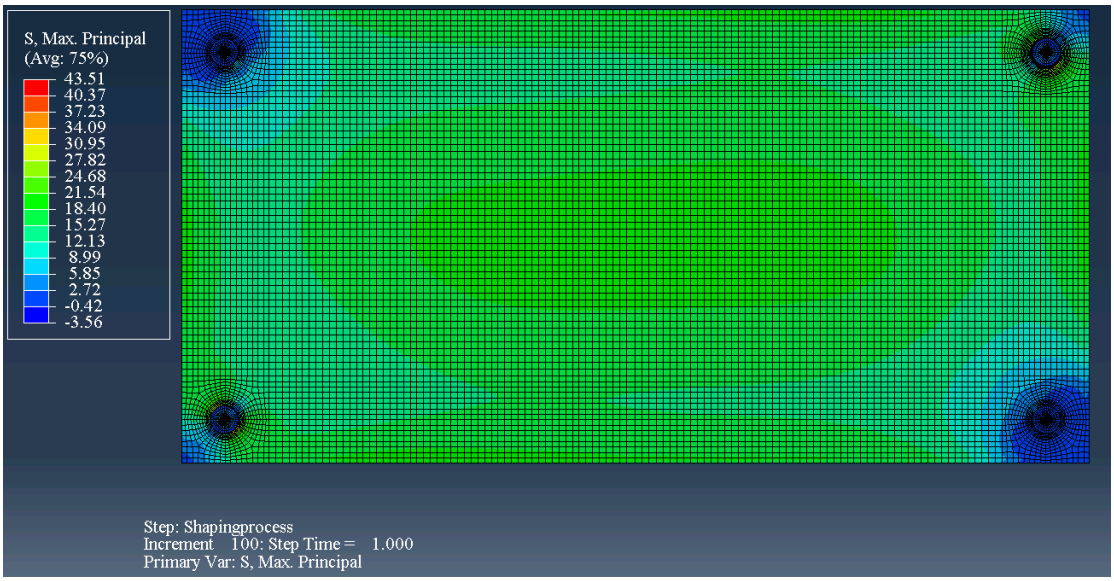

Figure 24 Maximum principal stresses after the instability (behind view; δ=100 [mm])

The in-plane tensile membrane, around 25[MPa], appears in the central part of the panel. From that it's clear that the most visible variation of stresses due to the instability appears in the extrados central part of the panel.

The difference of the stress between the "top" and the "bottom" surface from -3 to +25[MPa] is huge. Globally the stress is concentrate on the tensile surface.

The different screenshots show a “cross symmetry” of the panel stress built-up. This symmetry is due to the reaction forces, which are also cross, see Figure 26 and Figure 27.

The maximum stress before and after the instability takes place at the same place, that’s to say near the support. At the glue interface a peak concentration is reported. A special refinement mesh is then mandatory to capture the stress. The supports, “Free-X” and “Free”, are the most subject to that concentration, see Figure 25.

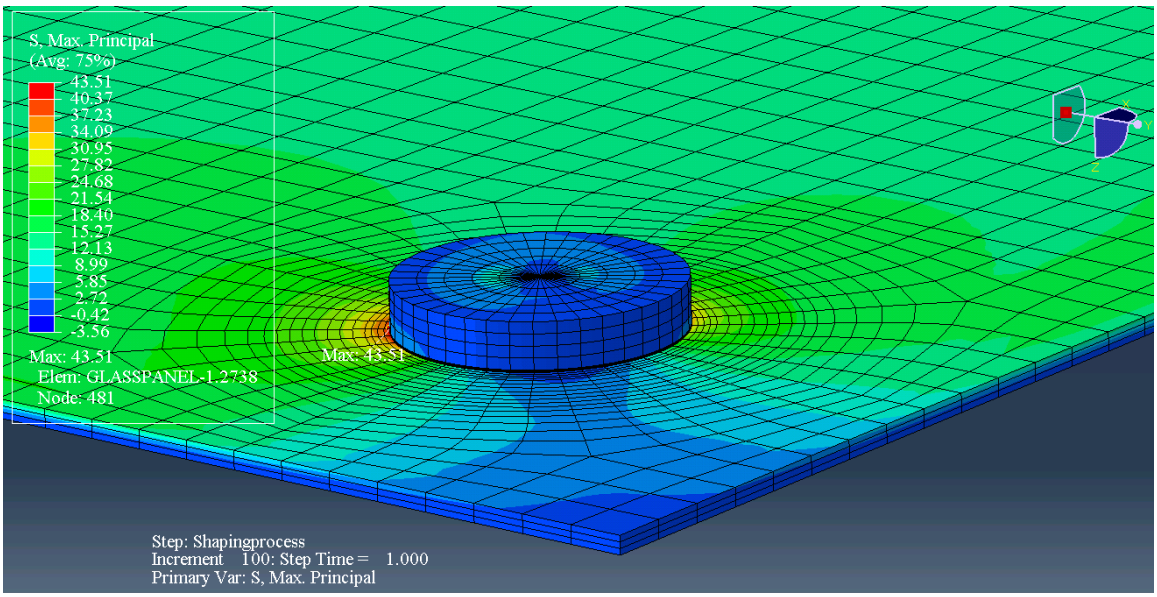

Figure 25 Peak stress at the Free-X support

The tensile stress concentration appears symmetrically from the diagonal axes at each sides of the support. As for a Brazilian test, the tensile stress, here, causes a perpendicular compressive stress. This effect is mainly due to the Poisson’s ratio.

However, the tensile stress concentration is the critical point. Appendix III shows that the peak stress could be decrease in despite of the glue’s rigidity.

2.2.3. Shell Model

Shell elements have been used in order to decrease the computational time. Shell elements are particularly interesting for monolithic plate problems as the thickness is integrated, during the analysis, following the Simpson integration rules.

In this part of the study the construction of the shell model is done in order to compute, quickly, the deformation behaviour, during the shaping process and the shaping-back process.

2.2.3.1. Global model

Almost the same global model is used as for the solid model. However, simplifications are done for the modelling of the support. In fact, the Appendix III has shown that the deformation of the plate during the shaping process is not influenced by the rigidity of the glue.

Thus, in order to decrease the computational time the support is modelling by a multipoint constraint, the master point is the joint ball and the slave nodes are the surface of the glass.

2.2.3.2. Element type

The Abaqus shell element library provides elements that allow the modelling of plate shells that can exhibit nonlinear material response and undergo large overall motions (translations and rotations).

The library is divided into three categories consisting of general-purpose, thin, and thick shell elements. Thin shell elements provide solutions to shell problems that are adequately described by classical (Kirchhoff) shell theory, thick shell elements yield solutions for structures that are best modelled by shear flexible (Mindlin) shell theory, and general-purpose shell elements can provide solutions to both thin and thick shell problems.

All shell elements use bending strain measures that are approximations to those of Koiter-Sanders shell theory (Budiansky and Sanders, 1963).

For most applications the general-purpose shell elements should be the user's first choice from the element library. However, for specific applications it may be possible to obtain enhanced performance by choosing one of the thin or thick shell elements. It should also be noted that not all Abaqus shell elements are formulated for large-strain analysis. [2]

Thin elements

Thin shell elements (Kirchhoff theory) may provide enhanced performance for large problems where reducing the number of degrees of freedom through the use of five degrees of freedom shells is desirable. However, they should be used only for the modelling of thin structures that exhibit at most weak nonlinearities in problems where rotation degree of freedom output is not required and for situations where the shell surface and the displacement field are smooth so that higher accuracy can be achieved with the use of second-order shells.[2]

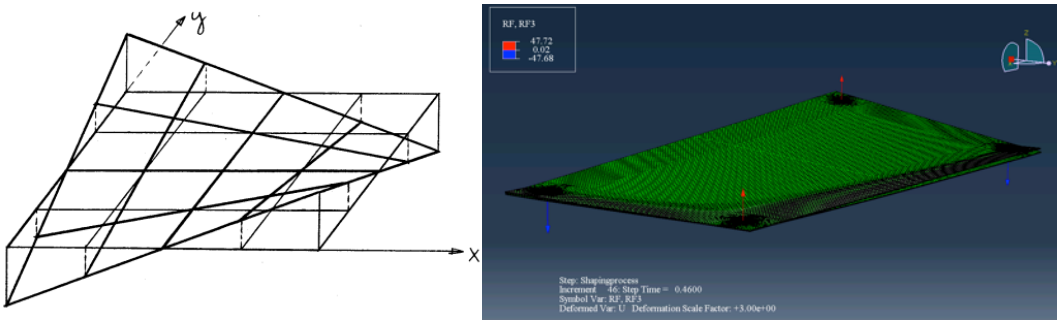

Figure 26 Hyperbolic paraboloid sketch (left) and in Abaqus for δ=46 [mm]

The linear Kirchhoff-Love theory predicts that if out-of-plane forces are applied at the corners, such as they twist (elastically) the flat rectangular plate; the deformed shape is a hyperbolic paraboloid, which preserves the straightness of the edges. Therefor the Kirchhoff-Love theory doesn't account for shear deformations.

Thus, the plate edges, as well as the fibres initially parallel to the edge, should remain straight during the shaping process, according to that theory.

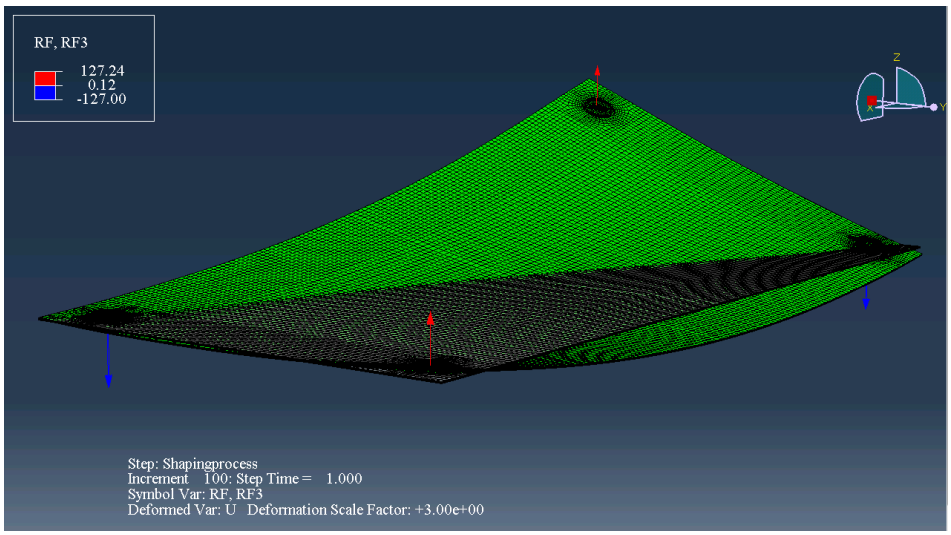

Figure 27 Instability form, loss of the straightness of the panel

However, after the instability the normal to the initial configuration don't remain perpendicular to the geometric reference and they even could warp. This warping is associated to the shear stress.

Moreover, Appendix X shows that before the instability the edges are already not straight anymore. That's to say shear deformations are already acting on the plate.

In conclusion, thin elements are not appropriate for the instability study during the cold-warping shaping process.

General Purpose elements, also called moderate thickness elements

The general-purpose elements provide robust and accurate solutions in all loading conditions for thin and thick shell problems. Thickness change as a function of in-plane deformation is allowed in their formulation. They do not suffer from transverse shear locking, nor do they have any unconstrained hourglass modes.

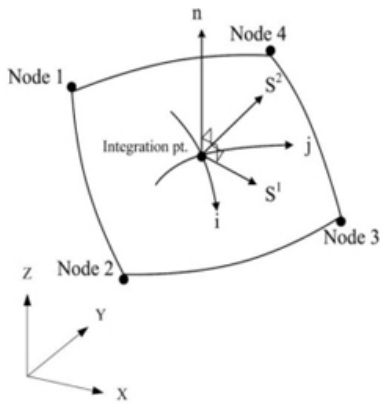

Figure 28 S4R shell elements, one integration point, [a]

The three-dimensional linear S4R, with hourglass control, elements are well suited for structures undergoing large-scale buckling behaviour, small strains but large rotations and severe bending. These elements use simplified methods for strain calculation and hourglass control.

S4R used the reduced integration to form the element stiffness (i.e. one integration point). The mass matrix and distributed loadings are still integrated exactly. Reduced integration usually provides more accurate results (provided the elements are not distorted or loaded in in-plane bending) and significantly reduces running time, especially in three dimensions. [2]

S4R is a 4-node doubly curved thin or thick shell, reduced integration, hourglass control, and finite membrane strains.

In conclusion the shell element model required the use of S4R elements, in order to enjoy the significant advantages in computational speed.

2.2.3.3. Mesh study

The mesh used is the one chosen in the mesh study Appendix I.

2.2.3.4. Applied Load and Displacement

The same load case as the solid model is applied. To catch the instability the selfweight AND an external pressure in the Z-direction are MANDATORY!

Without it the shell modelling didn't converge to the right solution and goes through the instability.

The load step and the external pressure are exactly the same as for the solid model. Nevertheless the applied displacement is different. In fact the shell model, due to its enhanced computational time, is used to simulate the shaping-process and the shaping-back process.

Thus, a first out-of-plane displacement is applied at the Ld_Point corner and then the same displacement is applied in the opposite direction. The plate goes back to its initial position.

2.2.4. Results of the numerical model with shell elements

2.2.4.1. Deformation U3 during the shaping and shaping back process

Only the displacement U3 is compute on this chapter.

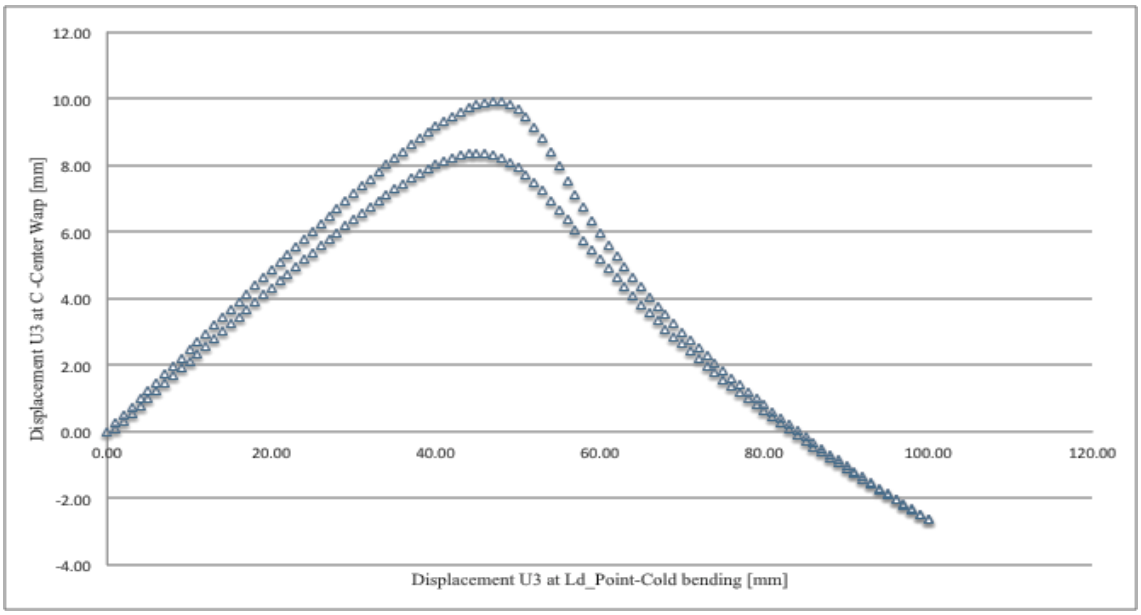

Chart 5 Displacement U3 at C in relation to U3 at Ld_Point during the shaping and the shaping -back process

Firstly, the shaping process gives exactly the same result as the solid model, Chart 1. The recommended simplification, Appendix II and Appendix III, are then useful in terms of saved time by the simplified model and the computational time.

The cold-warping is done elastically, so as expected, the centre point goes back to its initial position. However, the shaping back curved is not exactly the same as for the shaping process.

It has been shown by looking to the reaction forces in [3], that the whole panel is more rigid in the "buckle" configuration than initially. That's the reason why during the shaping-back process the curved is below the curved of the shaping process.

The shaping-back curved reaches the instability point for U3 at Ld_Point equal to 45 [mm] (U3 at C = 8.35 [mm]). So point C got more difficulty to meet its "shaping process" position. Therefore, it seems that for the shaping-back process the panel tend to join, naturally, directly its initial position, then point C didn't have to deform as many as for the shaping process.

Interesting things to do, would be to re-increase the applied displacement, at different stage during the shaping-back process. Then, one can see if the shaping-process curve shall prevail when the applied load increase and vice versa.

2.2.4.2. Deformation U3 for a precurved panel

An initial displacement $\delta_{initial}$=30[mm] is imposed to the Fix support. Thus, before the shaping process the panel is already warped. The instability of the panel is then investigated.

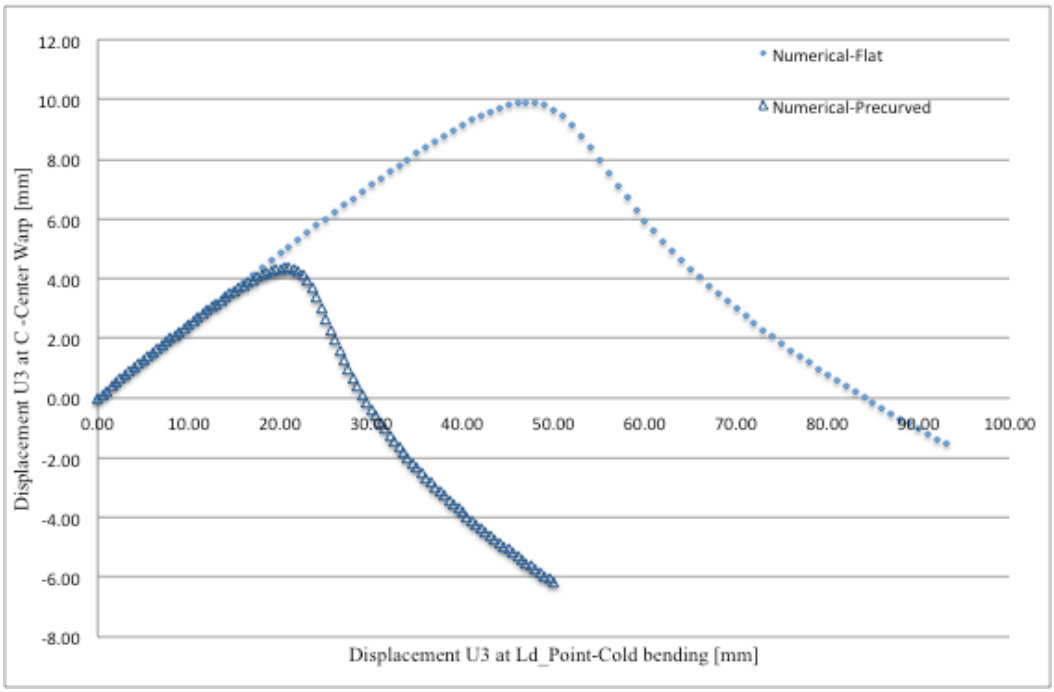

Figure 29 Displacement at C in relation to the applied displacement δ

The same slope before the instability is observed, it seems that the precurved model behave as a premature flat plate.

The instability occurs for δ=20.5[mm]. The displacement U3 of C due to $\delta_{initial}$ is equal to 7.48[mm], and due to δ only is equal to 4.35[mm]. Thus, the total displacement U3 at C during is equal to 11.83[mm].

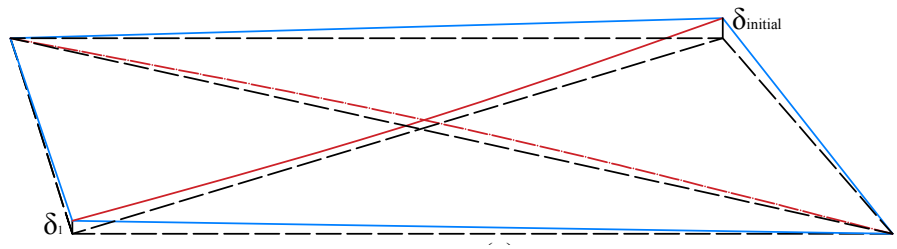

Figure 30 Initial deformation patterns before the instability

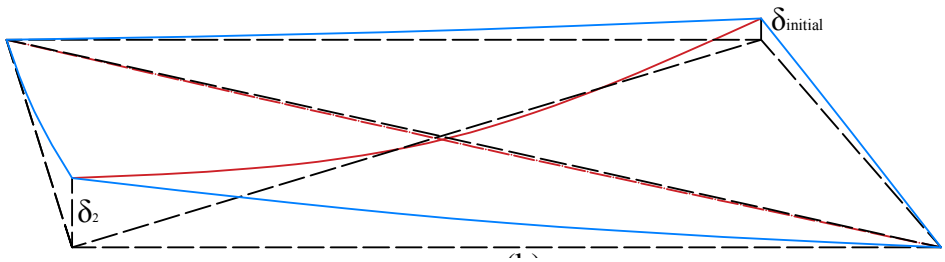

Figure 31 Second deformation pattern after the instability $\delta_1<\delta_2$

The same consequence as for the classical case is observed after the instability. That's to say ripples along the supported diagonal, curved edge and severe curvature for the forced diagonal are observed.

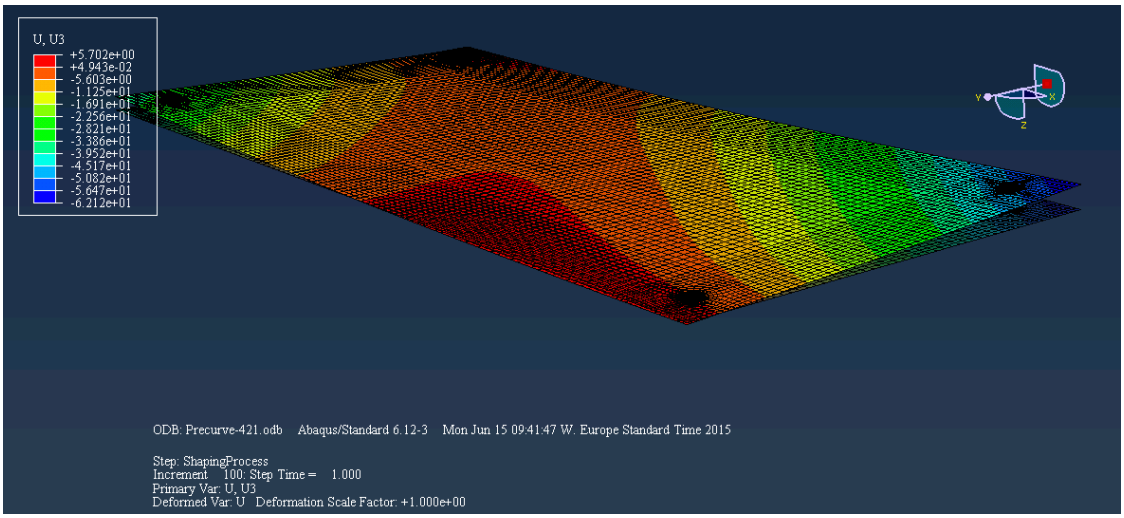

Figure 32 Displacement U3 for δ =50[mm] (after instability)

2.3. Experimental Work

Experimental tests are done in order to validate the numerical model.

2.3.1. Test setup preparation

The first part of the experimental test consists in doing the test setup. As, almost, for all the projects, one wanted the simplest setup with less economical cost.

Thus, the idea is not to limit the cost, in time and money, of the setup by optimizing it but rather by using old steel profiles, which were stock in the outdoor. That's the reason why they are rusted.

Figure 33 Old Steel Profiles

Moreover, the machine has to be an adaptive structure to carry different size of panel (in height and width). The vertical position of the glass avoids gravity deflection that will be considerable for a 4 x 1'000 x2'000[mm] panel. The measurements are as well easier than for a horizontal position of the plate.

Figure 34 Test Setup

Finally the machine (Figure 34) is divided into three steel profile parts; Two L assembly and one beam to link them. The two L part are the support of the glass. The beam between them fixes the distance between the L and ensures the parallelism and the planarity of the whole setup. Moreover, the self-weight of the beam helps against the mechanical dumping of the whole setup (due to the eccentricity) in case of heavy panel.

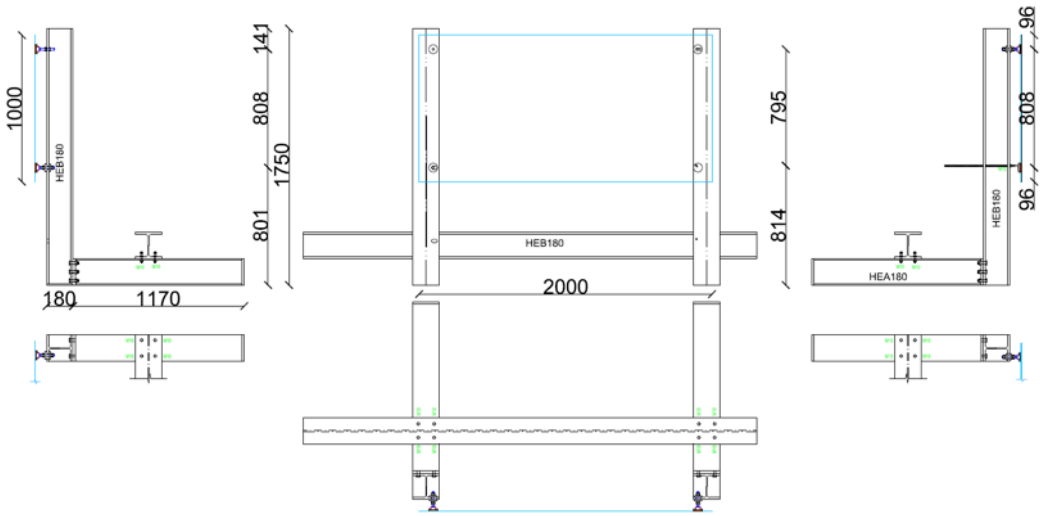

Figure 35 Frame description

Two different types of width have been considered, 1[m] and 1.5 [m], and four different lengths (1, 1.5,2 and 3.5 [m]). Indeed different studies [7] [10] have been done on 1'000 x 1'000, 1'500 x 1'500 and 3'000 x 1'000 [mm]. The test setup could be used to validate these different studies with further tests.

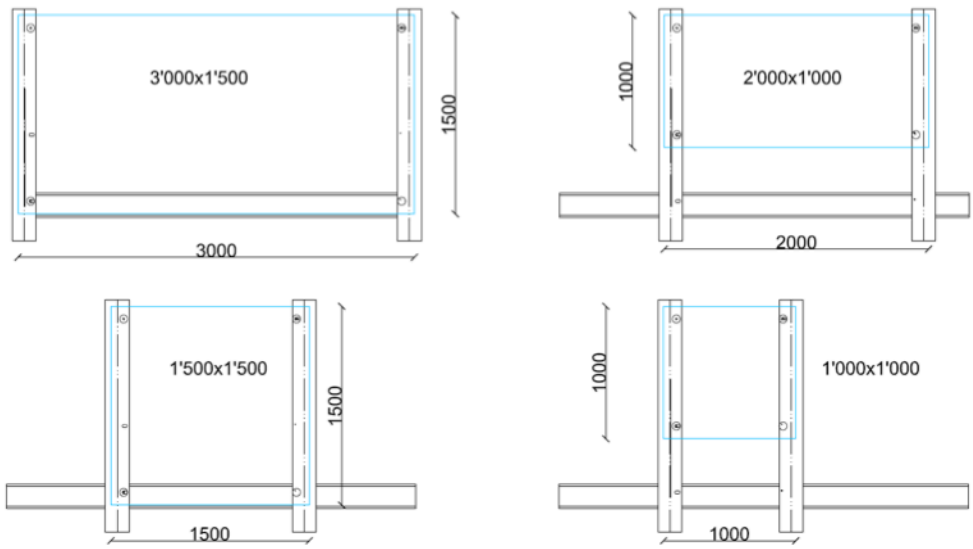

Figure 36 Setup declension

Afterward a wood beam has been placed between the tops of each L, in order to increase the global rigidity of the setup.

2.3.2. Support Conditions

As explained in the §2.1.2, glued spiders fitting are used. The boundary conditions are divided into two parts, the load point and the other Z- restrained support.

Contrary to real façade projects, the self-weight of the panel is undertaken by the point-supports. In the reality the selfweight of the glass plate goes directly to the plate below it thanks to tape between panel elements. Here it's too complicated to do it, as the edges of the plate are moving during the shaping process. However, the point fittings are sufficiently stiff to carry out the selfweight.

2.3.2.1. Z-restrained supports

These supports are ensured by the R1006TSSA. The system is free to rotate thanks to the ball joint, see Figure 7.

However, the translational conditions are ensured by the setup itself. Indeed a mechanical work has been done in order to offer to the support the right boundary conditions.

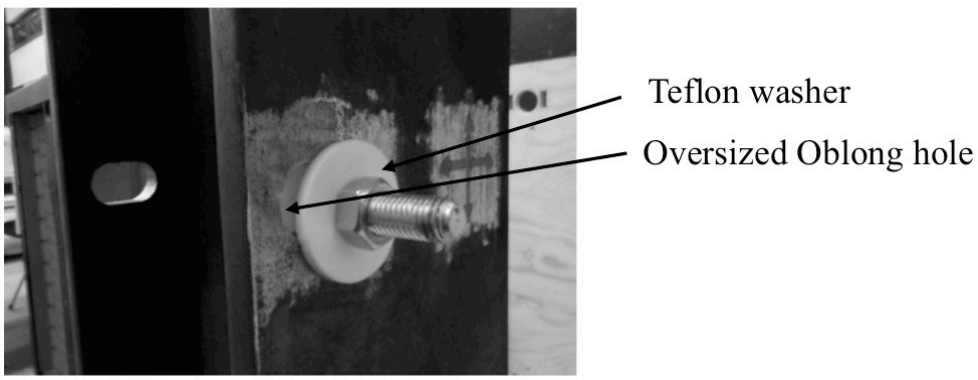

Figure 37 Support Condition offered by the test setup

Oblong and oversized oblong hole have been drilled into the L support. The dimensions of the hole were calculated with a previous numerical model. Teflon washer, special grease and a polishing were done in order to decrease the more possible the in-plane friction.

2.3.2.2. Load point

Pushing the panel at one corner does the cold-warping process. However, pushing the panel in the out-of-plane direction involve displacement in the in-plane direction. The load point is tricky since one want to push the corner in a fix position.

To avoid this problem, the idea was to glue to the glass a steel circular plate, 10 [mm] thick. The diameter of the circular steel plate is the same as the one of the R1006TSSA (i.e. ∅=60 [mm]).

The out-of-plane displacement is applied by a bolt, which is threated to the L support. An eccentricity is given to the bolt in order to offer a bigger in-plane displacement freedom. The eccentricity doesn't affect the behaviour of the panel during the cold-warped shaping process.

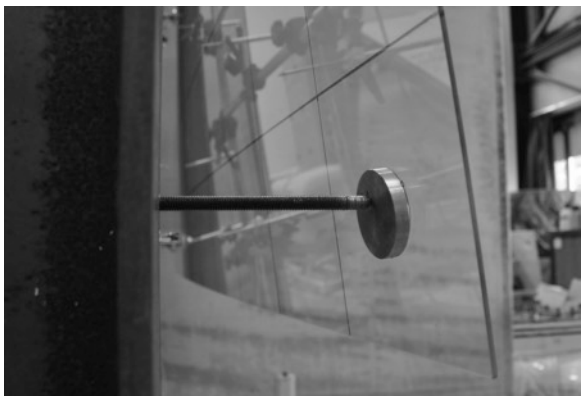

Figure 38 Load Point

2.3.3. LVDT setting up

LVDTs WA were used in order to monitor the out-of-plane displacement and the in-plane displacement during the shaping process. A total of twelve LVDT were place all over the panel. In the plane direction three LVDT were disposed; one on the Free-X support in the X direction and two in the Free support X and Y direction. The aim is to know if the in plane displacement are not restrained by the friction.

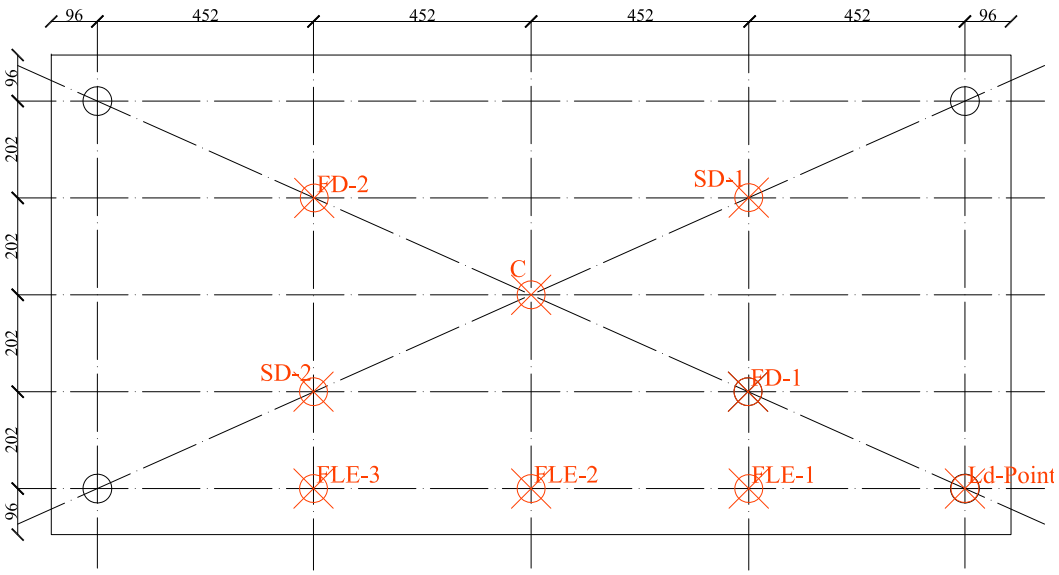

Figure 39 LVDT's position and terminology

Nine LVDT were disposed to record the out-of-plane displacement. The position and the terminology used is depict in Figure 39.

The Z-displacement along each diagonal and along the forced edge can be monitored along the shaping process. Thanks to the LVDT in C and in the Ld_Point the classical displacement at the centre (C) in relation with the applied displacement on the corner (Ld_Point) can be plotted.

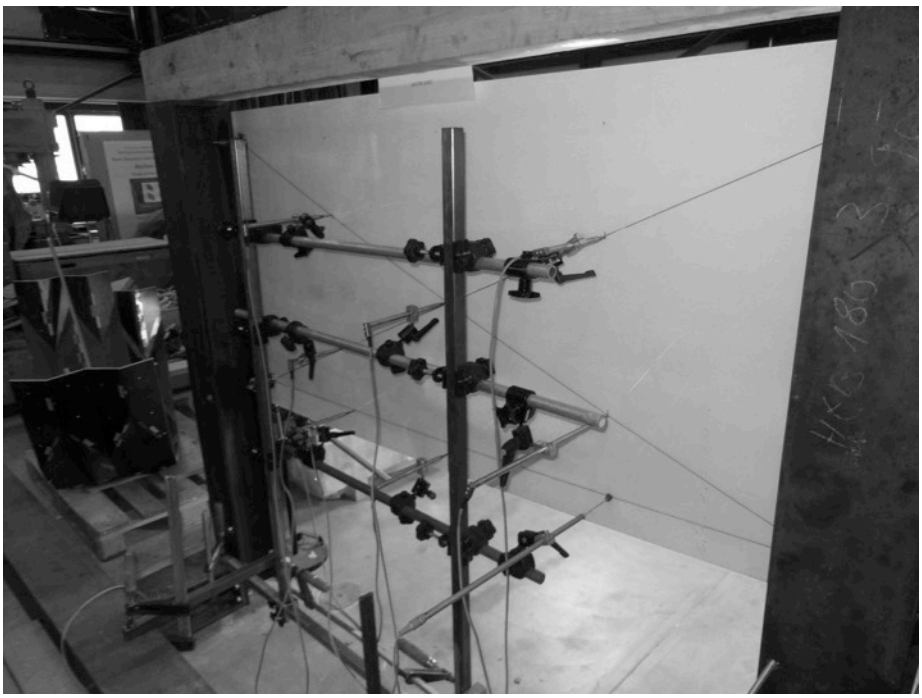

Figure 40 LVDT measuring the out-of-plane displacement

2.3.4. Strain gauges setting up

Strain gauges have been used to record the change in stress during the shaping process. **They have been disposed on the inside face**. The geometry of the panel changes during the process and particularly after the instability phenomena, then the stress inside the panel change during the whole process. Thus, height gauges are used to validate the numerical model.

Each gauge is glued to the glass panel, and then has the same deformation as the glass. They work by correlating the strain to the change in the electric resistance of the gauge.

Strain gauges have been disposed at the place where the stress is high (stress concentration) or where, due to the instability, the stress varies a maximum. S11 means strain measurement in the 1-1 direction (X axe) and S22 means strain measurement in the 2-2 direction (Y axe).

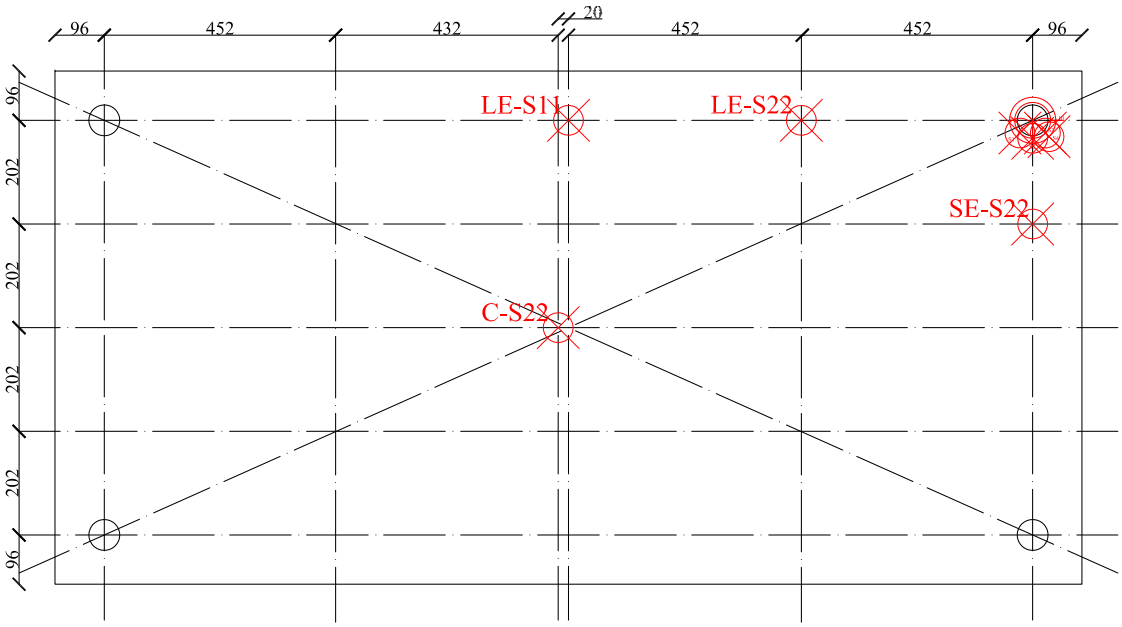

Figure 41 Global strain gauges position and terminology

LE-S11 and SE-S22 are the placed where the stress is higher compared to the rest of the panel[i]. C-S22 and L-S22 are the place where the stress should vary due to the buckle deformation mode.
Moreover, the glued point-fitted connection involved stress peak. To verify that the model is converging to the right stresses distribution, strain gauges have been disposed around the critical support.

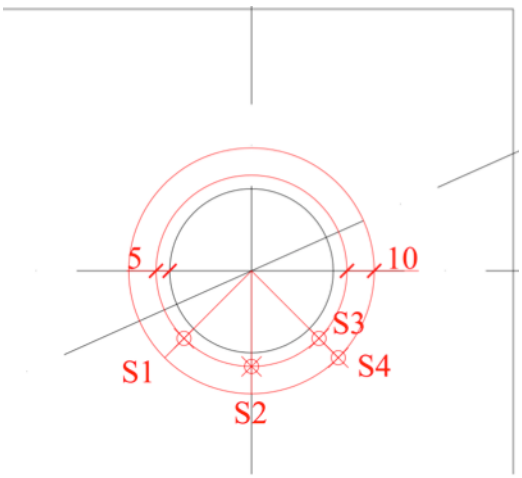

Figure 42 Strain gauges around the critical support

[i] The stresses inside the panel follow a central symmetry. So there are two maximum stress places.

The strain gauges are disposed in the radial direction. Indeed the circular support implies an almost perfect radial stress distribution around it. The strain in that direction should be the hugest one. S3 is the place where the stress is supposed to be the higher, the strain gauge S4 is used to show the peak concentration stress. S2 and S1 are used to show that the stresses vary from the tension to the compression around the support [i].

Figure 43 Strain Gauges

2.3.5. Digital image correlation setting up

A 3D camera measurement system has been used in order to validate the LVDT measure and to get the entire displacement of the whole panel.

The system requires a special treatment of the measured surface. A specific "moucheti" have to be paint on the glass surface. Indeed the used software, VIC-3D, works if only there is a huge contrast on the analysed surface. That's the reason why black dot are painted on the already, white painted, glass plate.

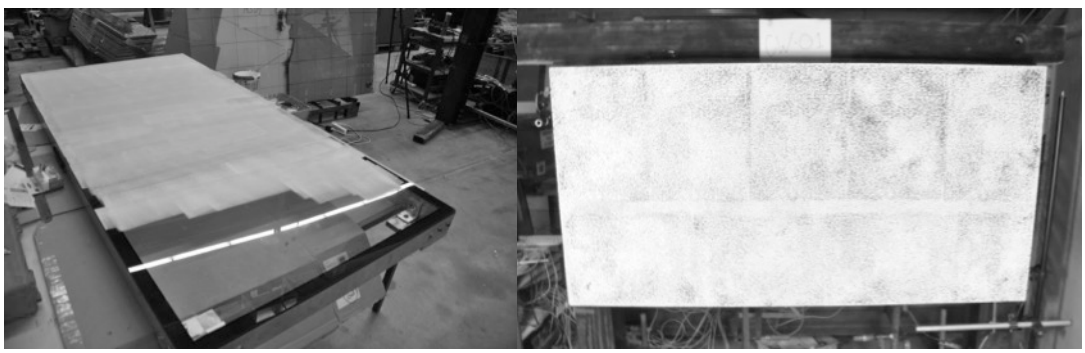

Figure 44 Preparation of the analyse surface

[i] The stress pattern follows a "cross symmetry", therefore only one quarter is treated.

The software is calibrated by creating a database of coordinates (x, y and z), which are used afterward for the calculation of the displacement. The software creates a mesh in the region of interest, and made the calculation of the grey level in each mesh element. Then, picture-by-picture the change of grey is analysed. These changes of grey ratio are correlated to the displacement.

In order to catch the big out-of-plane displacement an angle of 15°is given. The accuracy is about 1/100 millimetre. However, for small displacement the system didn't provide accurate results. As well for ε and γ the mesh is too coarse.

Figure 45 Digital image correlation system

2.3.6. Perform Cold-Bending tests

2.3.6.1. Aluminium Plate

Preliminary cold-warping tests have been done on an aluminium plate. Both glass and aluminium material have approximately the same elastic properties [3], therefore, the same behaviour for a same glass and aluminium plate is expected.

The aluminium has the advantage to be more manageable than the glass. Indeed there are no risks of fragile rupture in cutting sharp pattern. Therefore, the panel has been very useful for the painting phase, the gluing phase as well as for the laying into the test setup.

The only drawback of aluminium panel is the planarity of the panel. Due to the factoring process aluminium panels suffer from initial imperfections, which results in initial curvature (or deflection). The tested aluminium panel got an initial curvature such as the deflection at the middle was up to 10 [mm].

Problem is that the initial curvature has an influence on the cold-warping behaviour during the shaping process. Indeed, Figure 46 shows the behaviour of the aluminium plate. Only an out-of-plane displacement is imposed to the corner.

Figure 46 Cold-warping behaviour of the aluminium panel

The aluminium panel didn't buckle as expected. However, the edges developed a severe curvature in the opposite direction as expected. The geometry changes in a synclastic shape. The instability occurs in the opposite direction as expected.

Figure 47 Deformation pattern after the instability

It's observed that if an external pressure, in the opposite direction of the imposed displacement, is applied, then the initially expected instability occurs. Indeed, if an initial pressure is imposed to the panel the expected buckling become as the first deformation mode pattern. However, the higher the initial imposed displacement is, the higher the applied pressure has to be to get the expected deformation pattern. In other words, the initial curvature avoids the instability and the synclastic, developed, shape makes the panel more and more stiff to an external pressure.
Nonetheless, if the applied pressure is high enough, then a severe instability is observed. When the applied pressure is remove the panel stay in the instability deformation mode, see Figure 47.

2.3.6.2. HSG Plate

After the preliminary tests performed on the aluminium plate, heat strengthened glass have been tested. The planarity of the glass is better than for the aluminium plate, the edges are almost straight.
Thus, an instability is observed, as expected, without an external pressure, see Figure 48.

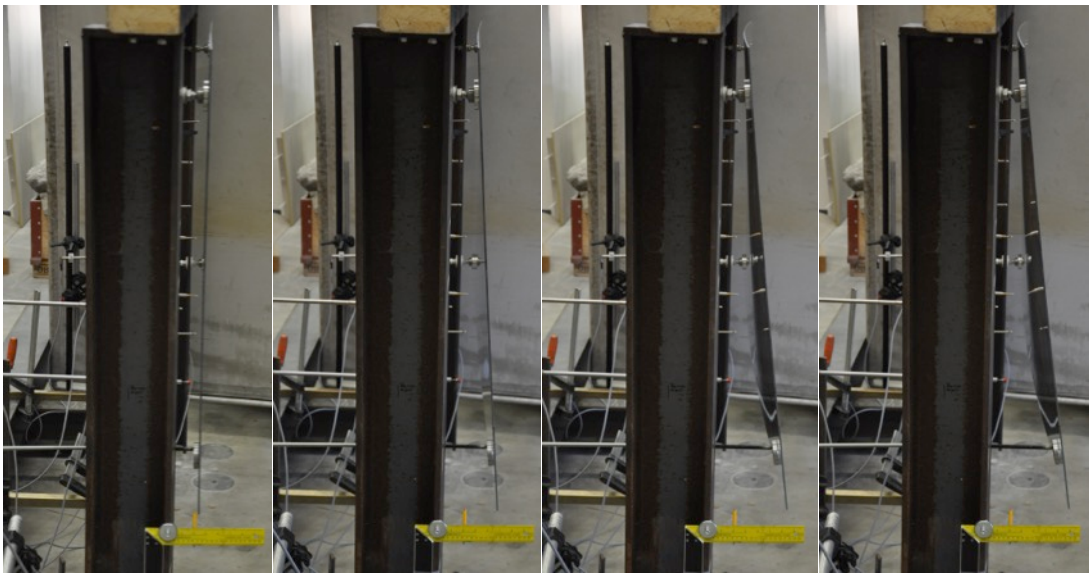

Figure 48 Cold-warping behaviour of a HSG plate.

2.3.6.3. Precurved model

Cold-warping test have been perform on the precurved HSG glass. Indeed thanks to the length of the threaded rod, an initial deformation $\delta_{initial}$= 30[mm] have been applied to the fix support. Then, the imposed displacement has been applied to Ld_Point.

Thus, the results could be compared to §2.2.4.2.

2.3.7. Results from the experimental test

The following results are coming from the tested HSG panel. Due to the LVDT influences reported in Appendix V, the test is performed without out-of-plane LVDT. Thus, only the digital image correlation system and the Ld_Point LVDT measure the out-of-plane displacement (Appendix VI).
Strain gauges are also used without the LVDT.

2.3.7.1. Instability phenomena

The instability phenomenon is investigated by plotting the displacement (C) of the centre of the plate in relation with the displacement on the corner (Ld_Point).

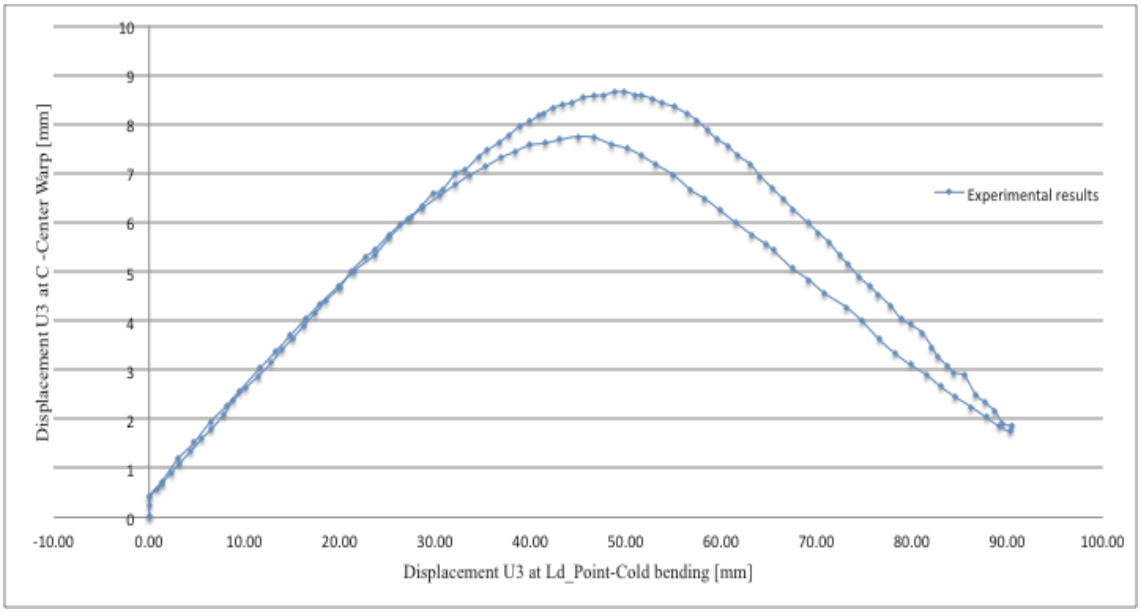

Chart 6 Displacement U3 at C in relation to U3 at Ld_Point during the shaping and the shaping -back process

The instability is reached after an applied displacement of 50.0 [mm], the displacement at C reaches a maximum value of 8.6 [mm]. The forced diagonal, supported diagonal and the forced long edge displacement are also plotted to see the effect of the instability.

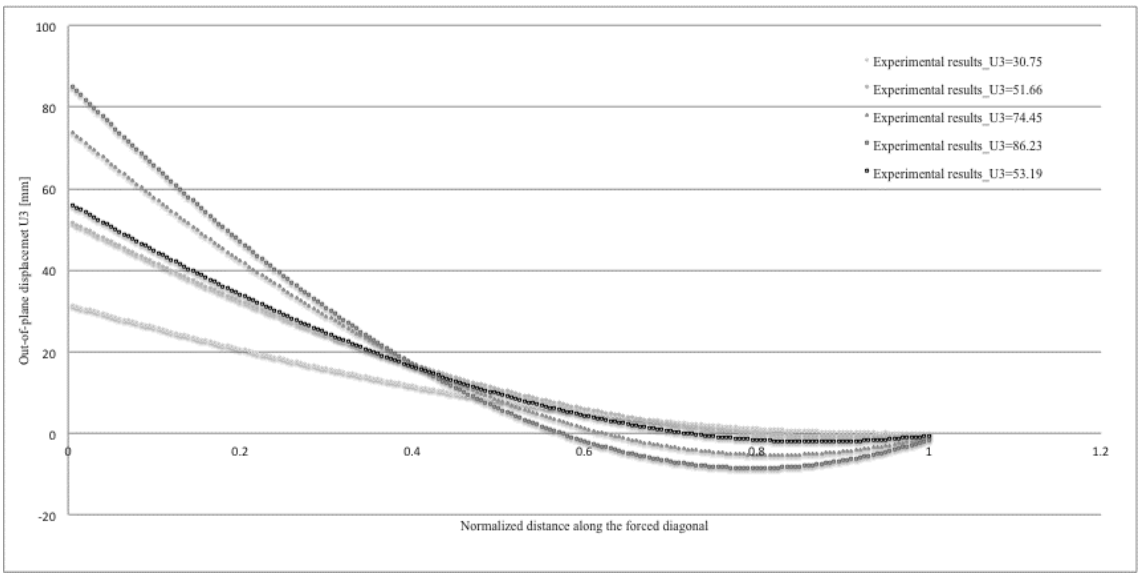

Chart 7 Forced diagonal behaviour during the shaping and the shaping back process

The change in form due to the instability implies a severe curvature of the forced diagonal. To reach this curvature the deformation of the diagonal have to be negative near the Fix support.

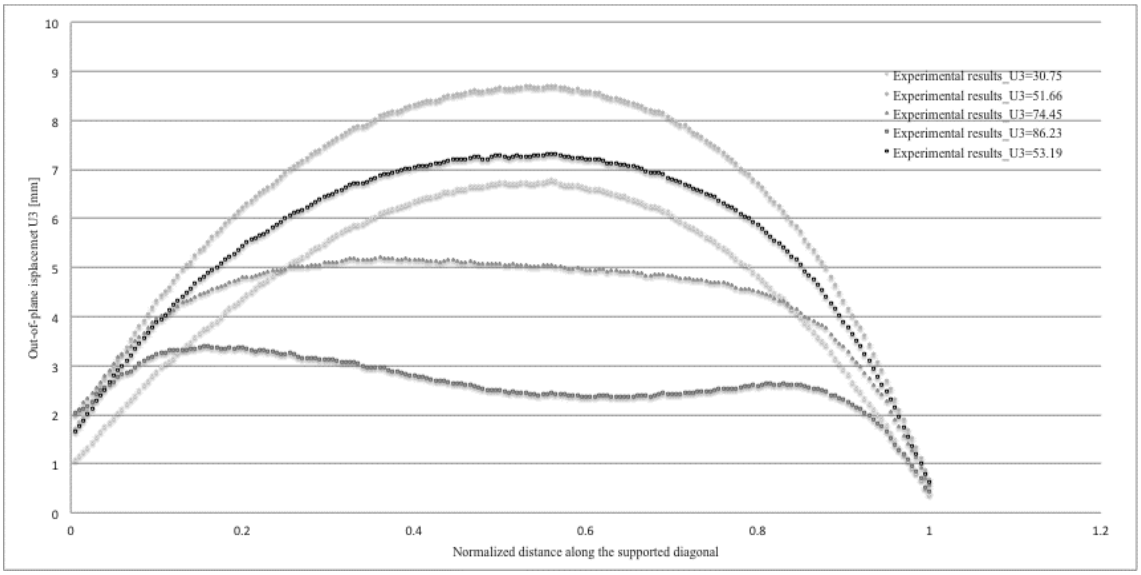

Chart 8 Supported diagonal behaviour during the shaping and shaping back process

Ripples are also observed at the surface of the plate. The amplitude of the ripples are larger than the limit fixed by the EN12150-1: 2000 [11]. Indeed the allowable limit for roller wave distortion on thermally toughened glass is 0.5[mm] over a length of 300 [mm]. The amplitude of the ripples affects the optical quality of the plate because of the implied distortions (similar of the roller wave distortions) [10].

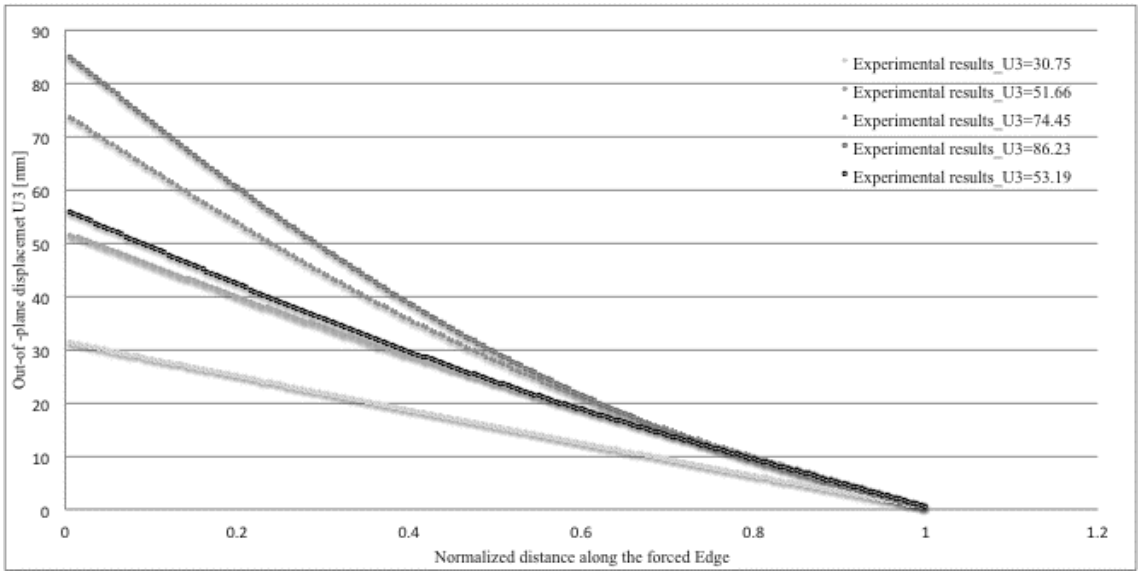

Chart 9 Forced long edge behaviour during the shaping and the shaping back process.

The edge seems not to be very straight before the instability (explain in Appendix X), although after the instability a clear curvature can be observed. As already said the Kirchhoff –Love theory is not anymore valid. That's why second geometrically order is used.

2.3.7.2. Stress built-up

The stress built-up is analysed thanks to the strain gauges. Thus, to get the stress the generalized Hook's law have to be applied. However, in order to compare the results with the numerical model, the strain is directly compared for both tests.

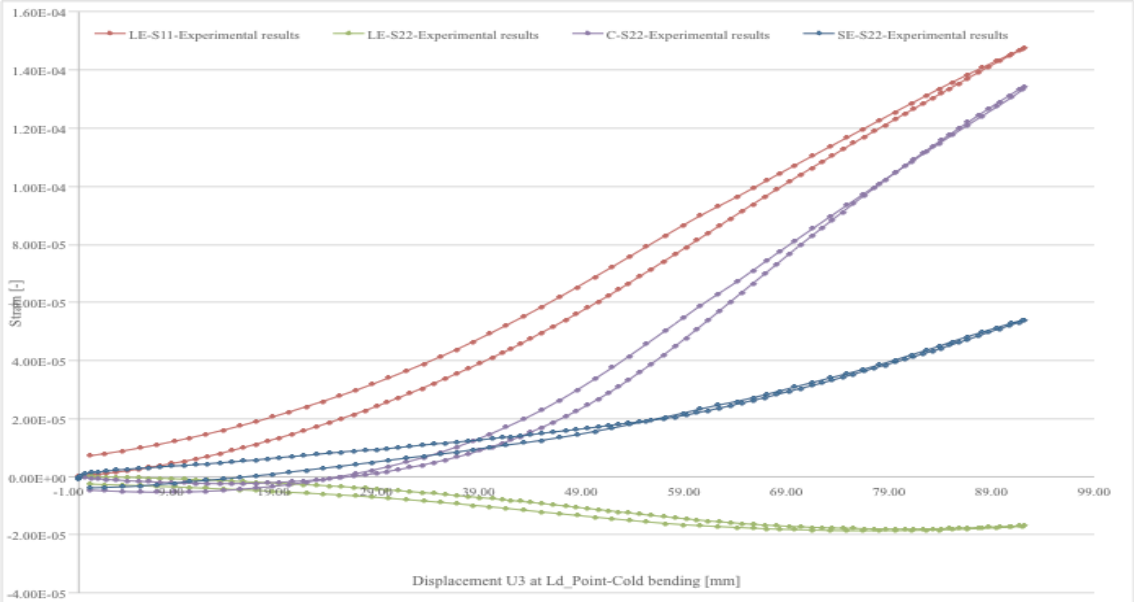

Chart 10 Strain on the extrados surface

The stresses vary in a smooth way from the beginning. There is no sudden increase of stress after the instability but one can notice a clear change of the C-S22 slope before and after the buckling. The change in stress at LE-S22 is less interesting than expected.

The strain concentration near the support is plotting apart from the rest of the strain gauges.

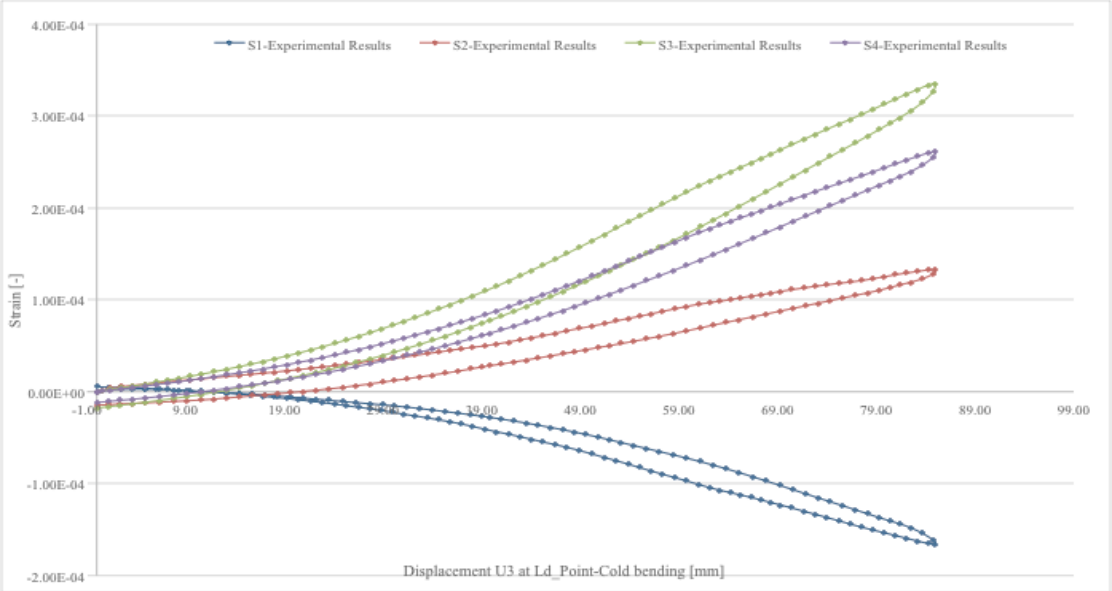

Chart 11 Strain near the critical support (Free-X)

As expected near the support stresses vary from the tension to the compression. The stress peak is localised near the S3 gauge. The stress is increasing in a continuous manner.
When the applied displacement decrease a sudden loss of strain is observed and the strain tends back to zero.

2.3.7.3. Precurved plate

The instability is investigated in the same manner as for the traditional model.

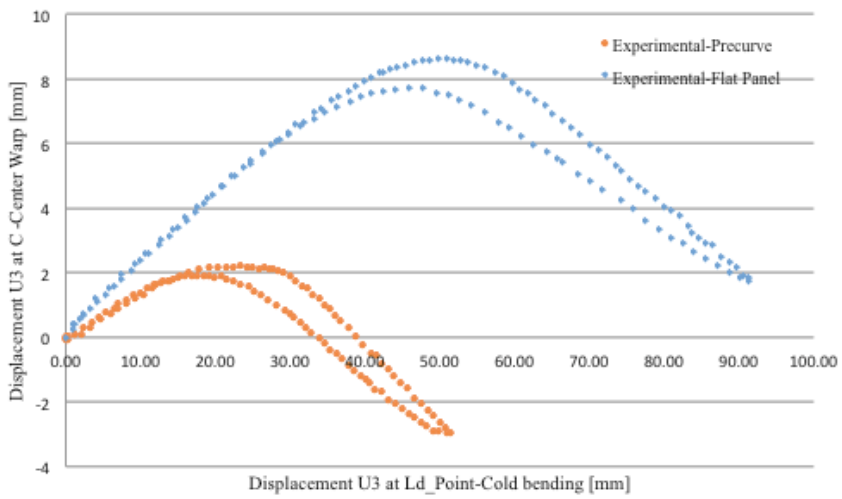

Figure 49 Displacement U3 at C in relation with δ

The instability is observed for δ=23[mm] for a *total* displacement U3 at C equal to 9.8[mm].

2.4. Numerical and experimental comparison

A comparison between the numerical modelling and the experimental is done to calibrate and validate the model. Both displacement and strain are compared.

2.4.1. Out-of-plane deformation comparison

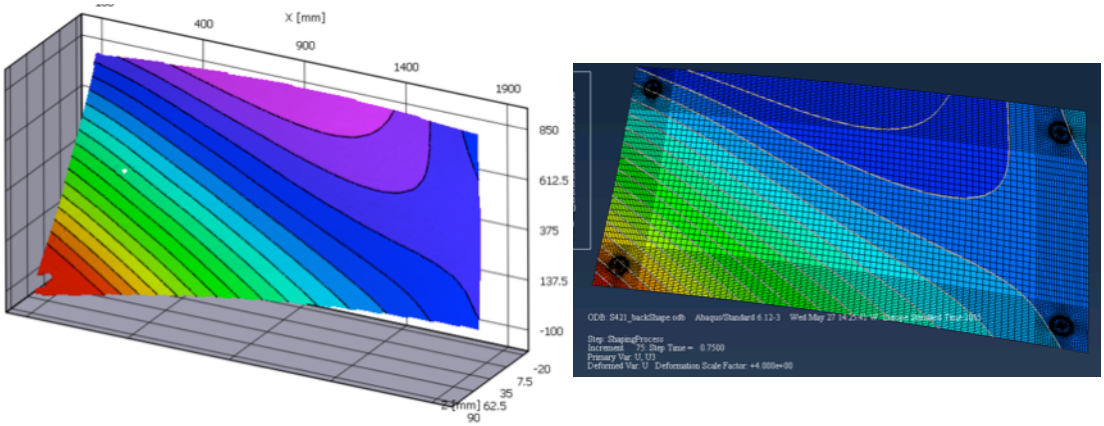

Figure 50 Deformation U3 pattern, experimental left and numerical right

The instability phenomena have been observed for both numerical and experimental results. However, even if the global behaviour is the same the values may differ. Hence the comparison is fundamental to validate the numerical model.

Displacement at C in relation with the applied displacement on Ld_Point

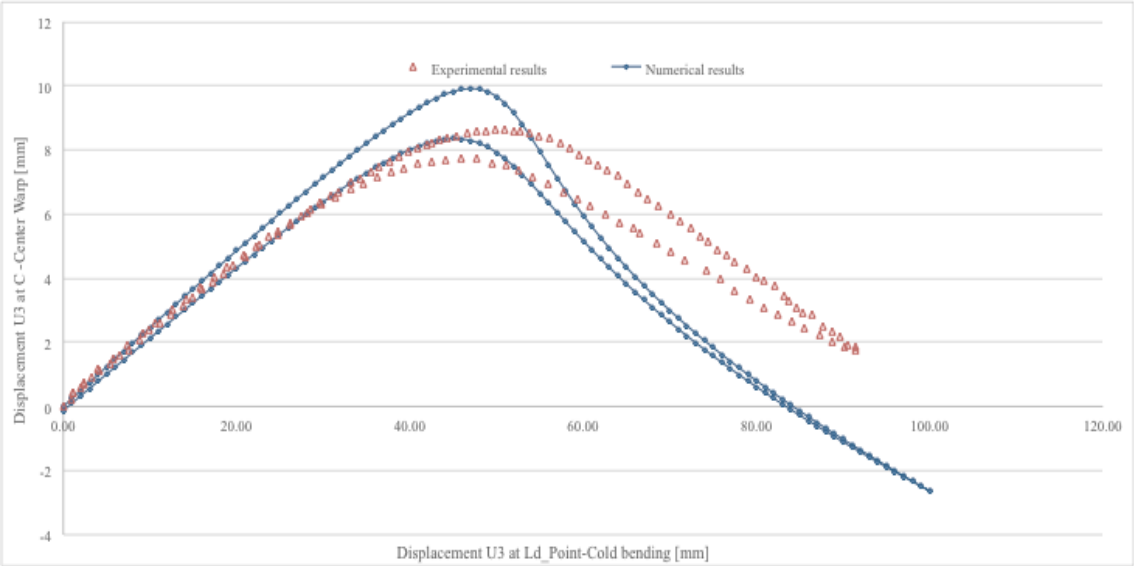

Chart 12 Comparison of the displacement of the centre C in relation with the applied displacement on Ld_Point

The instability occurs for an applied displacement of 47[mm] for the numerical results whereas the experimental results converge to an applied displacement of 50[mm] (+6%).

Nonetheless the point C doesn't have the same slope until the instability. Indeed when the instability occurs the displacement U3 of C is equal to 9.9[mm] for the numerical model and 8.7[mm] (-21%) for the experimental test. The difference is even greater because the instability doesn't occur for the same δ.
The experimental results give a smoother slope, witch decrease continuously until the instability. Before the instability a small plateau exist where the system is particularly unstable. Once the instability is reach the centre displacement starts moving in the opposite direction. The instability doesn't seem brutal since the slope after the instability is almost the opposite of the slope before the instability. Thus, the instability seems to occur continuously in a non-brutal manner.
The numerical results are different since the first part is completely straight (and not continuously decreasing) until a small plateau and the instability occur in a more severe manner. Indeed the slope just after the instability is steepest. However, after a certain displacement, after that the stability occurs, the slope is smoother and parallel to the experimental one.
In conclusion the numerical results give protective results for the $\delta_{instability.}$

Out-of-plane displacements U3 during the shaping process

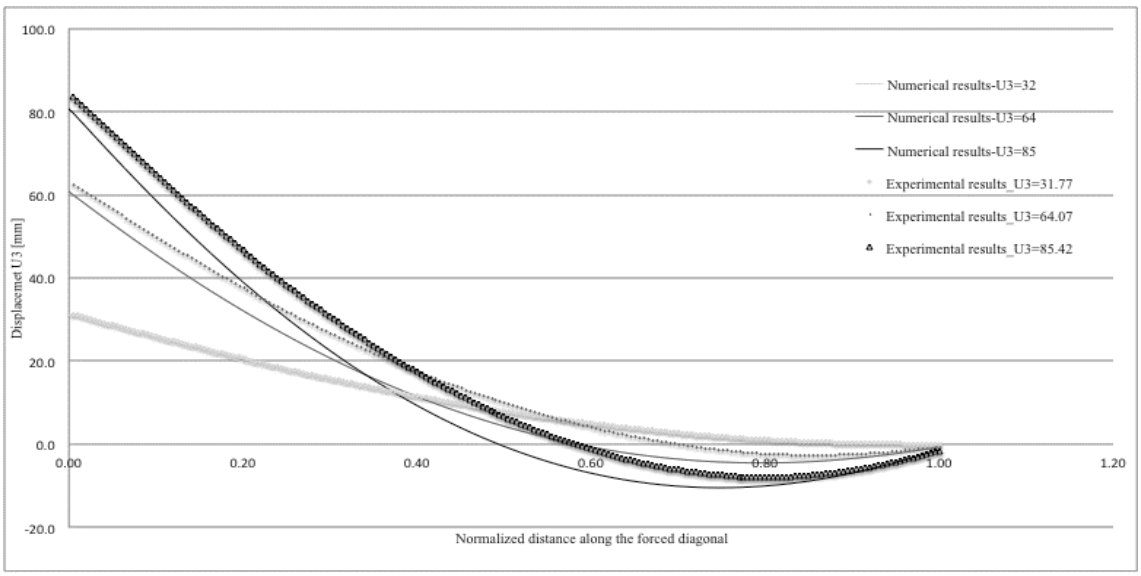

Chart 13 Out-of-plane displacements U3 along the forced diagonal during the shaping process

Before the instability occurs the curves match almost perfectly. Afterward the global behaviour is the same, except that numerical results give more severe curvature.

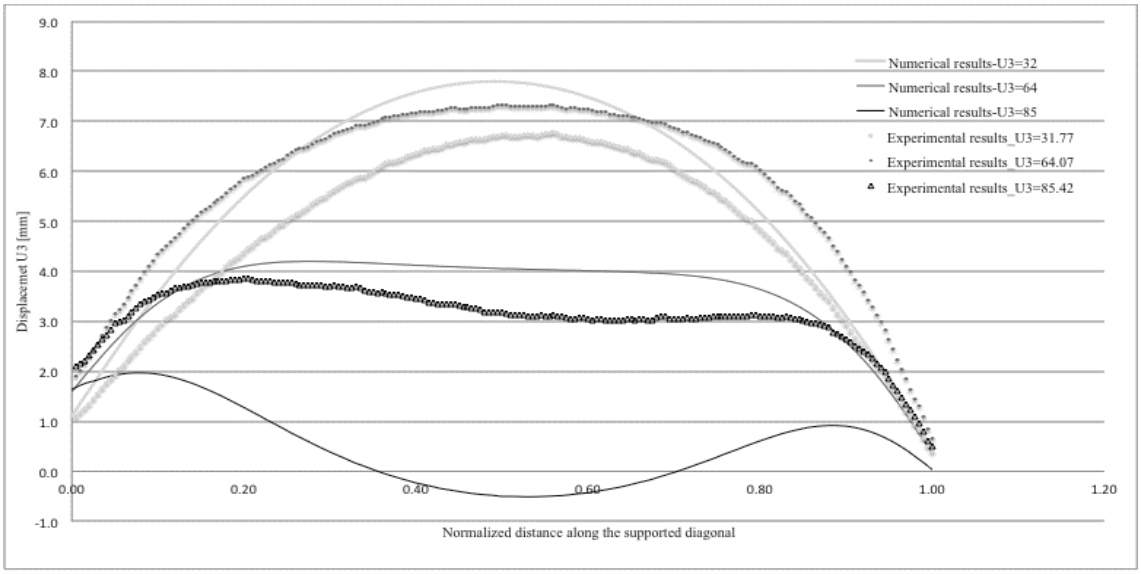

Chart 14 Out-of-plane displacements U3 along the supported diagonal during the shaping process

Here again numerical results increase the instability effect. The ripple amplitude for U3=85[mm] is 0.75[mm] for the experimental test and 1.5[mm](+100%) for the numerical model.

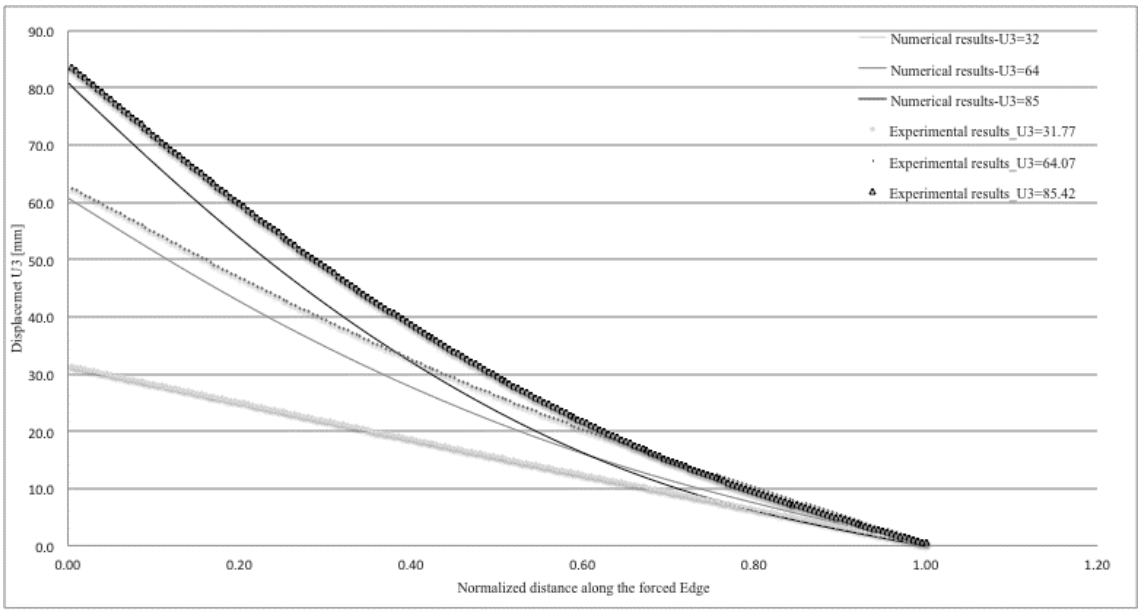

Chart 15 Out-of-plane displacements U3 along the forced edge during the shaping process

The same observation is reported for the behaviour of the edge.

In conclusion, concerning the out-of-plane deformation during the shaping process, the numerical model gives, incontestably, more protective results. The numerical model by increasing the effect of the instability on the deformed geometry becomes a lower bound limit of the instability occurring and effect.

2.4.2. Strain built-up comparison

The strain value, which is correlated to the stress by the Generalised Hook's law, is directly compared between the numerical and the experimental results.

Concerning the strain "on the panel" (Chart 16) the shapes of the curved are well correlated, particularly for (a) and (b). For (a), (b) and (c) the instability results in an increasing of strain. As expected from the deformation comparison, this increasing is more pronounced for numerical results.

In conclusion the instability, as expected, results in a huge change of the stress state inside the panel. The numerical model is close to the experimental test even if some differences, in the magnitude of the instability's effect, remain.

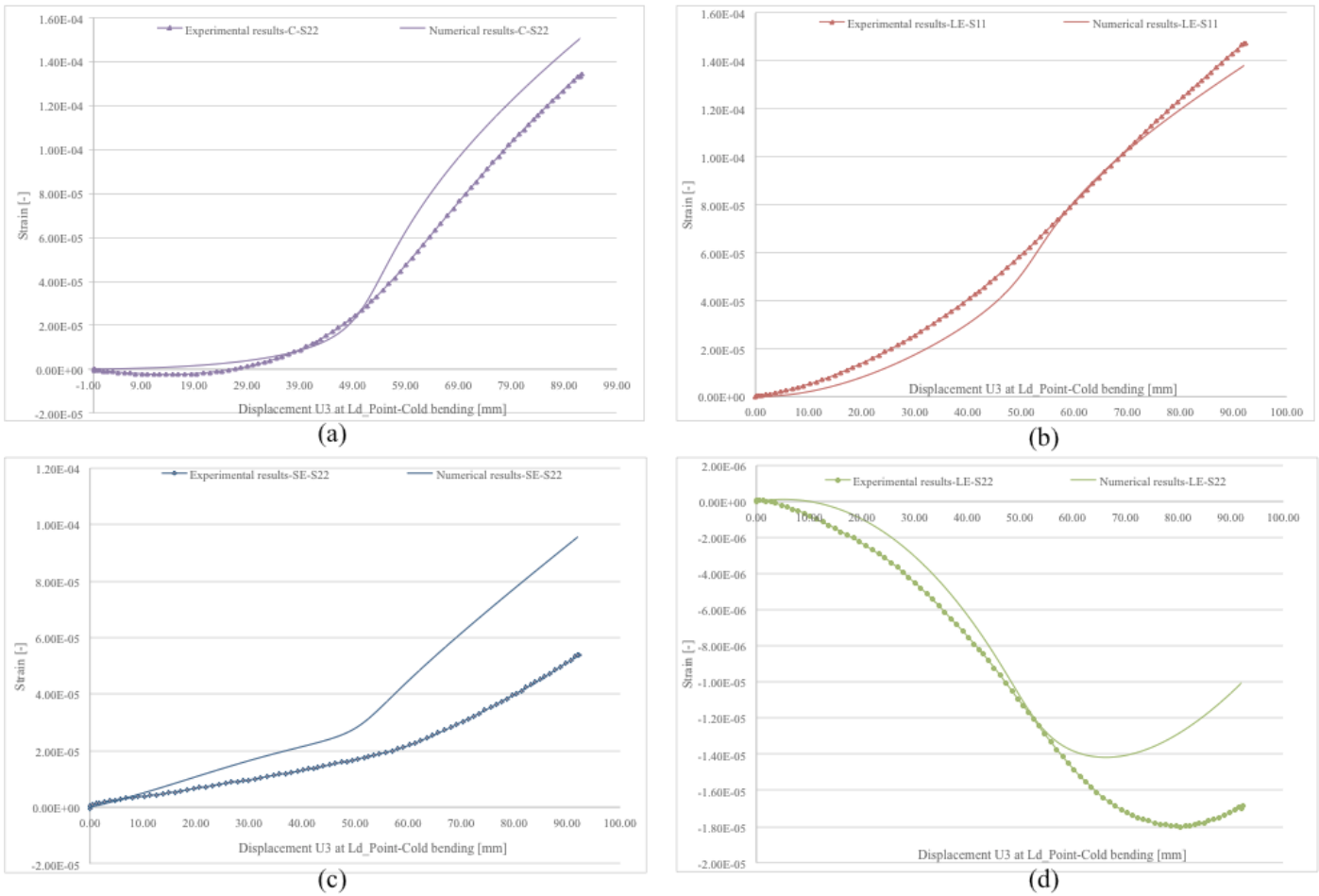

Chart 16 Strain built-up comparison on the panel; (a) C-S22 (b) LE-S11 (c) SE-S22 (d) LE-S22

Concerning the strain "around the support" (Chart 17), the curved are well correlated for (c) and (d). For (a) and (b) curves differ from the beginning of the shaping process. Moreover, the instability increases lightly this difference between the numerical and the experimental model. Hence strain around the support is less influenced by the instability.
The instability seems to relieve the rising of stress near in the concentrated peak.

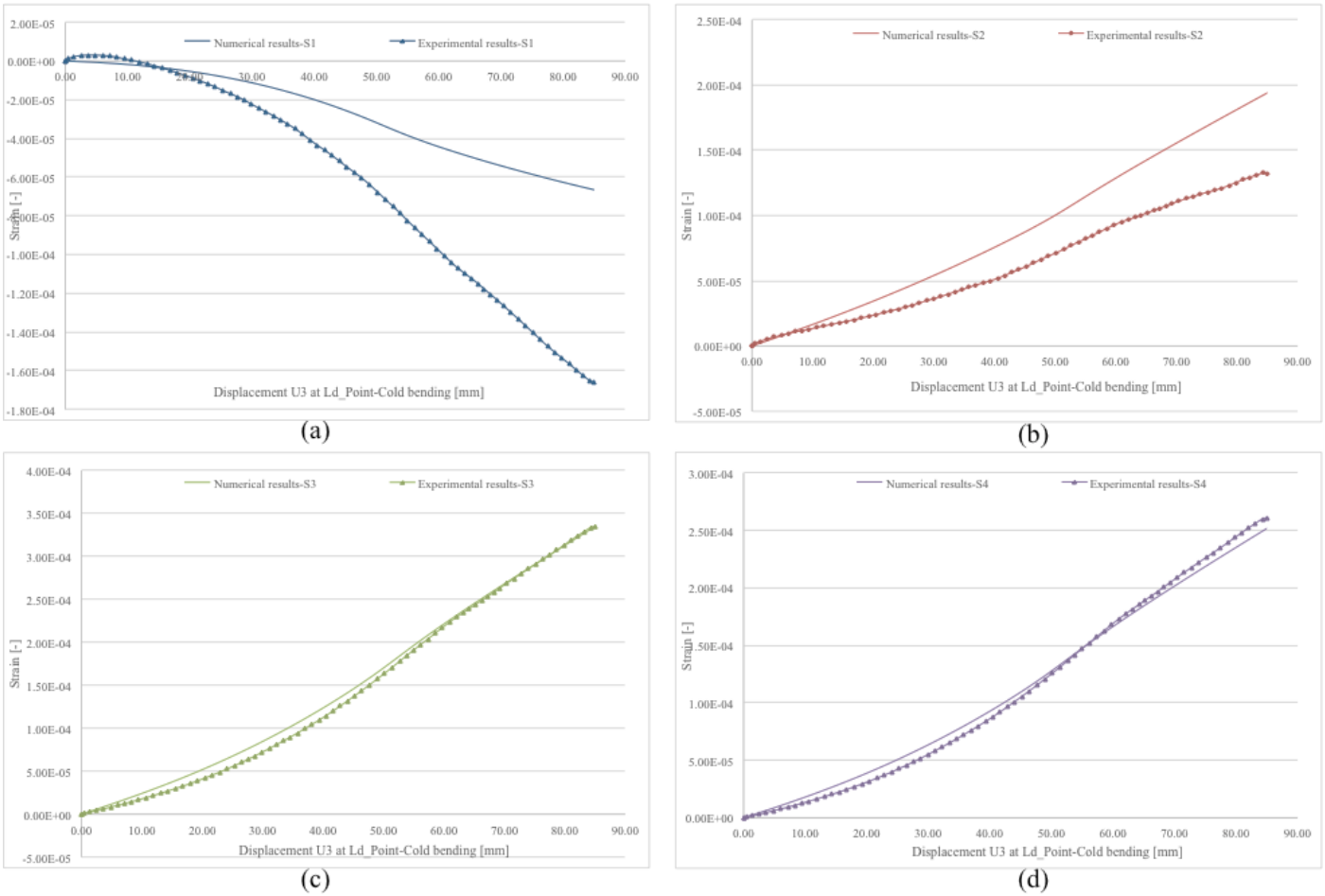

Chart 17 Strain built-up comparison around the critical support; (a) S1 (b) S2 (c) S3 (d) S4

In conclusion numerical model gives accurate results particularly where there are stress concentration. Even if the numerical model increases the effect of the instability, one can observed that its results converge, globally, to the experimental test. From that, the numerical model can be validates.

2.4.3. Precurved comparison

The results have shown that the numerical model was giving more protective results. However, the comparison, between both numerical and experimental results, has proved that the radius of curvature of the forced diagonal can characterize the instability of a cold-warped panel.

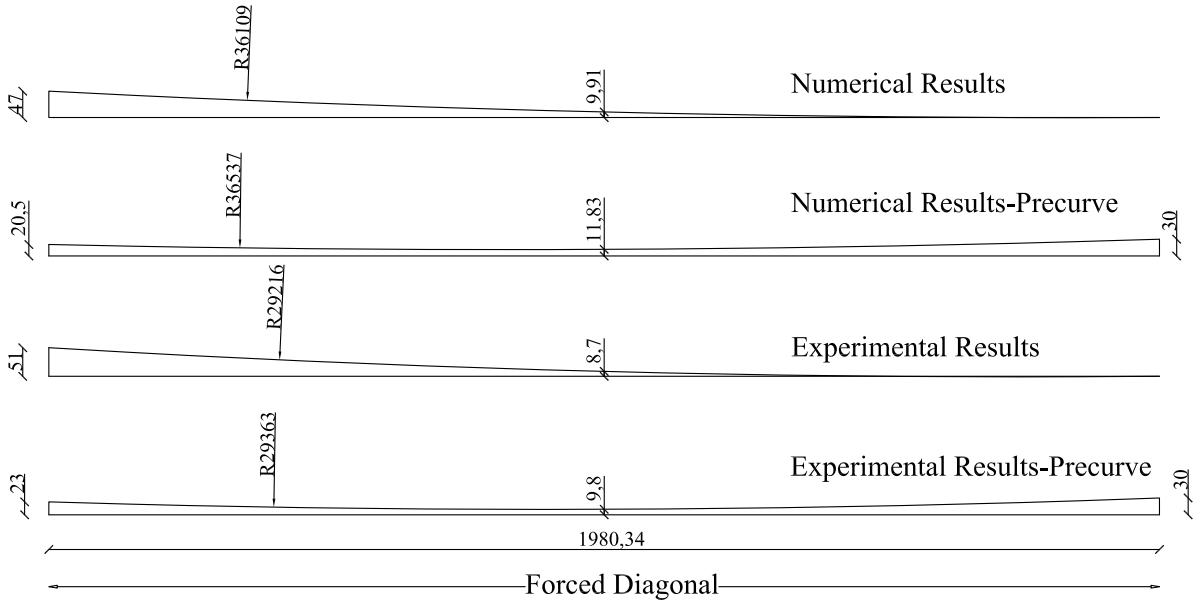

Figure 51 Curvature radius comparison for a 4x1'000x2'000

Indeed for each type of analysis the funded radius of curvature between the classical case and precurved one are almost equal.

3. Cold-warping of a Curtain Wall Element

The instability of the point-supported panel transforms straight edges (for small displacement) into curved one. So that, one may wonder if the stiffening of the edges would increase the stability range, delay the instability phenomenon or decrease the ripples amplitude.

In this part the cold-warping of a specific curtain wall panel is investigated. The plate is in the vertical position, as it would be for a cold warp façade. Silicone joints connect the frame to the glass, so that the whole unitized cell can be twisted by the imposed displacement at the Ld_Point corners.

Tests are performed on monolithic glass that's why the speed loading is not considered. The viscoelastic behaviour of the resin and the silicone is not taken into account.

3.1. Specimens definitions

3.1.1. Panel description

The experimental work is done on a 4 x 1'000 x 2'000 [mm] panel, such as the cold-warping of the point-supported panel.
For this experiment the FTG panel is used. Indeed there are no stress concentrations due to the punctual support and the risk of the failure of the panel due to the scratches is minimum.

3.1.2. Support description

The panel is linearly supported along its edge by an aluminium frame. The aluminium is a tubular rectangular profile 40x80[mm], 4[mm] thick.
A 6.4[mm] thick silicone joint is used in between the frame and the glass. The silicone used is a SIKASIL SG-500 bi-component (E=1[MPa] and ν=0.5).

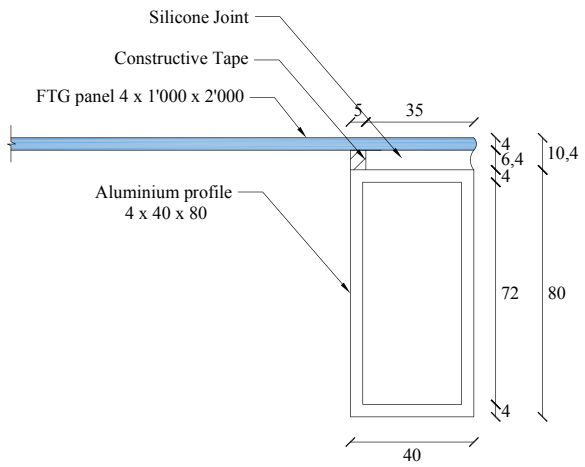

Figure 52 Glass to frame detail

The corner of the frame is rigid, an inside angle bracket is slip inside the tubular profile. Moreover, an aluminium plate is used in order to use the same test setup as for the point-supported panel.

Numerical model with pinned connection of the frame have been executed. Reaction forces and global stress were decrease compare to the rigid frame. Nonetheless pinned frame seems to be hardly realizable by the industry and as the rigid frame gives critical values, only “rigid” curtain have been tested (experimentally and numerically).

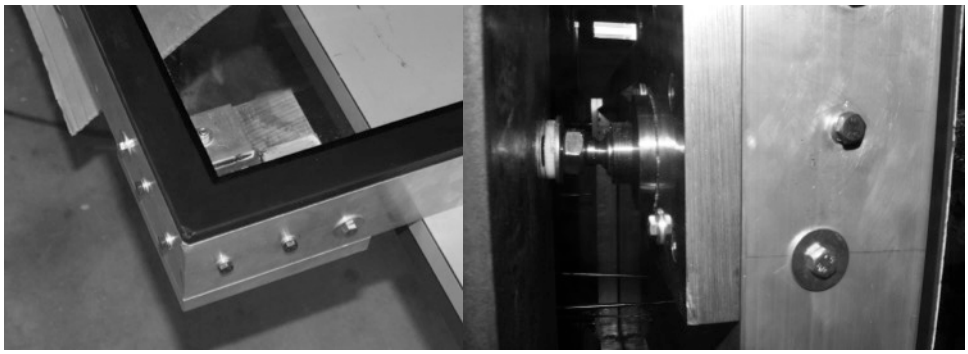

Figure 53 Reinforced corner of the curtain wall and fixing condition

The same circular plates are glued (epoxy resin DP490) to the aluminium plate, at each supported corner.

3.1.3. Boundary conditions

The fixing system is the same as the one used for the point-supported panel. Hence the boundary conditions used are exactly the same, see §2.1.3.

3.2. Numerical modelling

The finite element analysis was performed with Abaqus/CAE 6.12-3 software.

Results of the modelling will be the basis of the experimental test expectation (stress variation, displacement, reaction forces…).

The analysis type of the modelling is a geometrically non-linear one for the same reason as the point-supported panel.

The viscoelastic behaviour of the epoxy resin and the silicone and the plastic behaviour of the stainless steel support are not taken into account on this study; only the elastic behaviour is used.

3.2.1. Model

The model is divided into three main types of elements. To decrease the computational time some considerations have been done. In particular, beam elements are used for the frame modelling and spring elements for the silicone

3.2.1.1. Global Model

The complexity of the model is bigger than for the point-supported panel, therefore, the computational time is bigger. That's the reason why some simplifications have been done.

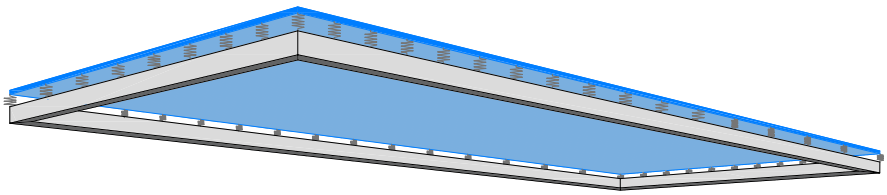

Figure 54 Curtain wall element.

The silicone joint is approximate by spring. An equivalent rigidity is given to the spring.

$$K_Z = \frac{E * A}{L}$$

$$K_X = K_Y = \frac{G * A}{L}$$

With: -L the thickness of the silicone joint
-E the E-modulus of the silicone joint

The tubular frame is approximate by beam element. The connection between each beam is rigid. Moreover, the influence of the aluminium plate is approximate thanks to the multipoint constraint. The master point is centre of gravity of the joint ball and the slave points are the beam's end.

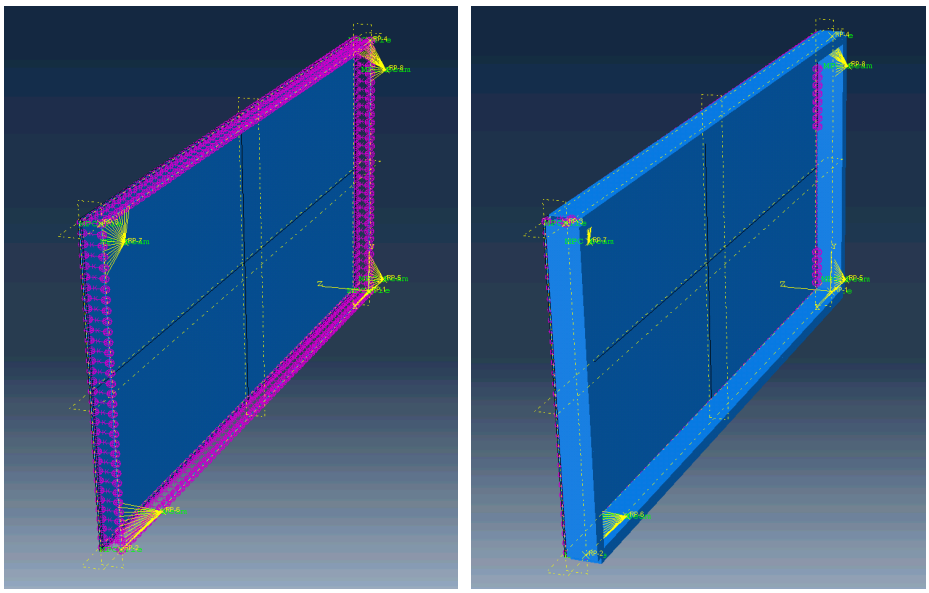

Figure 55 Modelling of the Curtain Wall, without rendering (left) with beam rendering (right)

3.2.1.2. Element types

Glass panel modelling

Shell (S4R) and solid (C3D20R) elements have been used for the modelling of the curtain wall. However, the continuous frame support gives rise to shear forces and twisting moment. The distinction between shear forces and twisting moment can be only maintained in higher-order plate theories accounting for shear deformation [8]. It's then no surprising that the use of shell elements give inappropriate results Appendix VII.
Thus, C3D20R elements are used for the modelling of the plate.

Frame modelling

To decrease the computational time beam elements (B33: A 2-node cubic beam in space) have been used. This element is an Euler-Bernoulli beam, which are only used to model slender beams [2].

Silicone modelling

The silicone viscoelasticity is not takes into account. Hence the modelling of the joint can approximate with springs along the edges. SPRING2 have been used, they are acting between two nodes [2].

In conclusion, apart the glass modelling, the computational is well decrease by the use of special purpose elements. The model is simplified to it's possible but the viscoelasticity cannot be investigated with this elements.

3.2.1.3. Mesh

A structured mesh of 16 [mm] has been provided to the glass panel. A light refinement has been done between the spring line and the edge.

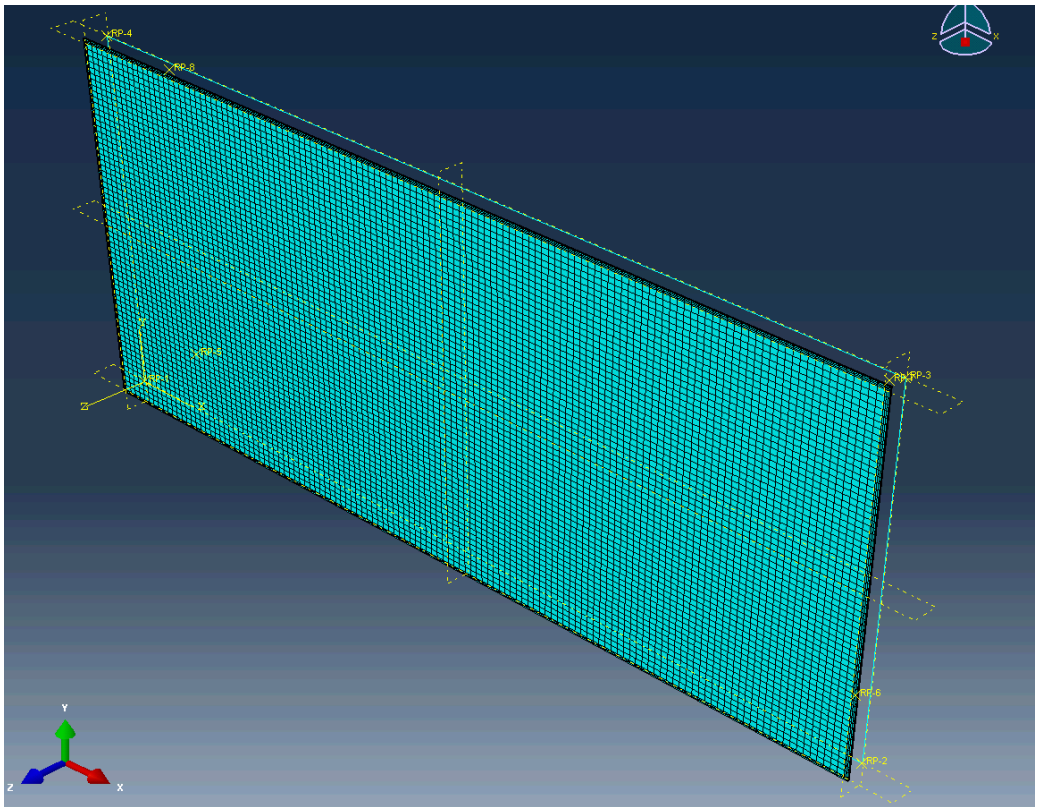

Figure 56 Mesh of the Curtain Wall

As there are no stress peaks due to the linear support. The mesh is assumed to be fine enough to provide accurate results.

3.2.1.4. Applied load and displacement

The same conditions as in 2.2.3.4 are used in order to help the model to converge.

3.2.2. Results of the numerical model

The same terminology as for the point-supported panel (Figure 17) is used.

3.2.2.1. Out-of-plane deformation

An instability is observed in Chart 18.The same slope as for the point-supported panel is reported until the instability occurs. The instability is less brutal than for the point-supported panel and the global stability is higher.

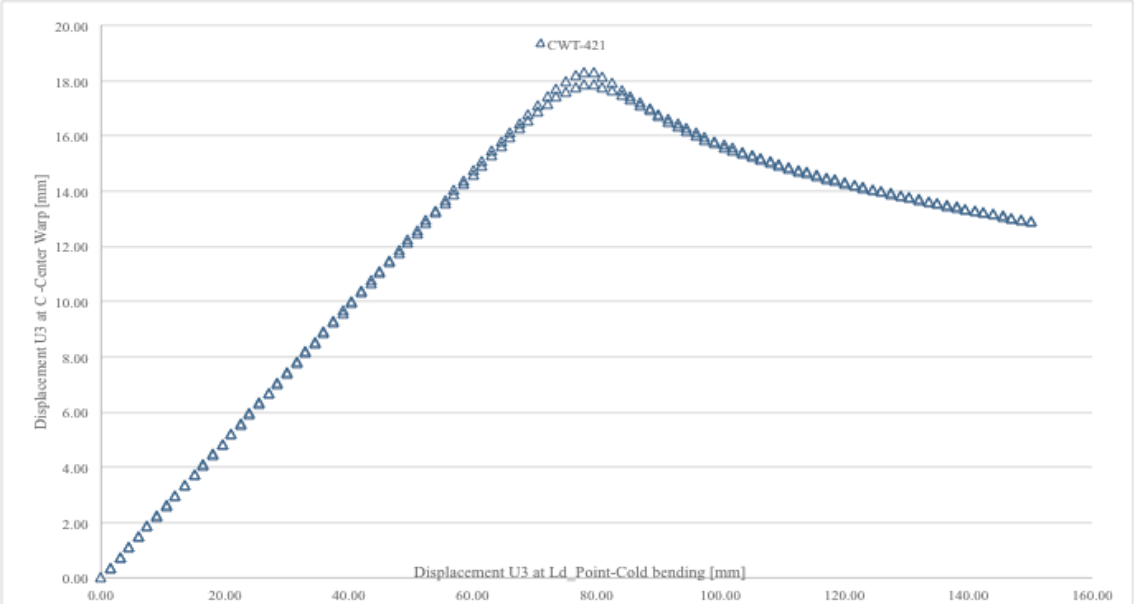

Chart 18 Displacement of the centre of the plate in relation with the imposed displacement

The instability phenomena act as curvature enhancer for the forced diagonal. However, the curvature is less severe than for the point-supported panel.

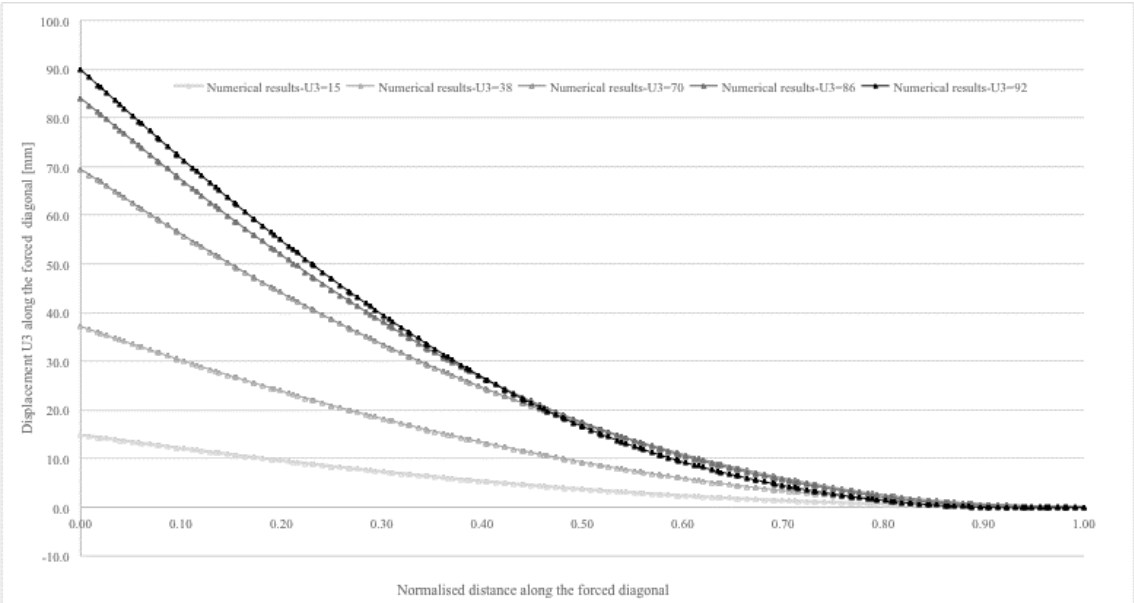

Chart 19 Displacement U3 along the forced diagonal during the shaping process

The instability acts as curvature inhibitor for the supported diagonal. The supported diagonal reach a ceiling and then decrease. Nonetheless the shape of the supported

diagonal becomes altered. In the case of curtain wall there are ripples only for very high δ, thus there is no need to investigate them further since the stress would be too high for the glass.

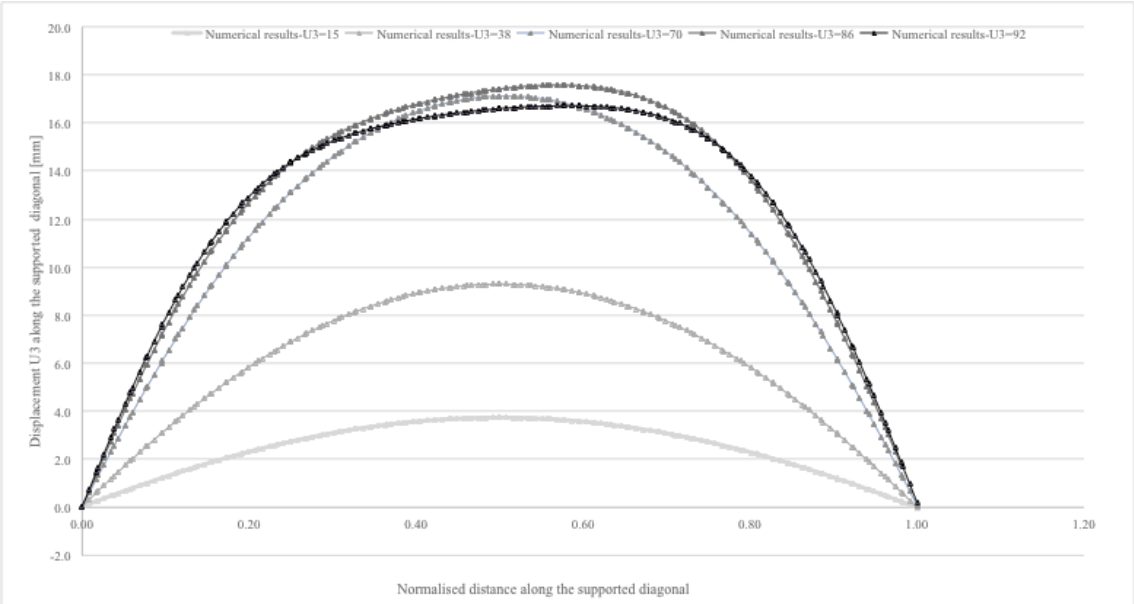

Chart 20 Displacement U3 along the supported diagonal during the shaping process

The frame has a stabilizing effect on the edges. Thus, they remain almost straight during all the shaping process. However, the instability is not avoided.

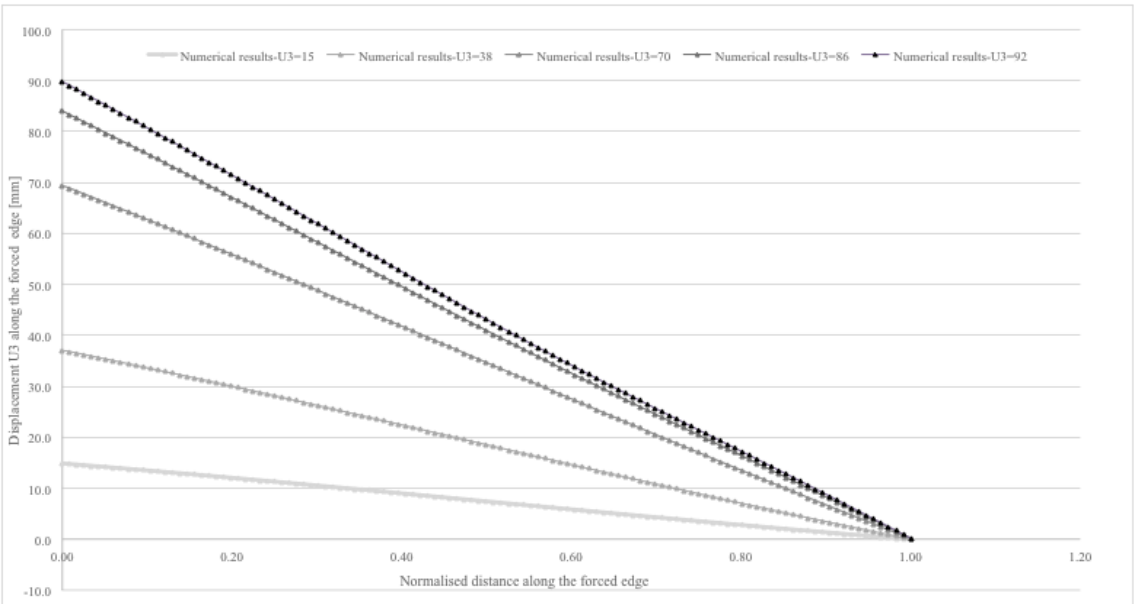

Chart 21 Displacement U3 along the forced long edge during the shaping process

Finally the frame acts as stability enhancer. The instability is not avoided but comes for a bigger δ. The effects of the instability are the same as for the point-supported panel (see Figure 57).

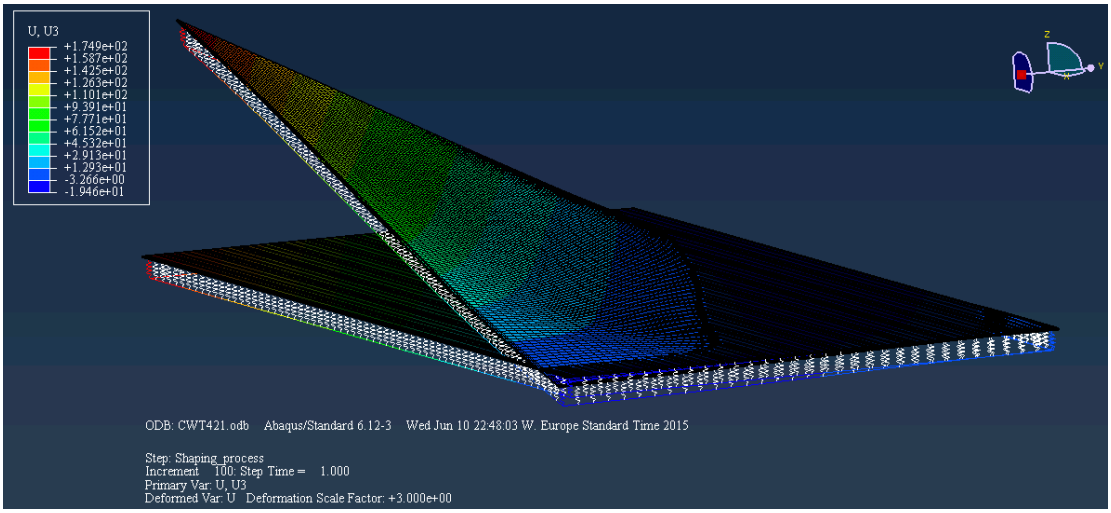

Figure 57 Global deformations U3 for δ=150[mm]

3.2.2.2. Stress built-up

As for the point-supported panel, the stress build-up on the glass is also investigated.

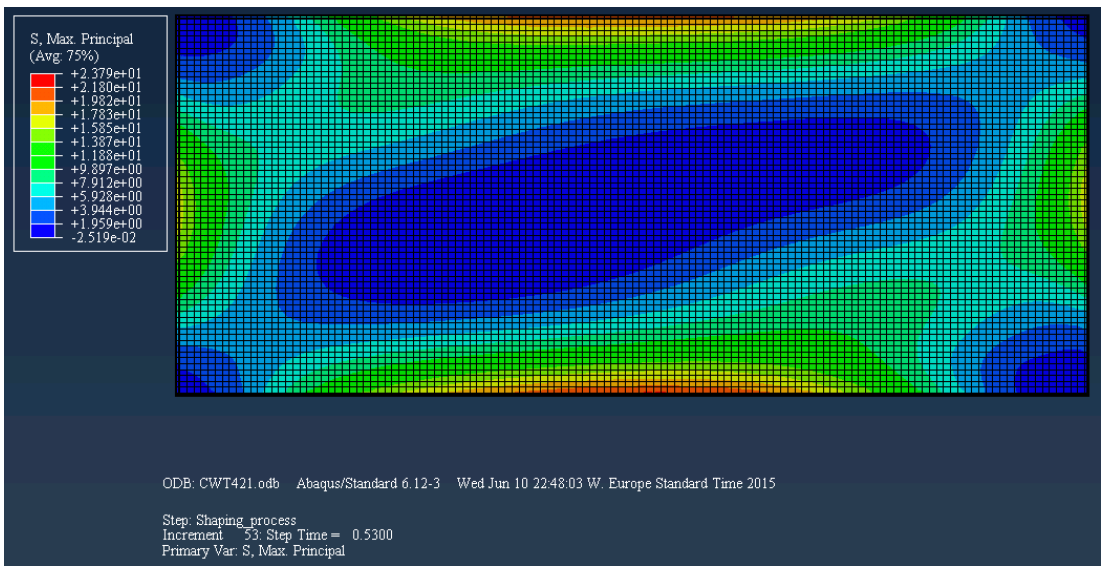

Figure 58 Maximum principal stresses before the instability (front view, δ=80[mm])

The frame-support makes the stress distributed along it, thus there are no peak stress. The design maximum stresses are thus smaller than for the point-supported panel. The intrados (inside) part of the panel is under compression or small tension. Only the borders are under tension stresses.

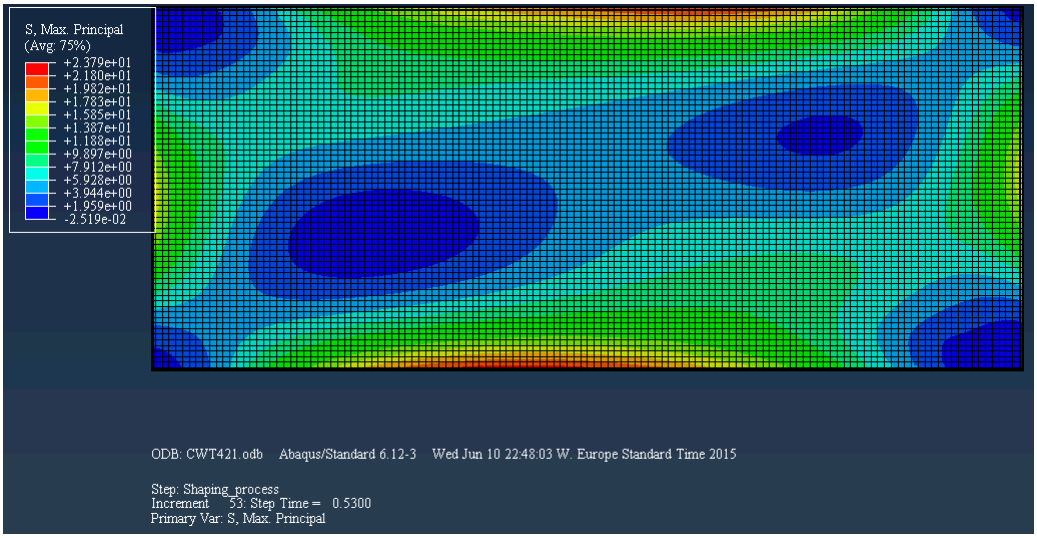

Figure 59 Maximum principal stresses before the instability (behind view, δ=80[mm])

The stress pattern at the intrados and the extrados are almost the same. Along the forced diagonal (at the extrados) some tensions stresses are observed, this due to the bigger curvature of the forced diagonal. The maximum stresses are localised for each side of the panel at the borders.

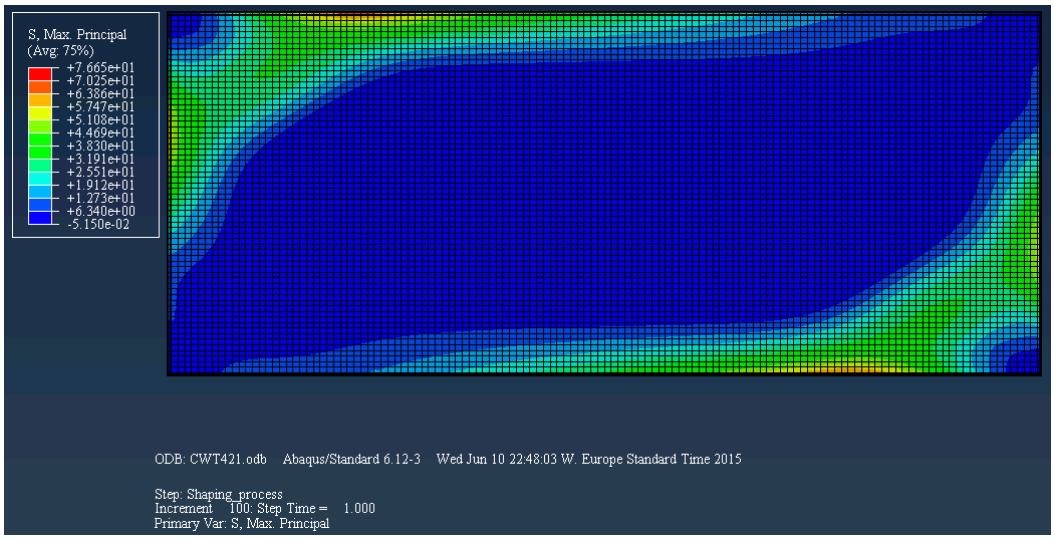

Figure 60 Maximum principal stresses after the instability (front view, δ=150[mm])

After the instability an in-plane compressive membrane is formed along the supported diagonal (at the intrados). The maximum stress becomes more localized along the border near the corners of the forced diagonal.

The extrados of the panel is under a tensile membrane at the centre of the plate. The stress concentration is along the borders near the corners of the supported diagonal this time (Figure 60).

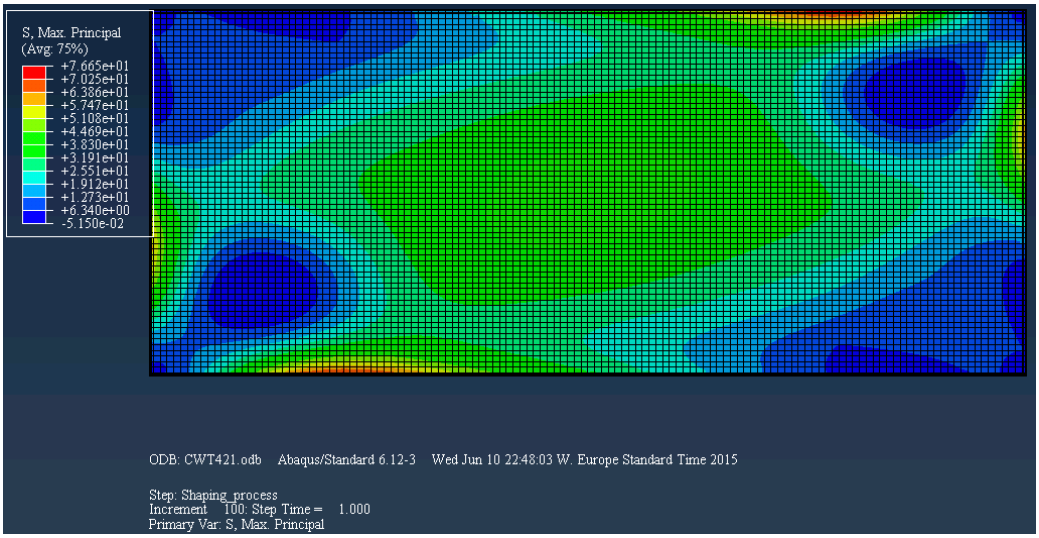

Figure 61 Maximum principal stresses after the instability (behind view, δ=150[mm])

In conclusion the geometry after the instability changes and the stress state changes with it. Some stresses concentrations are then reported. The level of stresses stay lower than for the point supported as there is no peak concentration.

3.3. Experimental test

Experimental tests are performed to validate the simplified model.

3.3.1. Test setup preparation

The test setup used is the same as for the point-supported panel. A bigger bolt (M16) has been used in order to carry the larger reaction forces.

3.3.2. Support conditions

The curtain wall panel has been adapted in order to have the same support condition as for the point-supported distance. A 20[mm] aluminium plate has been fixed at each corner in order to glue the circular plate to it. Due to the larger reaction forces (implies by the aluminium frame) the DP490 has been used.

3.3.3. LVDT setting up

The same LVDT setup has been used for curtain wall panel. Some LVDT have been removed (FD-1, FD-2, FE-1 and FE-3). The others LVDT have been maintained.

3.3.4. Strain gauges setting up

Two strain gauges have been used. Both are disposed at the inside of the panel. One gauge is installed at the centre (C-S22) to catch the change in stress. The other is placed where the concentrated stress is maximum.

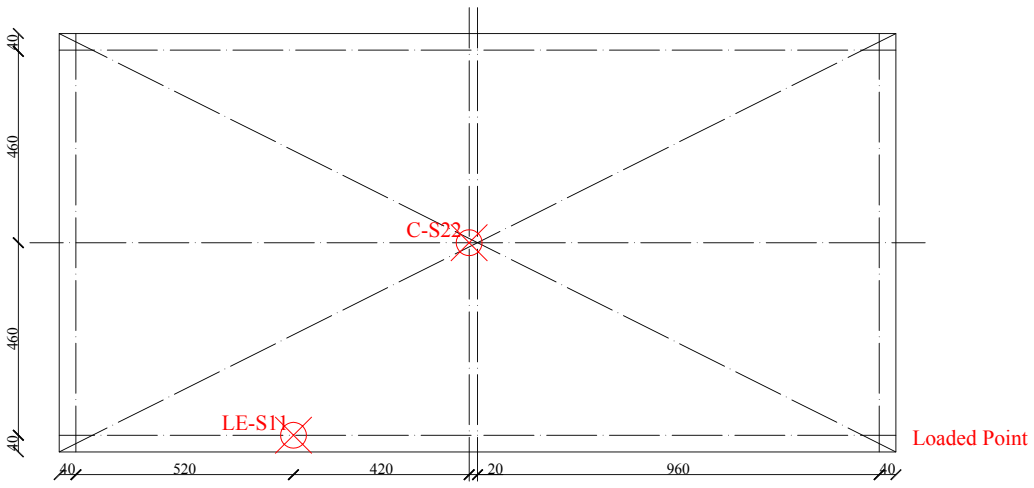

Figure 62 Strain gauges plan for the curtain wall

3.3.5. Digital image correlation system setting up

The same “moucheti” as the point-supported panel has been used, see Figure 44.

3.3.6. Cold-Bending test

The cold-warping of the curtain wall has been done without external pressure. However, any instability has been reported during the shaping process.

Figure 63 Global deformation of the curtain wall during the shaping process

Each edge stay straight and there is no instability, but the supported diagonal seems to be under tension (like a belt around the forced diagonal). Therefore, it's clear that numerical results and experimental results will give different values. One can directly compare both results to understand the source of the problem.

3.4. Numerical and experimental comparison

A first comparison between the numerical modelling and the experimental is done to calibrate model. Both displacement and strain are compared. Contrary to the point-supported panel, the forces of the LVDT's springs are negligible. Therefore, they can be use.

3.4.1. Out-of-plane deformation comparison

The instability phenomena have been observed for the numerical model but experimental results differ. Hence the comparison is fundamental to understand the differences.

Displacement at C in relation with the applied displacement on Ld_Point

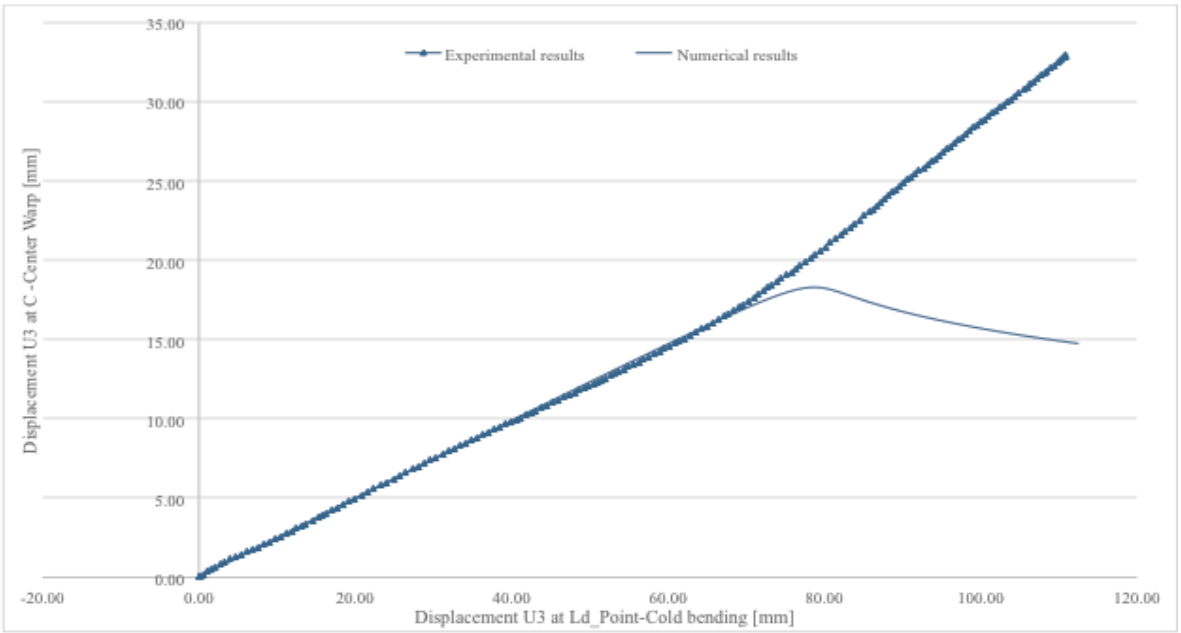

Chart 22 Comparison of the displacement of the centre C in relation with the applied displacement on Ld_Point

The comparison is pretty clear from that point of view. Indeed, it seems that instability occurs for each model for approximately the same δ (81[mm] for the numerical results and 71[mm] for the experimental one).
However, the instability occurs in an opposite direction for each test. The experimental case is then close to the behaviour of the aluminium plate §2.3.6.1.

The slope of the curve before the buckling point is exactly the same. Thus, the problem didn't come from the boundary condition.

Out-of-plane displacements U3 during the shaping process

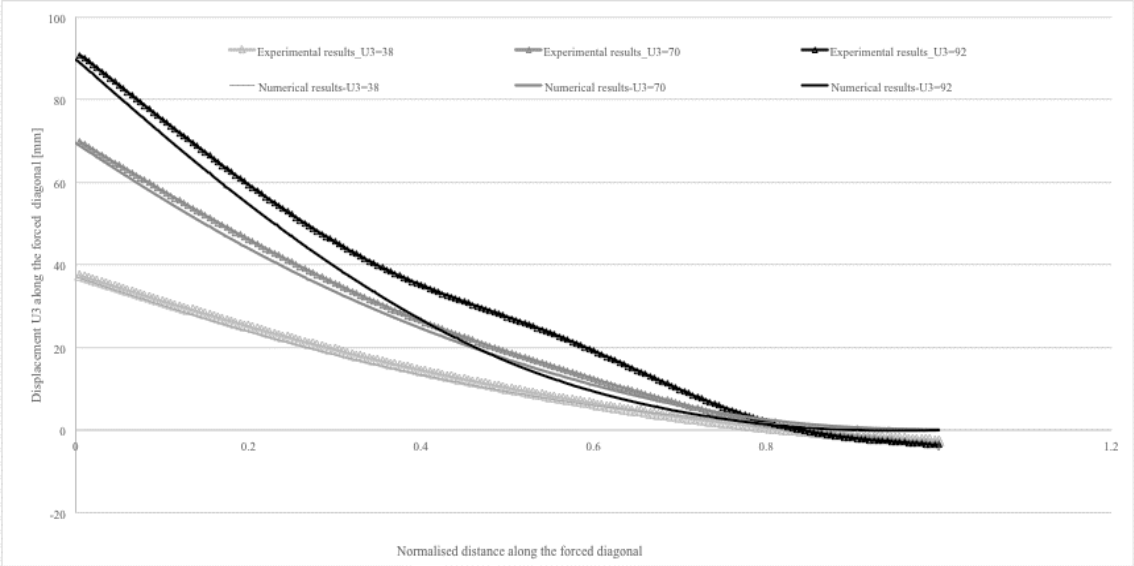

Chart 23 Out-of-plane displacements U3 along the forced diagonal during the shaping process

Before the instability, the displacements U3 along the forced diagonal are almost the same. The difference is lower than 5%. However, after the instability, the forced diagonal of the numerical model developed a severe curvature whereas for the experimental test the forced diagonal pops up. A quasi-straight line is developed in the centre of the diagonal. That's the "Belt-Effect" of the supported diagonal.

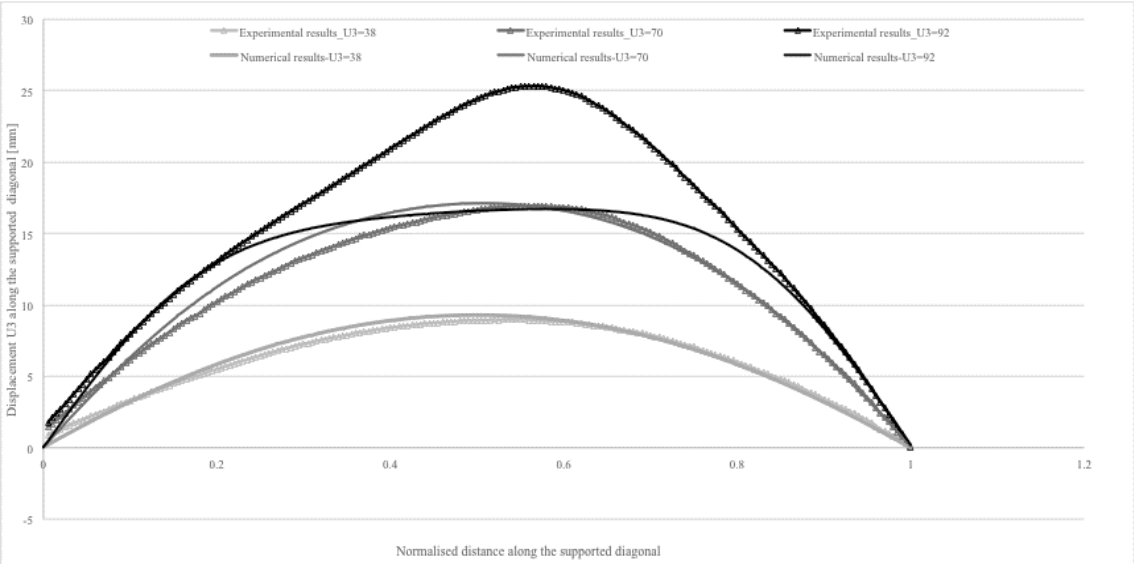

Chart 24 Out-of-plane displacements U3 along the supported diagonal during the shaping process

The "Belt-Effect" is also visible there; indeed one can observe that the shape of the supported diagonal after the buckling is completely pulled up by the forced diagonal.

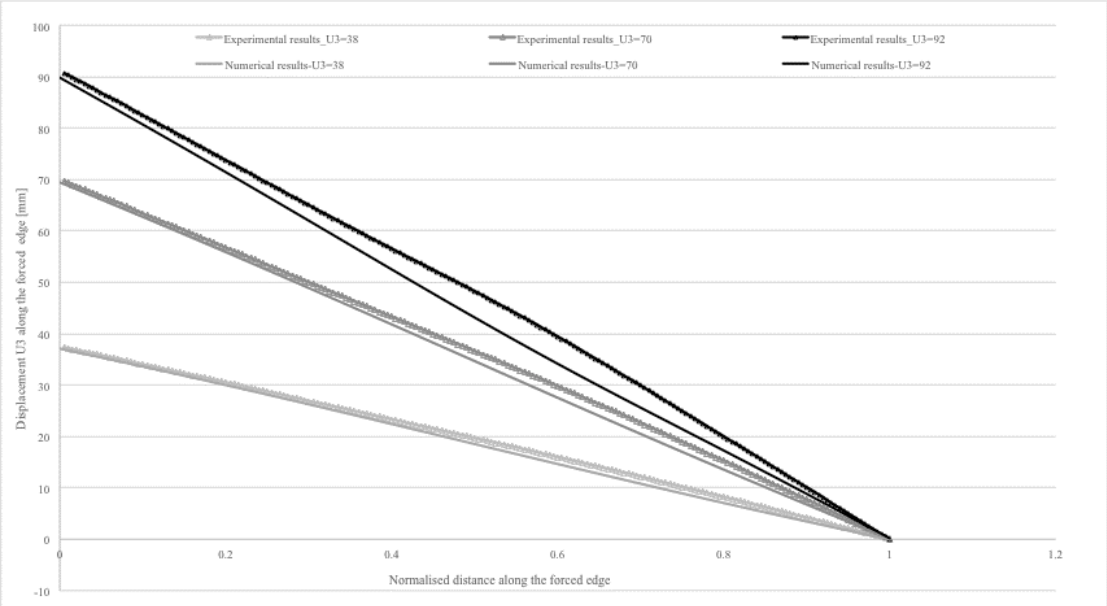

Chart 25 Out-of-plane displacements U3 along the forced long edge during the shaping process

The displacement along the forced edge shows that a light curvature is developed at the edge along the shaping process. This is not occurring in the numerical model. That developed curvature might help the glass to not buckle as expected.

3.4.2. Strain built-up comparison

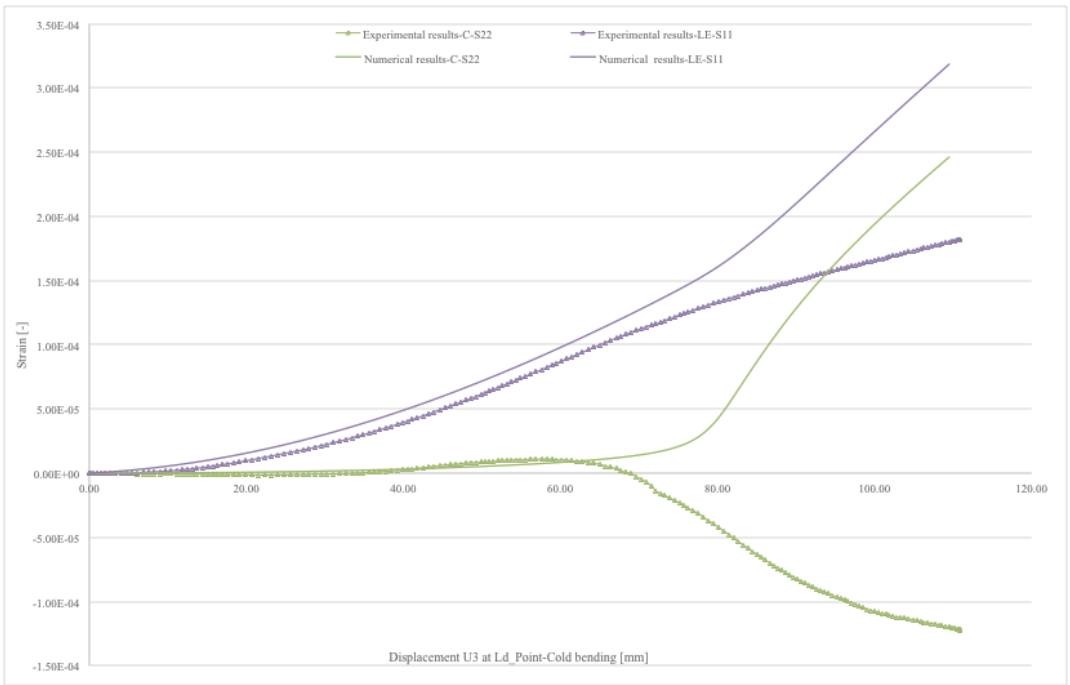

Chart 26 Strain built-up comparison for the curtain wall

Before the instability the curved are very close. Once the instability point is reach the curved diverge totally. Indeed, the instability acts as a stress enhancer for the

numerical model, the stress “Jump-Out” suddenly (that’s the reason why the gauges have been localised at this position).
However, the experimental results diverge totally from the numeral one. Indeed, as the expected change in form is not happening. The stress in point C is not increasing. For the same reasons in LE the stress is decreasing to the compression.

In conclusion, both analyses give different behaviour. It’s seems that the difference is coming from the linear support of the glass.

3.5. Numerical model with an improve rigidity of the silicone

A new numerical model has been done to understand better the differences observed in 3.4. As there is a lot of unknown concerning the silicone rigidity (a safety factor of 5.6 is used by the manufacturer), a new model with a very high rigidity (comparable to the steel) of the silicone has been done.
This is an extreme case but the results might be interesting.

3.5.1. Out-of-plane deformation comparison

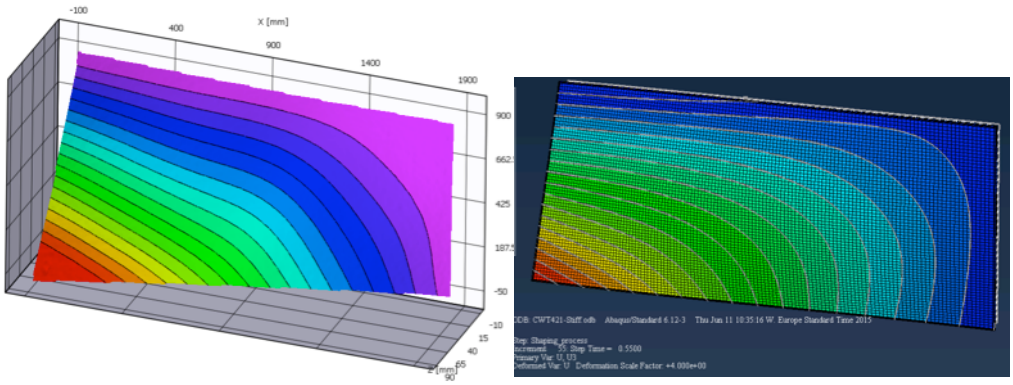

Figure 64 Deformation U3 pattern, experimental left, numerical right

Firstly it's interesting to observe the deformed shape of the cold-warped curtain wall.

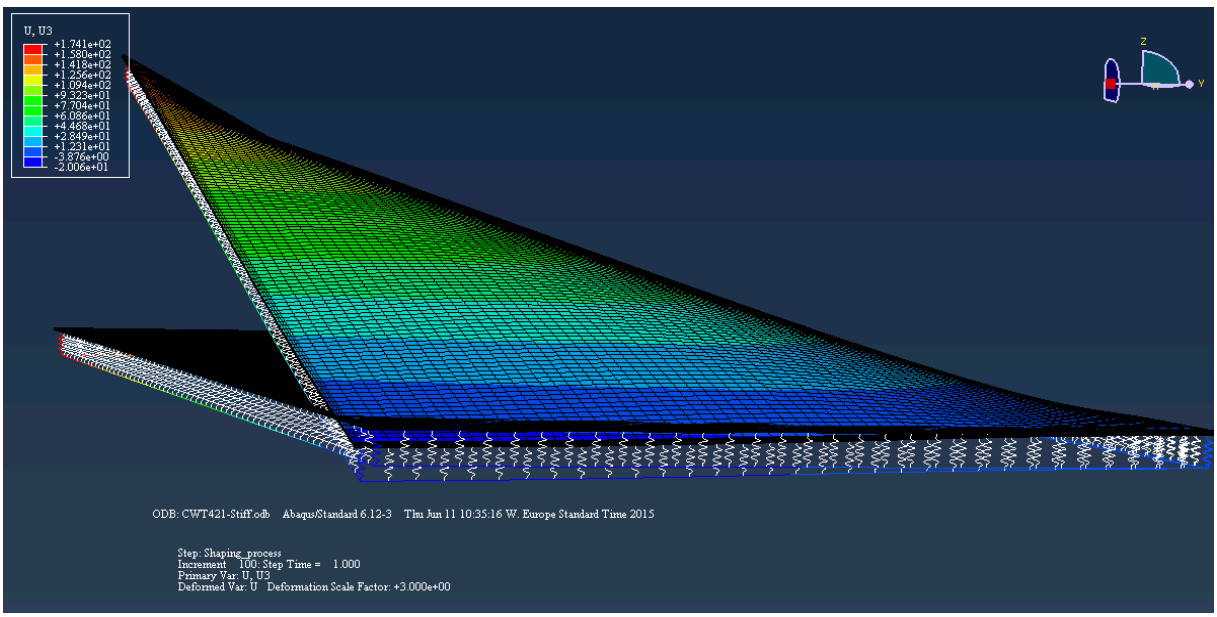

Chart 27 Deformation pattern with an enhanced rigidity of the silicone

The shape seems to be approximately the same as reported Figure 63. The "Belt-Effect" made by the supported diagonal on the forced one is clearly visible.

Displacement at C in relation with the applied displacement on Ld_Point

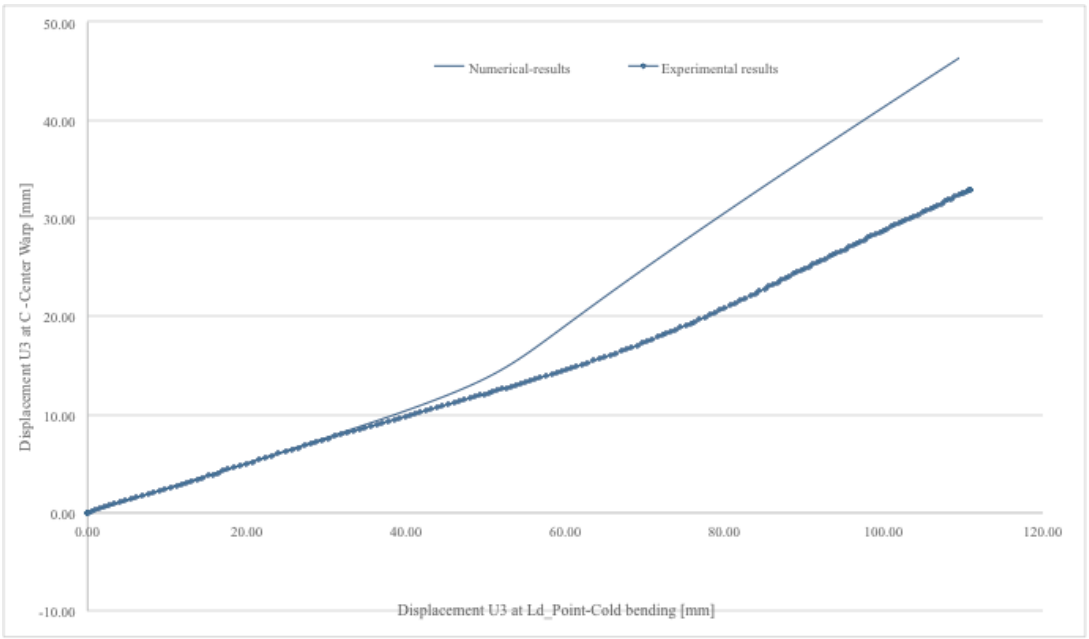

Chart 28 Comparison of the displacement of the centre C in relation with the applied displacement on Ld_Point

As expected by stiffening the edge the instability is going in the opposite direction. The instability of the numerical model comes sooner than for the experimental one. This is due to the bigger stiffness of the silicone. A convergence study of the silicone stiffness would be necessary to get the same results as the experimental test.

Out-of-plane displacements U3 during the shaping process

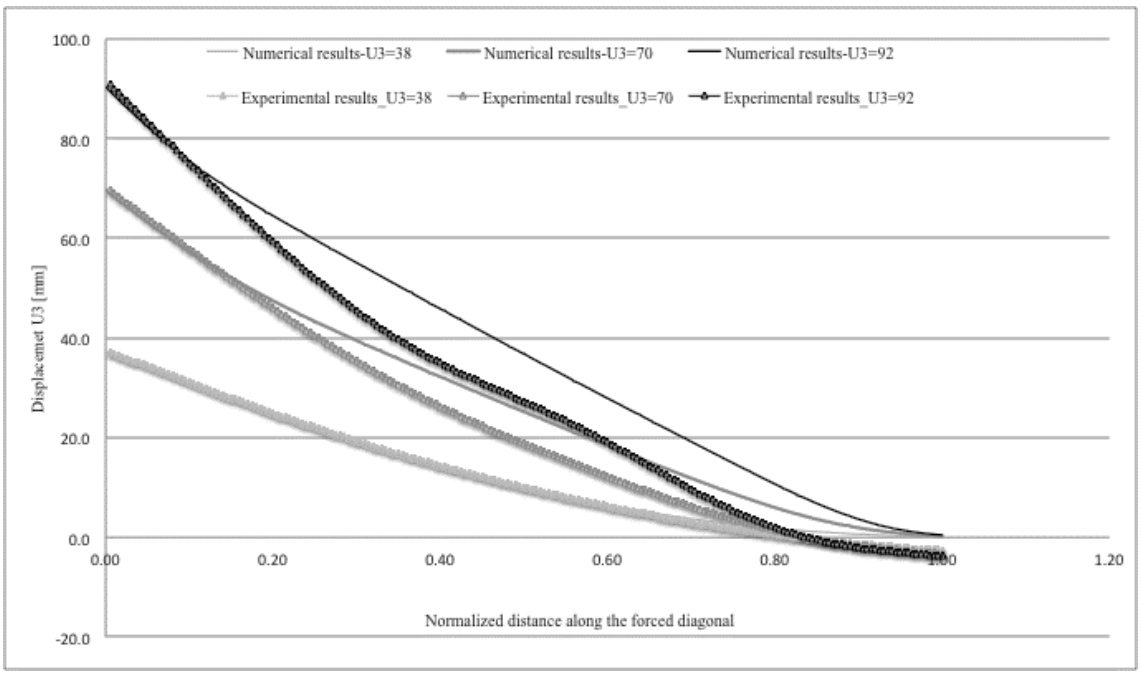

Chart 29 Out-of-plane displacements U3 along the forced diagonal during the shaping process

The displacement along the forced edge is different in magnitude. This is largely due to the fact that the instability become sooner for the experimental test. However, the same phenomenon is reported, at the centre of the forced diagonal a straight shape is observed (“Belt-Effect” made by the supported diagonal on the forced diagonal).

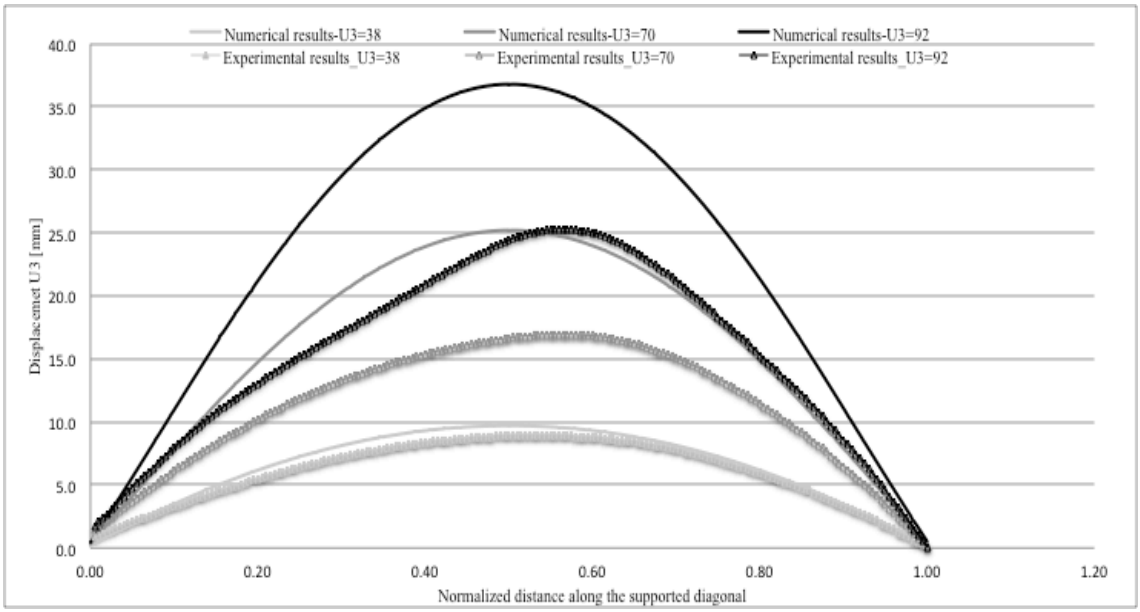

Chart 30 Out-of-plane displacements U3 along the supported diagonal during the shaping process

The experimental results give an asymmetric shape of the supported diagonal before and after the instability, which is not observed for the numerical one. This is probably due to the imperfection of the glass panel and/or to the different $\delta_{instability}$.

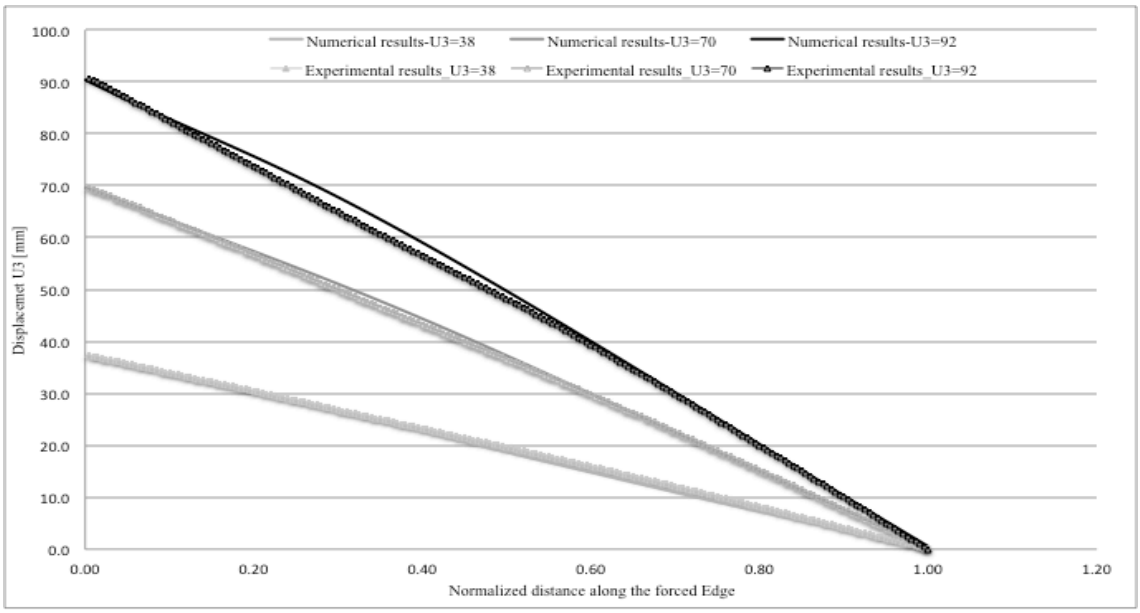

Chart 31 Out-of-plane displacements U3 along the forced long edge during the shaping process

As expected the borders after a certain displacement are not straight anymore with stiffer silicone rigidity. The displacements are really close during the whole shaping process.

3.5.2. Strain built-up comparison

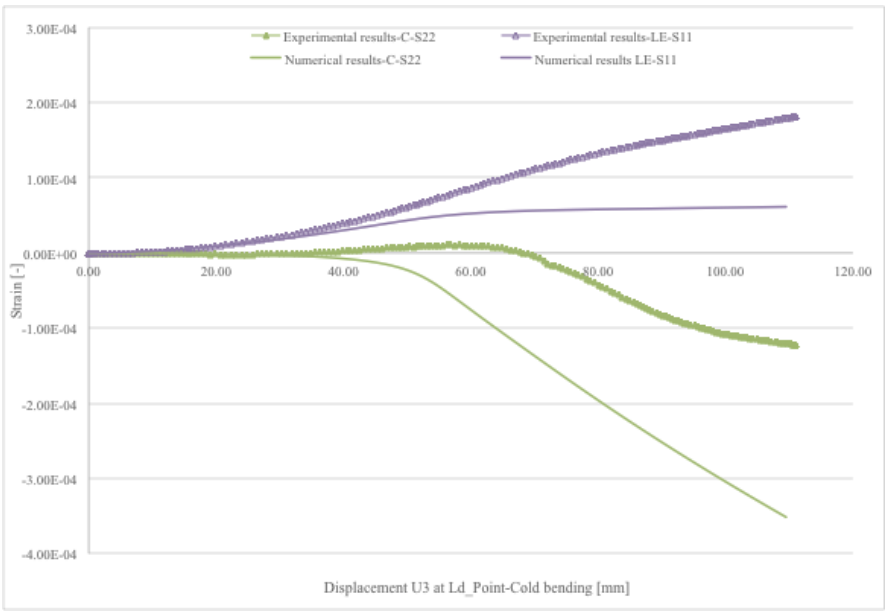

Chart 32 Strain built-up comparison for the curtain wall

The strain behaviour fit better with a higher rigidity of the silicone (due to the change in the instability direction). The shift of the curved is due to the different $\delta_{instability}$. However, the experimental stress at the centre (C-S22) seems to increase continuously whereas the numerical one seems to stabilize. The opposite things appear for LE-S11. This is probably due to the stiffness of the silicone and the way it is modelled in Abaqus.
The high rigidity of the spring induces localised peak concentration, which is not realistic. The borders of the panel have been removed from the plot.

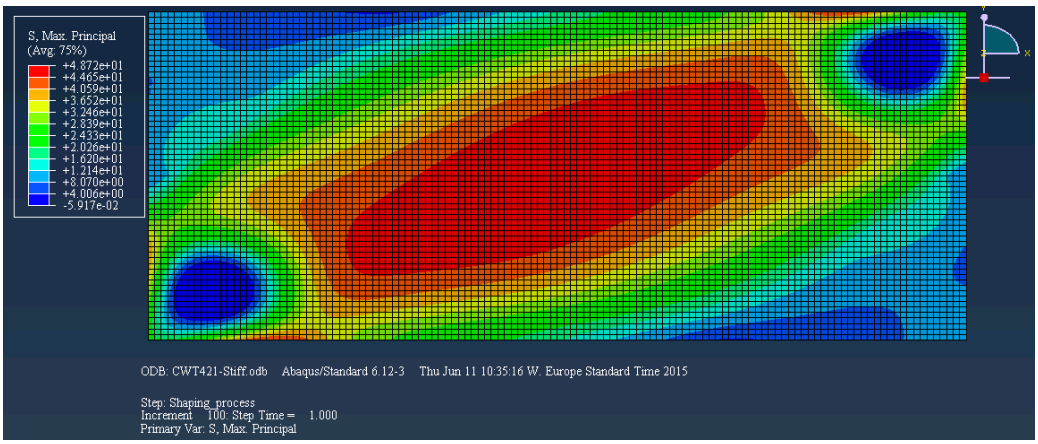

Figure 65 Stress pattern in the second instability's deformation pattern, (front view, δ=150[mm])

The whole stress pattern is completely different as expected before. However, as before the instability point, there are some stresses concentrations near the edges, but it's important to highlight the severe tensile membrane along the forced diagonal. The maximum stress is lower than in Figure 61; it's due to the fact that the borders aren't taken into account here.

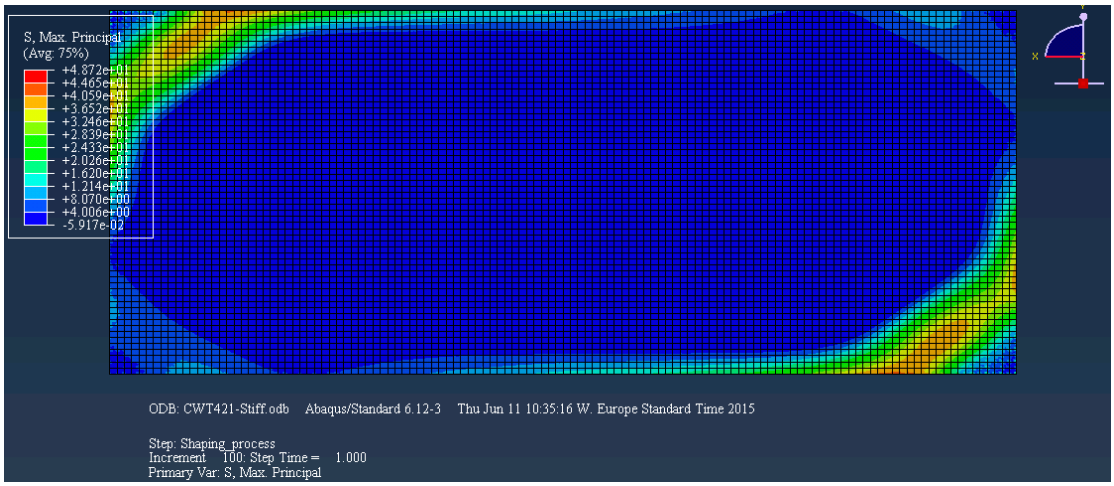

Figure 66 Stress pattern in the second instability's deformation pattern, (from behind, δ=150[mm])

At the inside of the panel the maximum stresses are not anymore at the same expected place. The position of LE-S11 seems therefore inappropriate. The whole stress pattern has change.

Stress inside the silicone

The different rigidity of the silicone has shown a high difference of solicitation.

With the first rigidity of the silicone the stress in the Z-direction was varying between -0.04 and +0.02 [MPa]. With a higher rigidity the stress was multiply by 100.
With the first rigidity of the silicone the stress in the X, Y-direction was varying between -0.1 and +0.1 [MPa]. With a higher rigidity the stress was multiply by 1'000.

Thus, it seems that in-plane rigidity of the silicone have a huge impact on the deformation pattern after the buckling. It would be interesting to measure the stress, which is actually acting on the silicone joint during the shaping process.

Reaction forces

Any differences concerning the reaction forces RF3 are reported for both models. Therefore, the global rigidity of the panel is the same for both kind of instability.

4. Numerical investigations of four point-supported panels

4.1. Parameter study of the panel size and thickness

The parameter study is focus on rectangular panel. They are the most commonly used by the industry. The parameter study is possible since the numerical model gives protective values of the behaviour during the Cold-Bending

4.1.1. Specimens definitions

A total of six different sizes of panel have been tested (size in [mm]):

- Three rectangular panels: 1’000x2’000, 1’500x3’000 and 1’500x4’500.
- Three square panels: 1’000 x1’000, 1’500x1’500 and 2’500x2’500

The ratio $\frac{L}{B}$ is then varying from 1 to 3. The panel sizes are realistic one and would constitute a good basis for a preliminary design of cold-warped panels.

For each panel size the effect of the thickness is investigated. Thus, seven different thicknesses are used (i.e. 4, 8, 12, 15, 19, 25 and 33). Up to 25 [mm] the thickness can be done in the manufactory or obtained by an effective thickness of laminated glass. The thickness of 33[mm] constitute the upper bound of the study, this thickness can be achieved by the lamination of five, 12 [mm] thick, glass panel.

4.1.2. Model definition and output request

Shell element model have been used. According to Appendix II and Appendix III, the modelling with shell elements plus MPC constraint (to model the support) gives an appropriate good protective result.
Indeed, the deformation of the panel is unchanged from a complex modelling with solid element, and the stress converges to an upper bound value (which is totally appropriate).

The mesh is the chosen one from the mesh study (Appendix I). A python script has been used for the parametric study purpose. δ to the instability point, δ to Smax=50[MPa], δ to Smax=100[MPa] and δ to the ripple amplitude equal to 0.5 [mm] have been plotted.
Each of this value can be seen as a limit of the cold-warped. Depending of the architect choice if the buckle configuration is a limit or not (then the ripple amplitude are a limit or not). Depending on the glass type (HSG or FTG) and the solicitation for the stress.

The reaction forces have been monitored, since it's a critical point for the construction stage. Indeed the cold-warping takes sense if the workers can bend the panel directly on site and preferably without mechanical device (like hydraulic jack).

4.1.3. Results

4.1.3.1. Displacement δ to the instability

Table 1 Instability displacement U3 [mm] at Ld_Point

Thickness	L/B					
[mm]	1'000/1'000	1'500/1'500	2'500/2'500	2'000/1'000	3'000/1'500	4'500/1'500
4.00	33.00	38.00	41.00	48.00	46.00	26.00
8.00	66.00	82.00	92.00	100.00	110.00	120.00
12.00	99.00	123.00	144.00	150.00	174.00	210.00
15.00	120.00	153.00	180.00	189.00	216.00	270.00
19.00	152.00	192.00	230.00	234.00	276.00	362.50
25.00	194.00	250.00	302.00	302.00	362.00	480.00
33.00	250.00	322.50	397.50	387.50	470.00	640.00

The instability behaviour for the 4x1'500x4'500 panel is different. Indeed, the panel is too slender and then the global behaviour during the shaping process is different. In order to have consistent results, this case has not been considered.

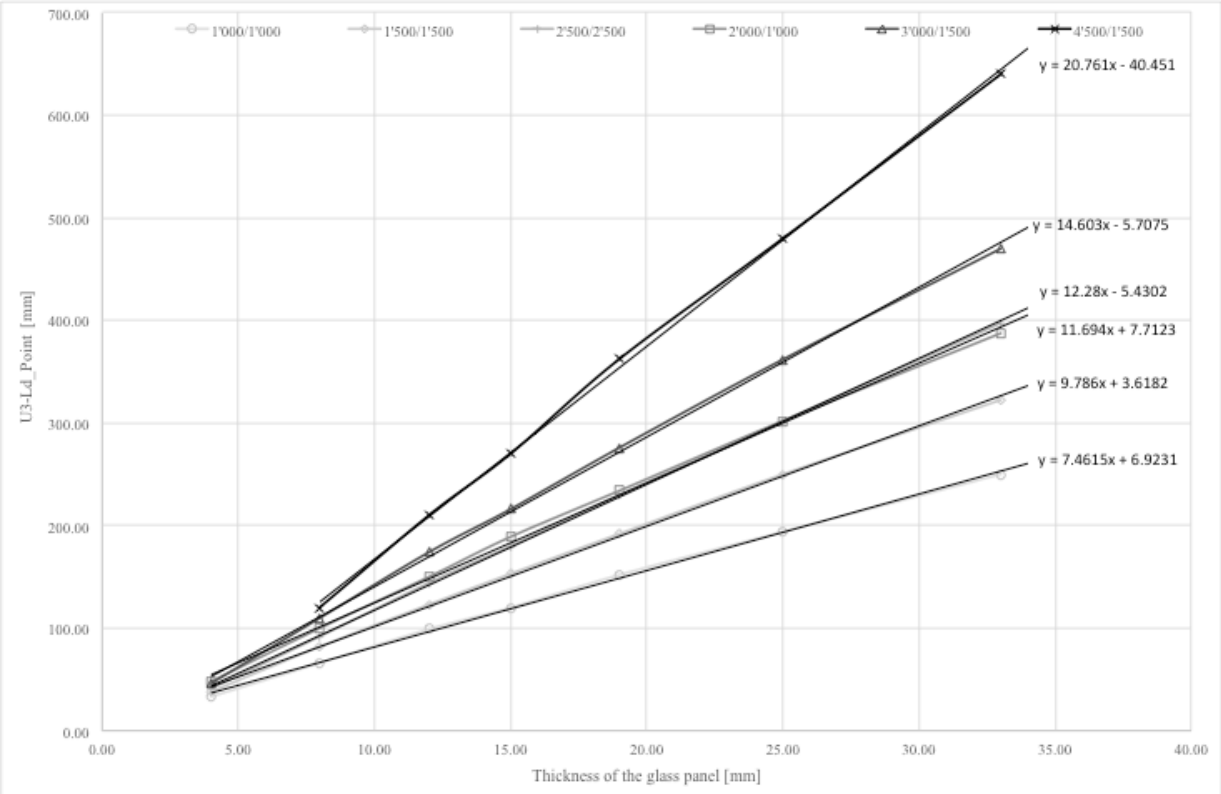

Chart 33 δ at Ld-Point to the instability in relation with the thickness of the panel

From that one can observed that:

-The thicker is the panel the larger is δ to get the instability

-The longer is L the larger is δ to get the instability; L seems to be a good indicator

-The δ to get the instability can be well correlated to a **linear trend line (a linear relation exists between $\delta_{instability}$,** that's to say the thickness is a good indicator when it's correlated to L.

-The diagonal cannot be directly correlated to δ since the 2'500x2'500 and 2'000x1'000 have almost the same δ to get the instability.

-Contrary to the Staaks theory concerning the square panel, (i.e. $\delta_{instability}$ equal to16.8 times the thickness), the constant $\delta_{instability}/t$ change for the different size of square panel. The Staaks law is then no more available for four point-supported panel.

Until now, no real relation have been find between $\delta_{instability}$, L, t. Furthermore, it seems that the ratio L/B have an influence on the results.

4.1.3.2. Ripple amplitude

If the new geometry of the panel after the occurring of the instability is not considered as a limit, the ripples amplitude have to be check.

Table 2 U3 at Ld_Point for ripples amplitude equal to 0.5[mm]

Thickness	L/B					
[mm]	1'000/1'000	1'500/1'500	2'500/2'500	2'000/1'000	3'000/1'500	4'500/1'500
4.00	-	80.00	80.00	80.00	80.00	-
8.00	160.00	160.00	180.00	160.00	180.00	180.00
12.00	210.00	210.00	240.00	240.00	270.00	300.00
15.00	240.00	270.00	300.00	270.00	-	-
19.00	280.00	320.00	360.00	320.00	-	500.00
25.00	360.00	-	-	-	-	-
33.00	500.00	-	-	-	-	-

Ripple amplitude greater than 0.5[mm] have not been reported for all the geometry. For some cases the applied displacement was not high enough, that's why there are some empty case in Table 2.

The thicker is the plate the more the applied displacement is high to get ripple amplitude equal to 0.5 [mm]. The size of the panel seems to have light influence on the ripple, particularly when the thickness is thin.

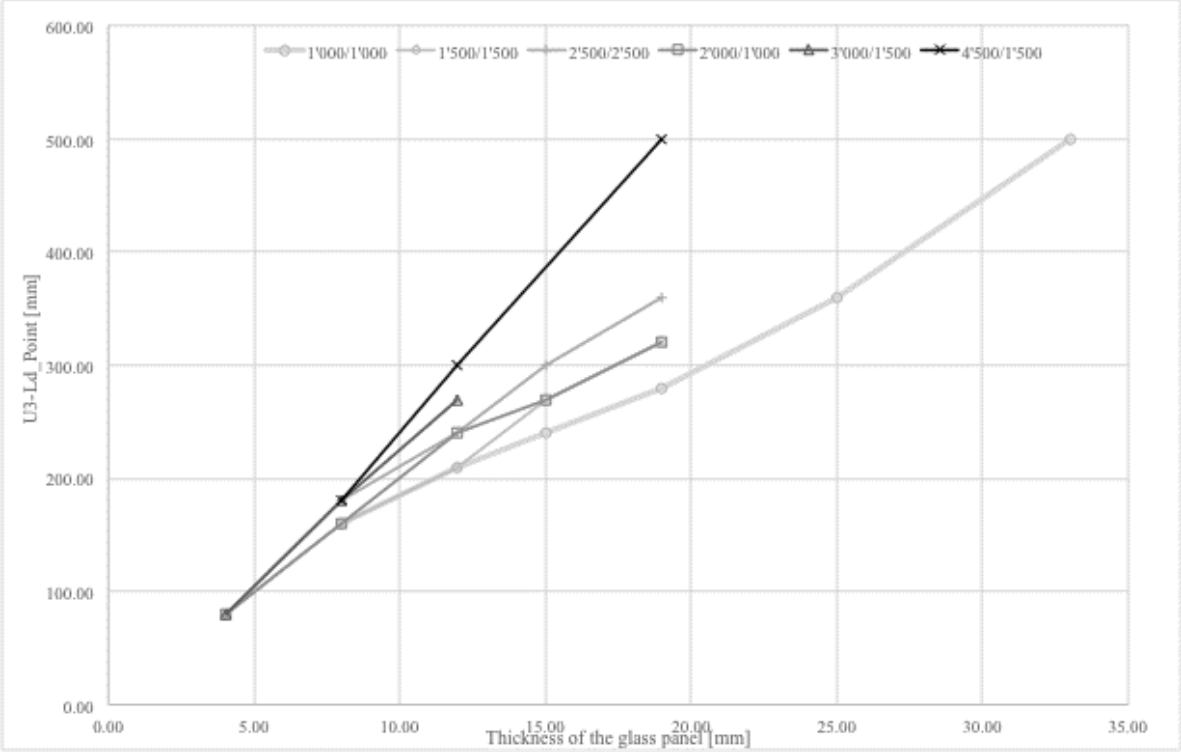

Chart 34 U3 at Ld_Point for ripple amplitude equal to 0.5 [mm] in relation with the thickness

4.1.3.3. Maximum stress

Table 3 U3 at Ld_Point for Smax equal to 50[MPa]

Thickness	L/B					
[mm]	1'000/1'000	1'500/1'500	2'500/2'500	2'000/1'000	3'000/1'500	4'500/1'500
4.00	45.00	-	-	100.00	-	-
8.00	30.00	80.00	200.00	70.00	155.00	-
12.00	25.00	70.00	170.00	60.00	135.00	180.00
15.00	20.00	60.00	160.00	50.00	120.00	167.00
19.00	17.00	50.00	150.00	45.00	105.00	160.00
25.00	15.00	40.00	125.00	35.00	90.00	145.00
33.00	12.00	35.00	110.00	30.00	75.00	110.00

When the plate is relatively flexible (slender), the plate can be deformed without a huge increasing on stress. At the opposite rigid plate will imply a huge amount of stresses during the shaping process.

Thus, the thicker is a plate the larger will be the generated stress. It's the same regarding the plate size. The shorter is the short edge of the panel the more the stress will be high.

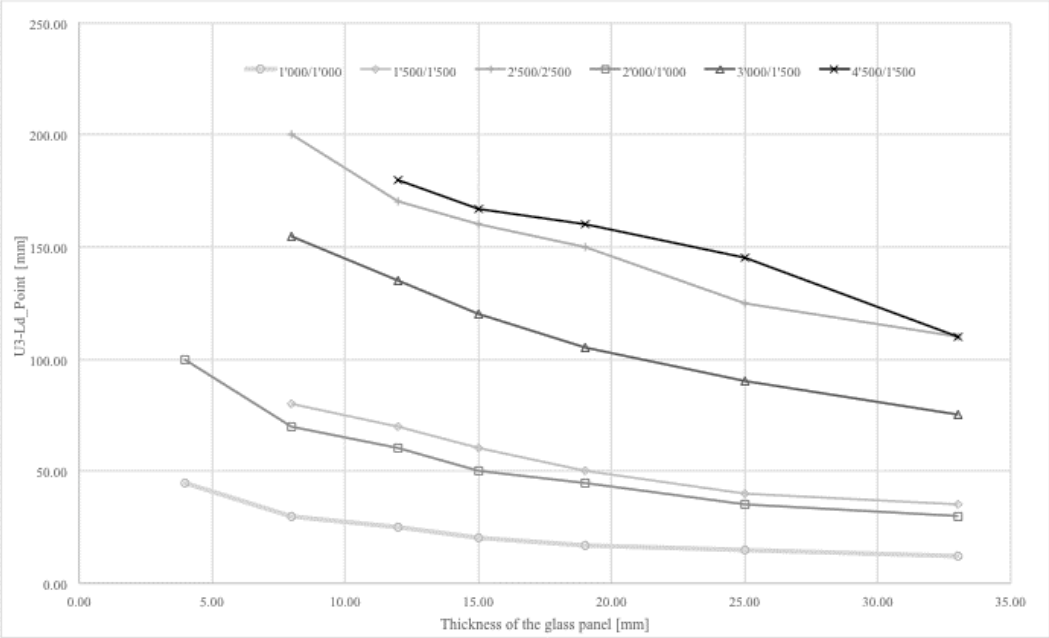

Chart 35 U3 at Ld_Point for Smax equal to 50[MPa] in relation with the thickness

Table 4 U3 at Ld_Point for Smax equal to 100[MPa]

Thickness	L/B					
[mm]	1'000/1'000	1'500/1'500	2'500/2'500	2'000/1'000	3'000/1'500	4'500/1'500
4.00	85.00	-	-	-	-	-
8.00	60.00	140.00	-	120.00	-	-
12.00	45.00	120.00	300.00	100.00	215.00	310.00
15.00	40.00	100.00	265.00	90.00	200.00	300.00
19.00	35.00	90.00	240.00	80.00	180.00	275.00
25.00	30.00	80.00	220.00	70.00	165.00	250.00
33.00	25.00	65.00	200.00	55.00	150.00	220.00

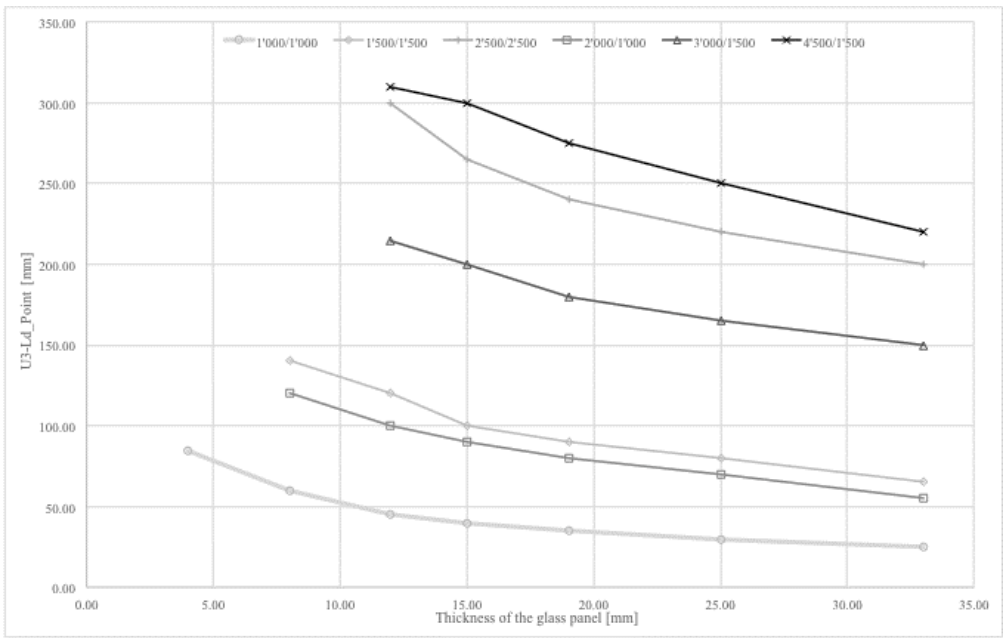

Chart 36 U3 at Ld_Point for Smax equal to 100[MPa] in relation with the thickness

4.1.3.4. Reaction forces

Table 5 Buckling reaction force RF3 [N] at Ld_Point

Thickness	L/B					
[mm]	1'000/1'000	1'500/1'500	2'500/2'500	2'000/1'000	3'000/1'500	4'500/1'500
4	88	32	11	51	13	6
8	1'404	576	182	865	332	210
12	7'139	2'918	969	4'418	1'821	1'317
15	16'595	7'084	2'363	11'104	4'411	3'389
19	43'177	18'077	6'168	28'038	11'637	9'787
25	125'142	53'990	18'520	85'027	35'536	31'072
33	377'764	161'642	56'589	266'295	109'436	105'596

The thicknesses and the length of the edge have a huge effect on the reaction force magnitude. The length of the short edge is determinant; the shorter is the edge the higher is the reaction forces.

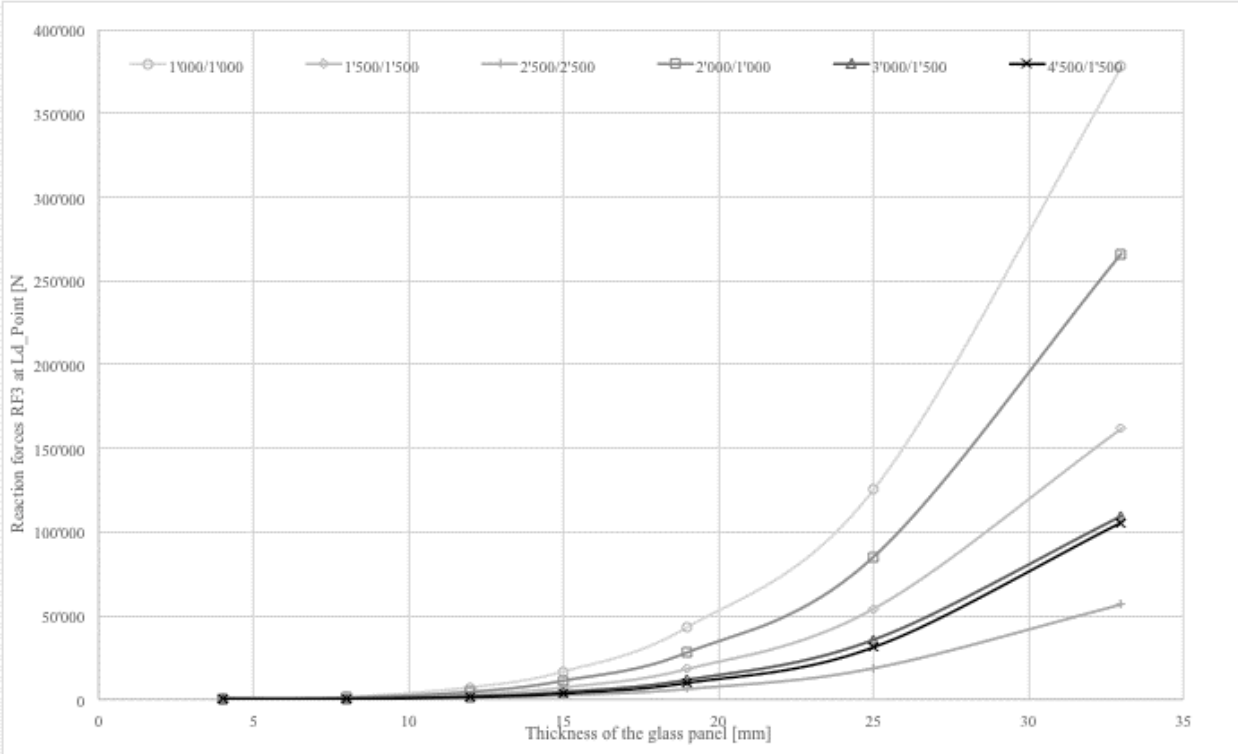

Chart 37 Reaction forces at $\delta_{buckling}$ in relation with the thickness

The relation RF3=f(t) can be well defined by a polynomial (order 3) curve for each panel size.

4.1.4. Design table

Design table can be obtained by crossing the different table. Depending on the limiting parameter, fixed by the architect and the engineer, different limits can be used. The design table is presented in Appendix VIII.

4.2. Effects on an external pressure

One may wonder is the panel under an external pressure will behave in the same manner. An external wind load is applied against the glass.

4.2.1. Model

The shaping process is done right after t. Thus, the pressure before the shaping process already deforms the panel. The applied load act in the opposite direction of the applied displacement.

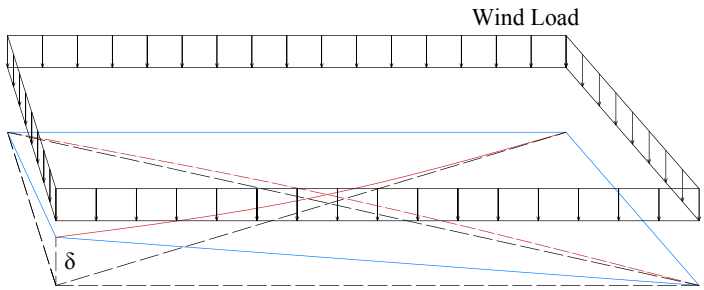

Figure 67 Sketch of the panel under wind load during the shaping process

The panel is in the vertical position. Shell elements (S4R) in combination with the same choice of modelling as in §2.2.3 have been used.

Different magnitudes of pressure have been used (0, 0.2, 0.5, 1 and 2[kN/m^2]) on a 1'000x2'000 [mm] panel. As for the design table, the thicknesses vary from 8 to 33[mm]. The thickness of 4[mm] wasn't pertinent due to the large deformation under wind load

4.2.2. Results

Table 6 Buckling displacement U3 [mm] at Ld_Point for different external pressure.

Thickness	Pressure				
[mm]	*0 [kN/m2]*	*0.2 [kN/m2]*	*0.5 [kN/m2]*	*1 [kN/m2]*	*2 [kN/m2]*
8.00	100.00	90.00	104.00	154.00	-
12.00	150.00	141.00	135.00	135.00	147.00
15.00	189.00	183.00	177.00	171.00	165.00
19.00	234.00	232.00	228.00	224.00	216.00
25.00	302.00	300.00	300.00	296.00	292.00
33.00	387.50	385.00	385.00	385.00	385.00

NB: The precision of the results can differs by 2.5[mm] for thick plate (from 19[mm] to 33 [mm]), due to the fixed number of output (200) and the maximum applied displacement (500).

As expected the thickest is the plate the less the external pressure will influence the behaviour. For thinner plate the instability occurs for a smaller δ.

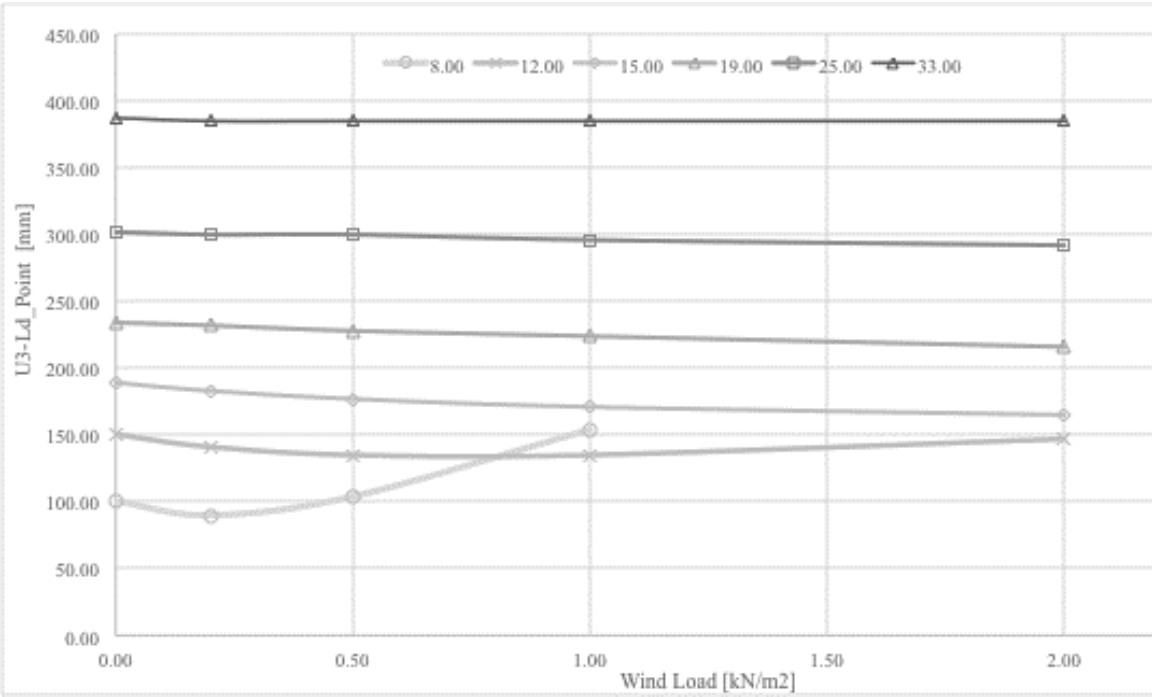

Chart 38 Instability displacement U3 in relation with the wind load

Globally wind loads make the panel more willing to the instability. Indeed the δ to the instability decrease with the pressure.

However, for thin plate, the deformed shape due to the initial pressure is huge. Therefore, the instability occurs for a bigger δ and the consequences of the instability are really light.

4.3. Effects of imperfection

The aluminium panel has showed that an initial imperfection in the same direction of the applied displacement δ would change the instability behaviour.

4.3.1. Model

The imperfection is modelled by an initial deflection W [mm] in the middle of the panel. The deformed geometry is imported from an Abaqus result with an imposed displacement W as in Figure 68

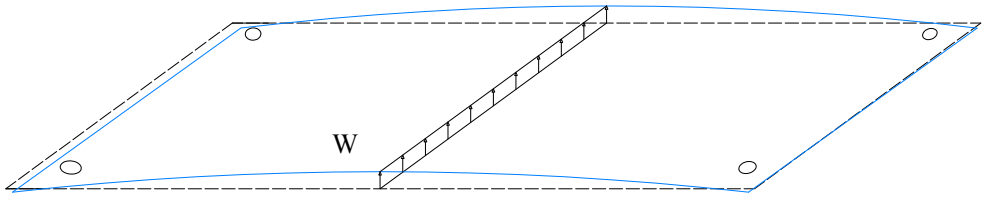

Figure 68 Imperfection input in Abaqus

A solid model is used; indeed as the system is very instable the solid model is more willing to converge to a realistic result. The mesh used is the same as the one from the mesh study.

Different value of W are used (0, 1, 5, 6.5 and 10 [mm]) with a 4x1’000x2’000 [mm] and a 12x1’000x2’000 [mm] glass panel.

4.3.2. Results

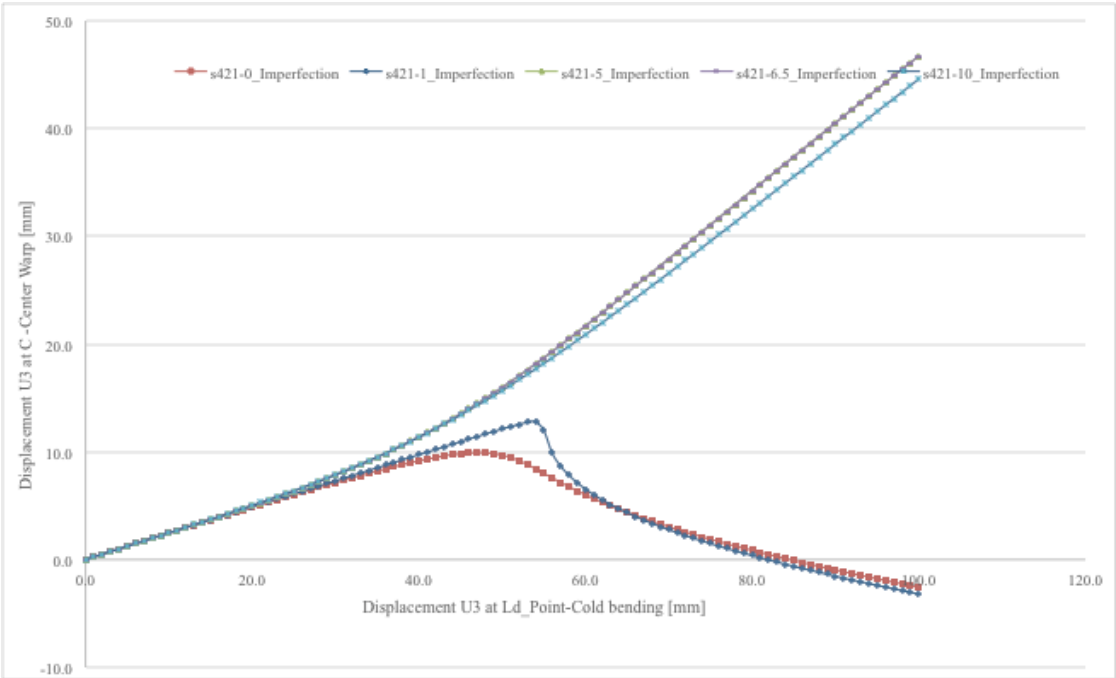

Chart 39 Effect of the imperfection on a 4x1'000x2'000 panel

One can observe the two different instability phenomena. Without instability the buckling induce a “Jump-In” of the point C. The opposite phenomenon appears when imperfection is applied. However, for small imperfection the model reach a very instable configuration.

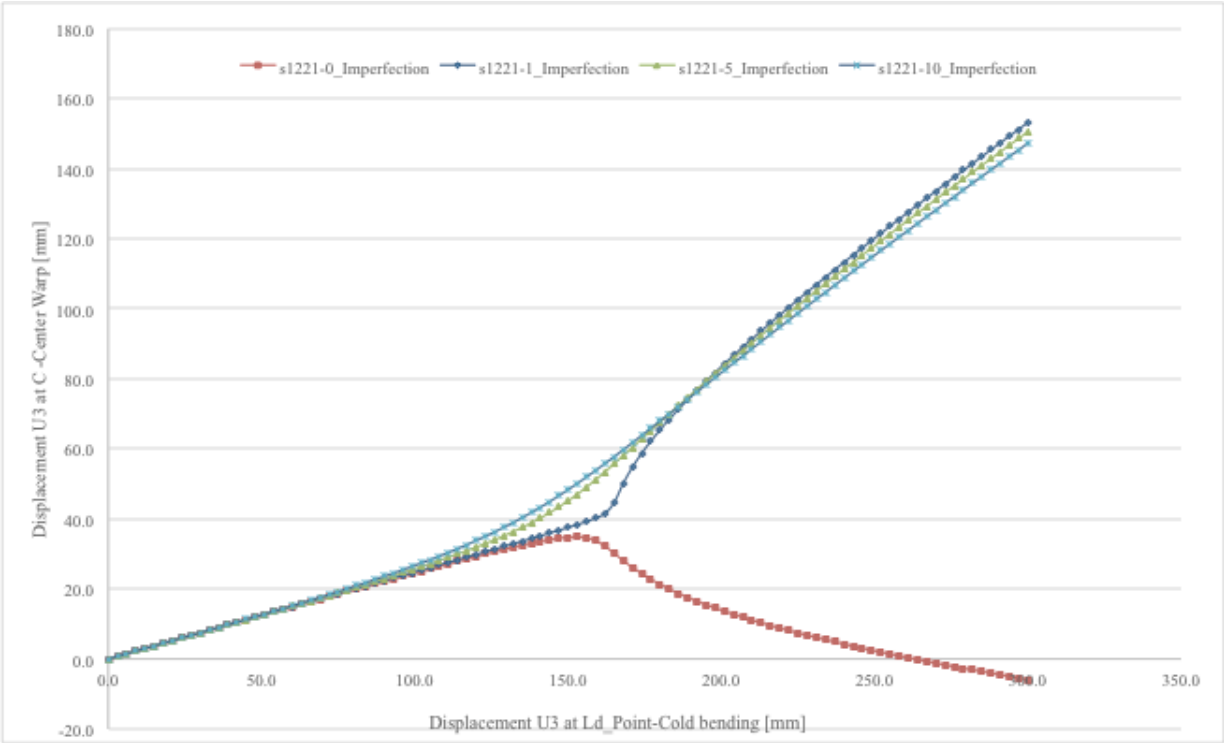

Chart 40 Effect of the imperfection on a 12x1'000x2'000 panel

Indeed, for the two different thicknesses the instability appears whether as a “Jump-In” or as a “Jump-Out”.
Thus, the numerical results have to be take carefully, the model might not converge to the real solution.

In conclusion imperfection in the same direction as the δ, implies a change in the instability (“Jump-Out” instability). The instability occurs approximately for the same δ as the usual instability. However, the geometry differs and the stress pattern is totally different for both instability phenomena.
The deformed configuration in case of “Jump-Out” do not induce ripple along one diagonal. Then, it would be preferable to cold-warped panel with appropriate imperfection or lightly hot bent panel.

4.4. Insulated Glass Unit Investigation

It has been shown that the stiffening of the edge has a favourable effect for the cold-warping. Thus, one may wonder the influence of the edge sealing in case of cold-warped insulated glass unit (IGU).

4.4.1. Models

As for the curtain wall model, the edge sealing has been replace by spring. The IGU is supported by four points-fitting (glued) support on one face. A surface-to-surface interaction constraint has been defined between both glass plates.

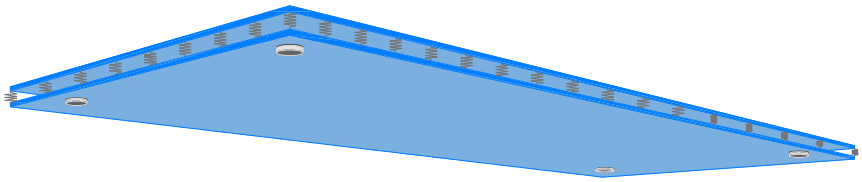

Figure 69 Abaqus IGU Input

The two plates are 4 [mm] thick, the spacer is 12 [mm] thick and has a width of 12[mm]. Three different rigidity of the spacer have been used (Cz=1, 5 and 210000 [N/mm]/mm) on a 1’000x2’000[mm] panel.

4.4.2. Results

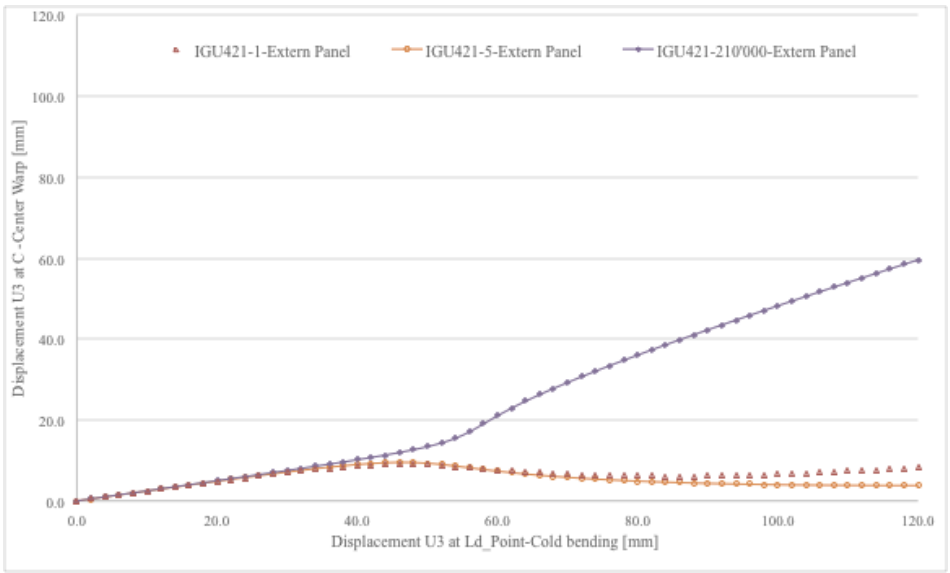

Figure 70 Instability behaviour for IGU panel, extern panel

One observed that there are no favourable effects for traditional spacer (Cz = 1 to 5 [N/mm]/mm). Indeed the buckling appears for the same δ=47[mm] as 4x1’000x2’000[mm] monolithic panel. As expected for really stiff spacer the second

instability phenomenon is reported. The IGU react in the same manner as the curtain wall panel.

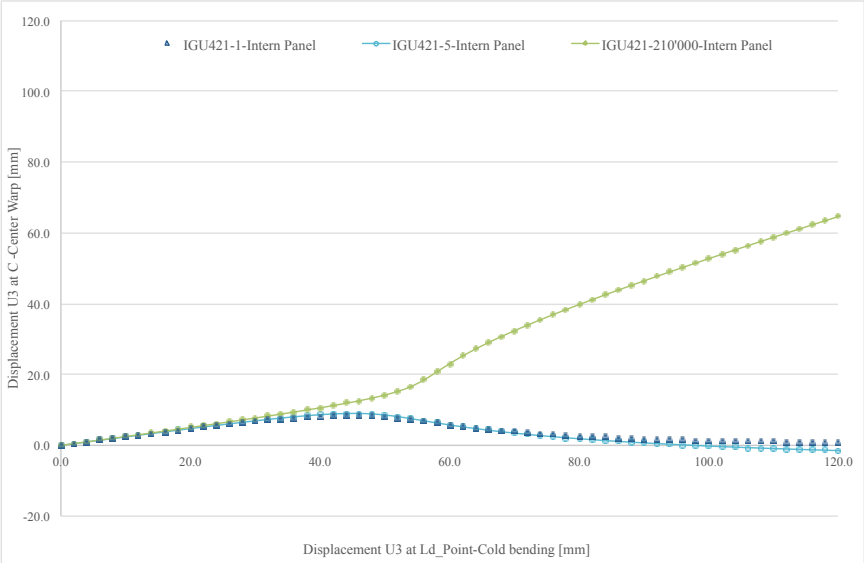

Figure 71 Instability behaviour for IGU panel, intern panel

Both extern and intern panel behave in the same manner. Thus, the ripples are also observed on the external panel. Therefore, the IGU is not a solution against the visual distortions due to the ripples.

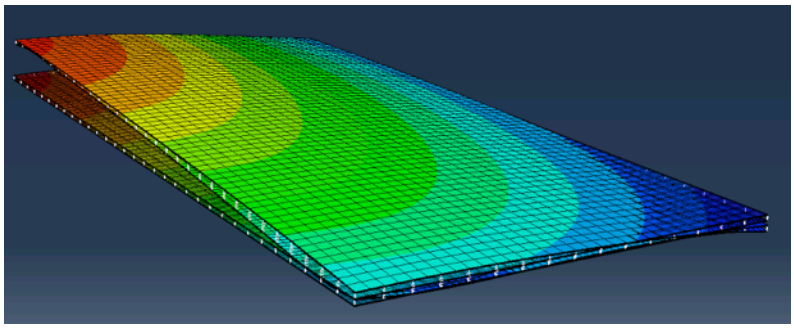

Figure 72 Deformed behaviour for Cz=210'000 [N/mm]/mm

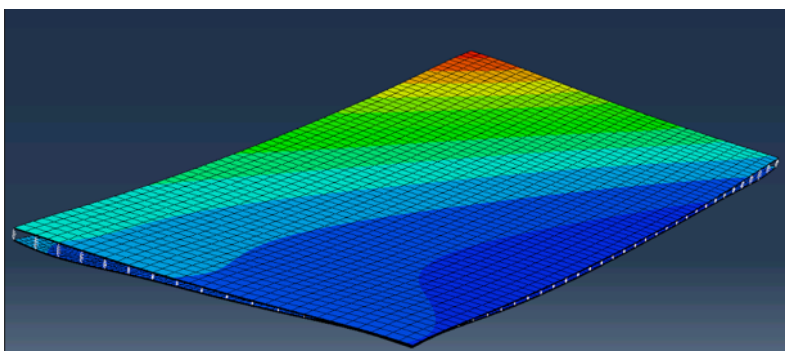

Figure 73 Deformed behaviour for Cz=1[N/mm]/mm

4.5. Double-displacement

In this part the displacement δ is applied on Ld_Point and on the Fix support. The reaction forces are the same as in the traditional case, as well as the bending moment.

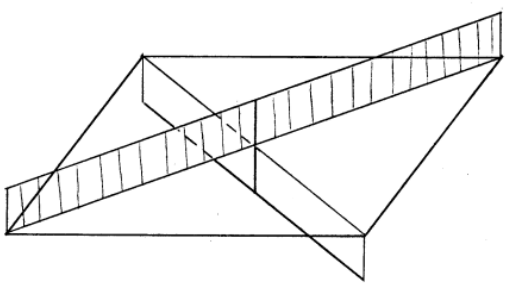

Figure 74 Bending moment acting for a cold-warped panel

However, the deformation pattern is not exactly the same, the instability is then investigated.

4.5.1. Model

The same model as §2.2.3, is used. The only difference is that the same imposed displacement is applied on Ld_Point and the Fix support.

4.5.2. Results

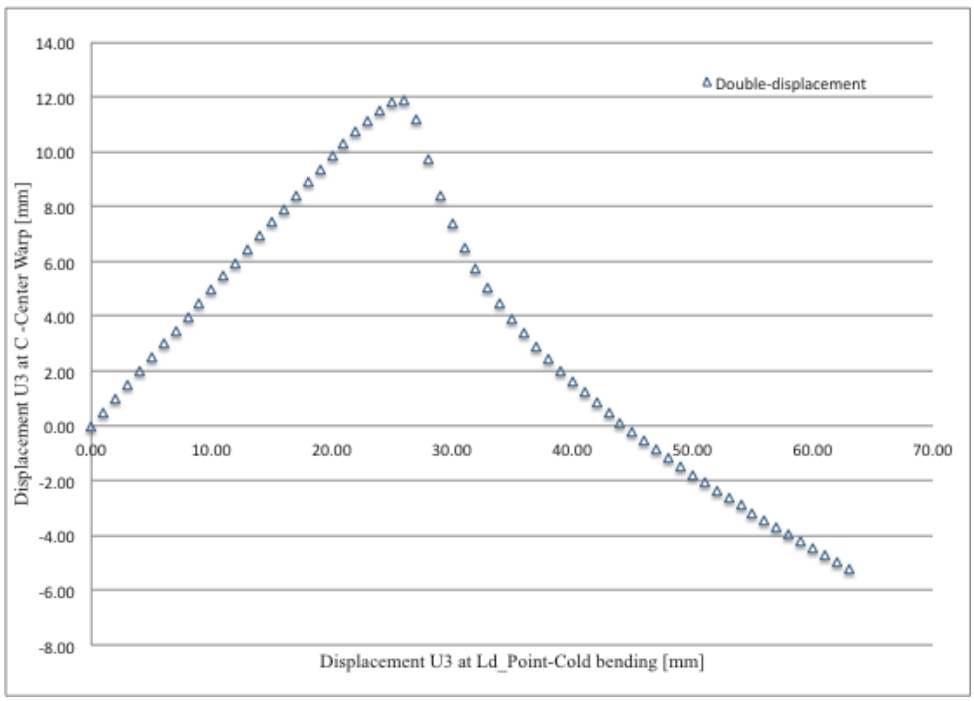

Figure 75 Instability investigation for a double imposed displacement

The instability occurs for δ=25 [mm], thus the same radius of curvature at the instability point is funded.

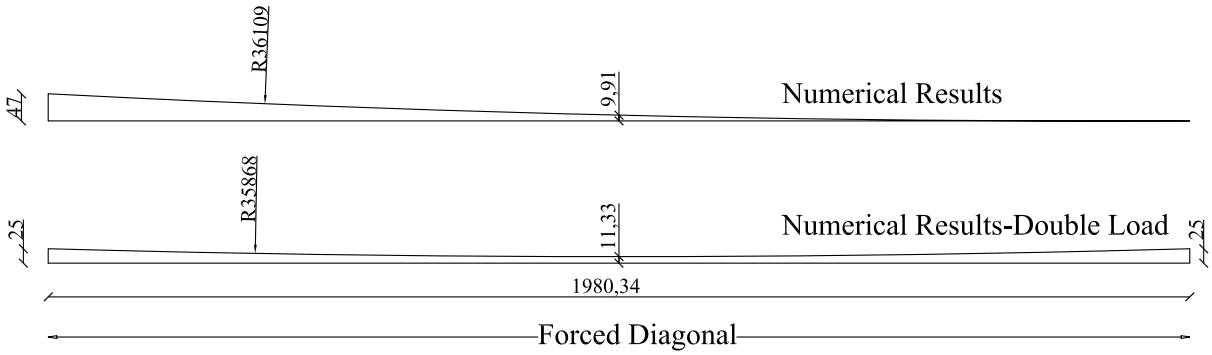

Figure 76 Maximum radius of curvature until the instability, comparison

The small difference between both radiuses comes from the precision (1[mm]) of the imposed displacement. In conclusion, the instability of a cold-warped panel can define by the achievable radius of curvature of the forced diagonal.

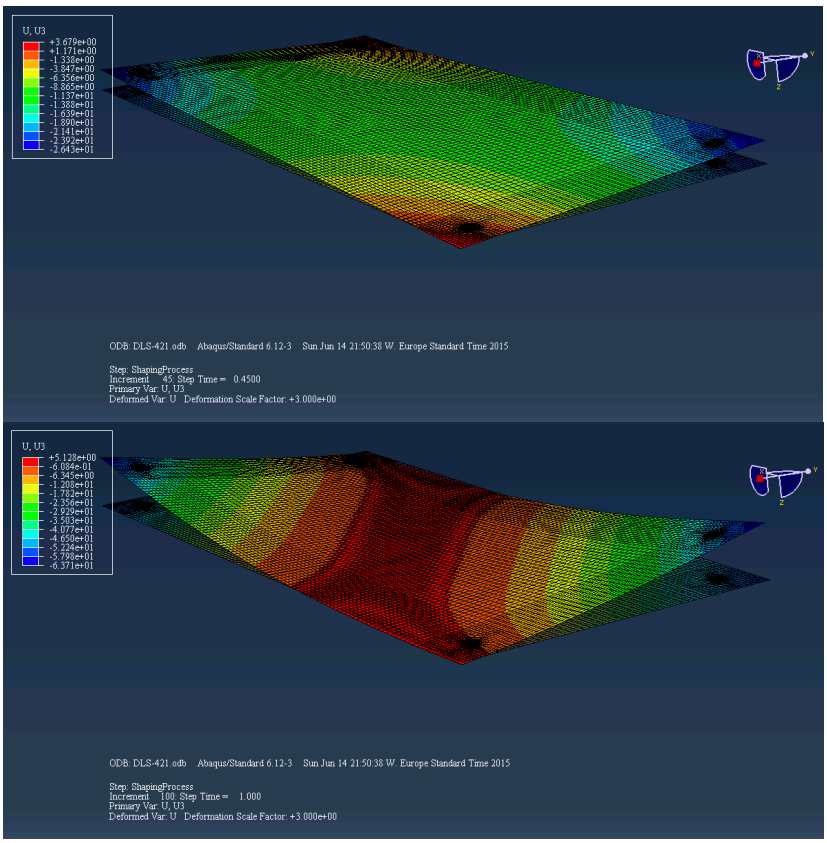

Figure 77 Deformed shape before and after the instability.

The instability implies the same consequences as for the traditional case. That's to say ripple along the supported diagonal, curvature of the edge and a severe curvature of the forced diagonal are observed.

5. Numerical Investigation of Curtain Wall

Curtain wall elements are complex model since they are composed by three main parts; the glass, the silicone and the frame. For this reason it's quite complicated to build a design table since there are at least four variable parameters (i.e. glass size and thickness, silicone rigidity and frame rigidity). However, the following chapter investigates the main parameters of a 2'000x1'000[mm] curtain wall element.

5.1. Glass thickness influences

In this part the glass thickness influences during the shaping process is investigated.

5.1.1. Model

The same model as the one describe in 3.2.1 is used. Thus, the same aluminium frame 84x40x80) and silicon parameter are used (Sikasil SG-500-E=1[MPa] and ν=0.5). Five different thicknesses of the glass are treated (i.e. 4, 8, 12, 15 and 19) on the 2'000x1'000[mm] panel.

δ to the instability ripples amplitude and Smax are recorded. Because it might be a critical factor (concerning the setting up on site). The reaction force RF3, at the instability displacement, is also plotted.

5.1.2. Results

Due to the rigidity used in the numerical model, a "Jump-In" instability occurs. However, it has been shown that there is, in any case, an instability for the same $\delta_{instability,}$ which is characterized by a "Jump-Out" or down of point C.

Table 7 Maximum δ [mm] f (instability, ripple and Smax)

Thickness	Limiting Parameters			
[mm]	Instability	Ripple	Smax=50[Mpa]	Smax=100[Mpa]
4	78	-	-	-
8	153	-	115	170
12	207	-	110	170
15	246	-	105	165
19	296	-	90	155

Thus, Table 7 gives realistic values for the occurrence of the instability. Nonetheless special regards should be given to Smax. Indeed, the stress pattern depends on the deformed geometry of the panel; the Smax pattern would be different for a jump-up instability. However, the *maximum* value of stress should be in the same order of magnitude, therefore, Table 7 gives accurate results.

The δ of the instability occurrence is well described by a polynomial (order 3) trend line.

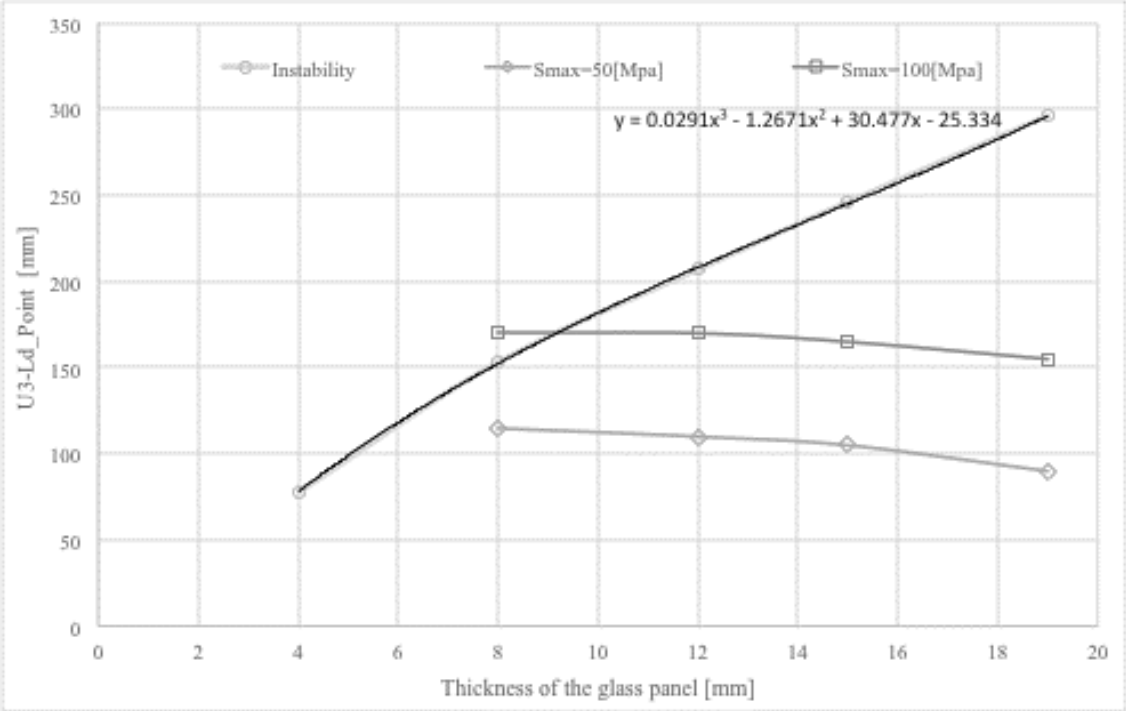

Figure 78 Maximum δ in relation with the thickness for different limiting parameters

The ripples are not a determining factor since the amplitude of them is lower than 0.5[mm].

Table 8 Reaction forces RF3 at the instability in relation with the thickness

Thickness	Reaction Forces RF3
[mm]	[N]
4	3'882
8	9'772
12	19'385
15	31'581
19	56'465

The change in thickness of the glass implies an important change in the reaction force; a polynomial (order 3) trend line defines the relation pretty well:

$$RF3 = 8.9t^3 - 90.4t^2 + 1538.7t - 1384.2$$

5.2. Influence of the frame and the silicone on the deformation

It has been shown that the rigidity of the silicone has a huge influence on the type and the δ of the instability. Thus, the linear support rigidity has an effect on the behaviour during the shaping process. The influence of the silicone and the frame is then investigated.

5.2.1. Model

The main model is composed by a 12x1'000x2'000[mm] glass panel. A thickness of 12[mm] is used, in order to have a realistic stiffness of the glass for that size of frame. Four different combinations are made concerning the stiffness of the silicone and the stiffness of the frame:

1) Silicone SG-500 (E=1[MPa], ν=0.5) and aluminium frame 4x40x80[mm] cross section, initial model
2) Stiff[i] silicone and aluminium frame 4x40x80 cross section
3) Silicone SG-500 (E=1[MPa], ν=0.5) and stiff frame
4) Both silicone and frame are stiff

5.2.2. Results

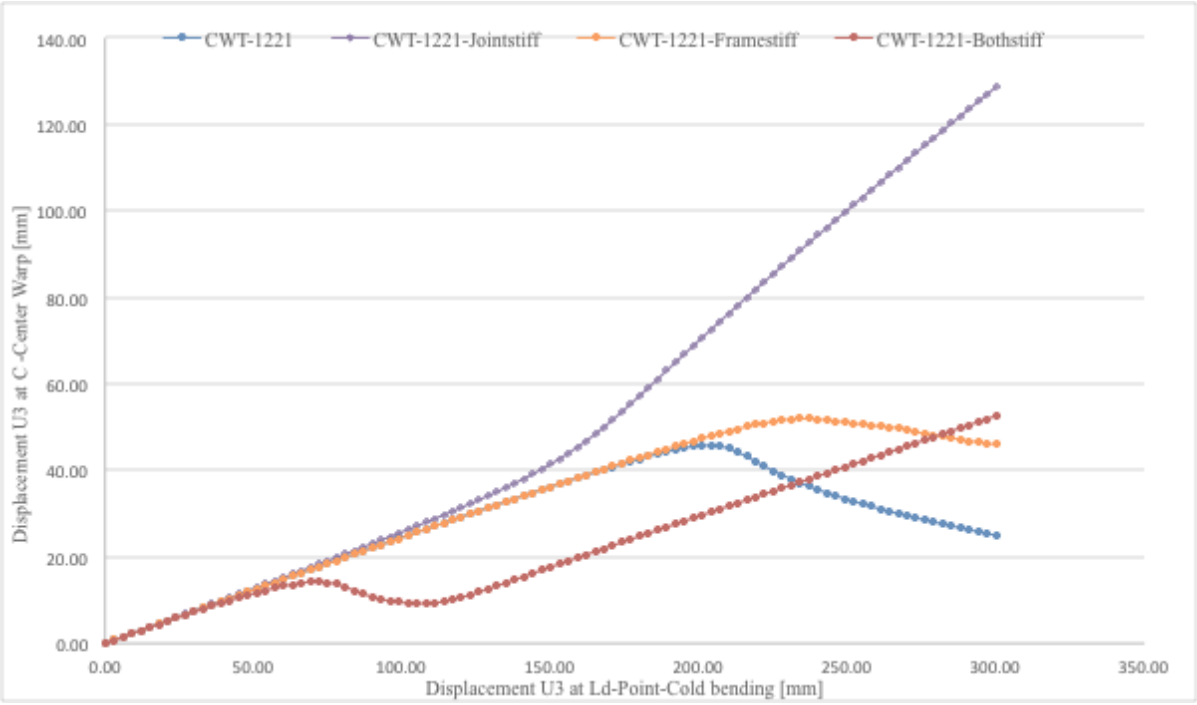

Chart 41 Silicone and Frame influence during the shaping-process

[i] Stiff means that the rigidity is infinitely bigger than the one used in the initial model

Stiff joint will result in a jump-up instability of the glass. This effect has been already shown on chapter 3.5.The imposed displacement induced a deformation to the panel. This deformation can be carried out by the initial plate geometry until a certain point, the instability point $\delta_{intstability}$. When $\delta_{intstability}$ is reached, the plate cannot carries the imposed deformation anymore and have to change its geometry. The change in geometry occurs by the first mode of the instability, a "Jump-In" of the surface panel. However, when the edges are hold a second mode of instability appears. A "Jump-Out" of the surface is then observed. That's the reason why stiff silicones induce the second mode of the instability.

It's observed that $\delta_{intstability}$ is bigger for a super stiff frame. The difference is light, but it's maybe due to the fact that the initial frame has already an important stiffness. However, that result highlight the facts that stiff (enough) frame have to be used to benefit from the curtain wall advantages.

When both silicone and frame are stiff a premature instability is observed. Indeed the support is too rigid and a transversal in plane compression is causing the buckling of the glass panel. The whole geometry is then modified and visual distortions are observed. This case could happen if a stiff frame is used in combination with a considerable width of silicone (acting like a fully fixed connection). Special attention should be paid to the silicone widths to avoid a premature buckling or failure of the glass (increasing of stress due to the fully fixed support).

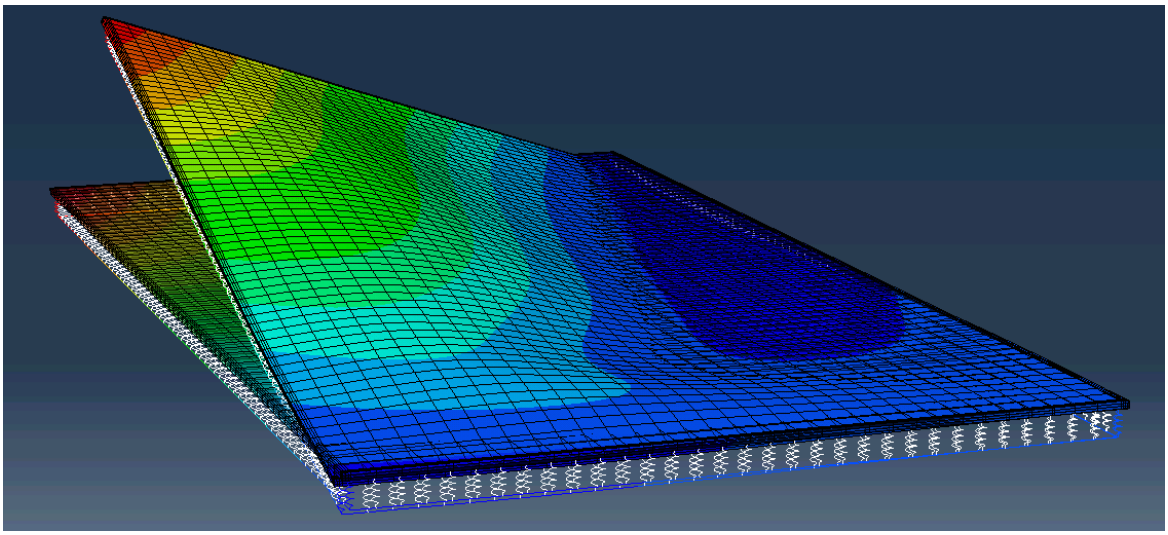

Figure 79 transversal buckling for the "bothstiff " model

5.3. Two sides supported panel

It has been shown that the straightness of the edge has a real influence on the instability behaviour. Thus, the classical curtain wall has been investigated. This part investigated the behaviour of a cold-warped panel for which the two-long edges are supported by a frame.

5.3.1. Model

The same silicone and aluminium frame is used as for the curtain wall model (SG-500 and 4x40x80[mm] aluminium frame). The glass thickness is 12[mm] and the size is maintained to a 1'000x2'000[mm] plate.

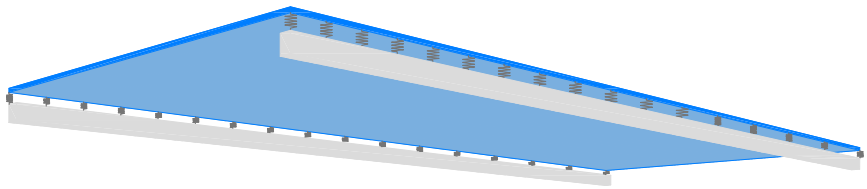

Figure 80 Two sides supported panel model

Springs are used to model the silicone and beam element model the long edge. The punctual supports are applied at each frame end. An additional torsional constraint has been given at each aluminium beam. In the practical case of a real building, that could be associated to the continuity of the frame.

5.3.2. Results

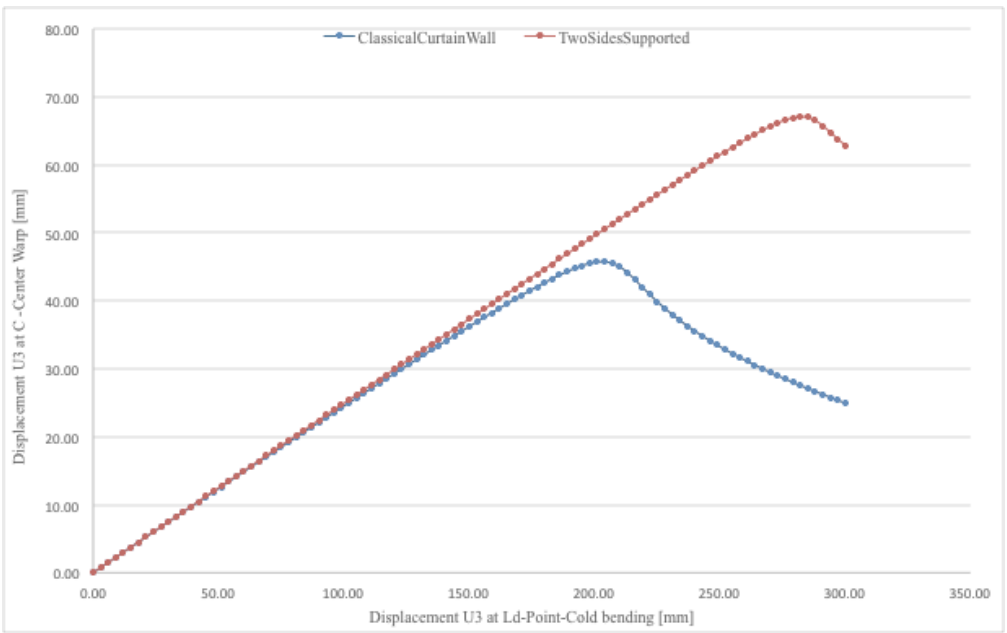

Chart 42 Instability comparison between a curtain wall and a two sides supported panel

The result is pretty eloquent, since the instability occurs for $\delta_{instability}$=282[mm], it's an increasing of 138% compared to the classical curtain wall. In addition the stress acting on the glass is decrease. Indeed, to reach 50 [MPa] the δ is140 [mm] (increasing of 137%) and to reach 100[MPa] the δ is 225 [mm] (increasing of 136%).

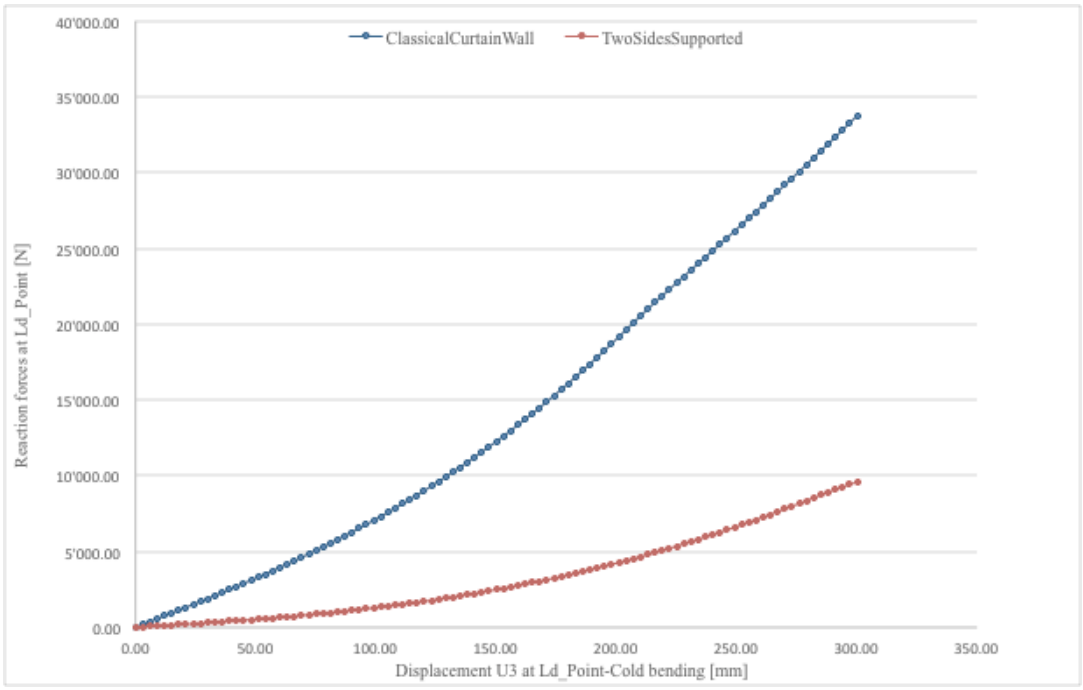

Chart 43 Reaction forces RF3 comparison between a curtain wall and a two-sides supported panel

The advantage is pretty clear concerning the reaction forces; the setting-up on site would be greatly facilitated by the lower reaction forces.

The only drawback of the two sides support panel could be the lower rigidity concerning the deflection due to the wind.

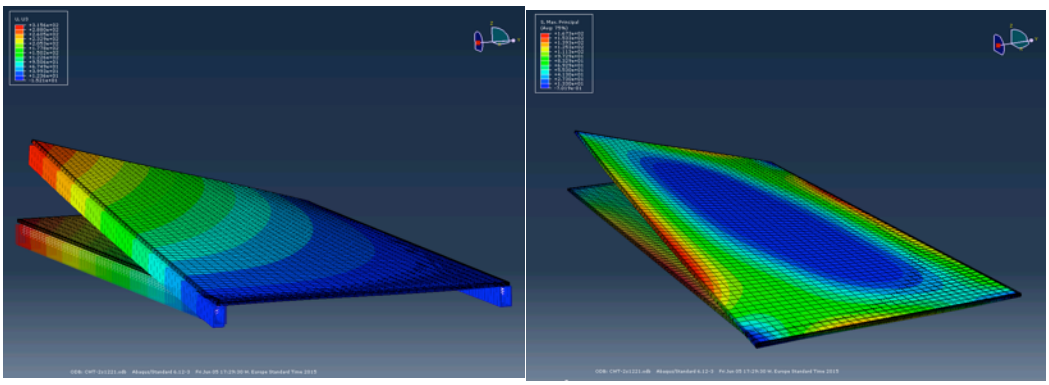

Figure 81 Deformation U3 and maximum principal stress pattern

6. Conclusions

Throughout the previous chapter, the instability phenomenon of a cold-warped panel during the shaping has been investigated. The main conclusions are presented in this chapter as well as a recapitulative plan.

At the beginning of this research the following objectives were stated.

- Investigation of the instability phenomenon reported by M.Eekhout and D.Staaks by means of numerical models validate by experimental tests.
- Investigation of panels supported by glued point-fitted spider connection and frame supported
- Numerical investigation of different ways to avoid the instability phenomenon

Firstly, a numerical and experimental programme was composed. 4x1'000x2'000[mm] HSG panels samples were used as they were made available by the ICOM, and have the same ratio L/B as the most common used glass.

The first tests have been done on the four point-supported glass panel. Both experimental and numerical model were globally well correlated. Nonetheless, the numerical model lightly overestimates the instability consequences on the panel. Thus, numerical results could be used to form an upper bound limit of the instability's effects.
Moreover, experimental results on the aluminium were completely different from the expected one. Afterwards, it has been seen that the plate was initially lightly curved; the imperfection due to the manufacturing process was in the same direction of δ. As a result of the cold-warped process, the edges were severely curved as well as the forced diagonal, in the opposite direction as expected and consequently the supported diagonal didn't buckle. Additional tests have shown that, for a specific panel, the instability occurs for a same radius of curvature of the forced diagonal.

Additional tests were performed on a frame-supported glass panel. It has been reported that the stiffness of the silicone and the frame were significant. Since factories give mechanical properties of the silicone for the long-term (with high safety factor γ=5.6), it's complicated to have the real values. However, results have shown the existence of two regime of instability.
The first one is the traditional, that's to say after that $\delta_{instability}$ is reached, point C displacement starts moving in the opposite direction. That's why this instability can be associated as a "Jump-In" of the centre surface. This instability is achieved when the stiffness of the silicone is small. $\delta_{instability}$ is larger than for the four-point supported panel and the ripples amplitude are smaller. The stress inside the glass is well distributed thanks to the linear support and there are no peak stresses (contrary to the point connections). The only drawback of the frame-support is the reaction forces needed to bend the entire element, which could be too high for the workers.

The second one can be seen as the opposite of the traditional instability mode. This instability is achieved when the silicone is sufficiently stiff. After that $\delta_{instability}$ is reached, point C displacement suddenly "Jump-Out" the same direction as δ. That's why this instability can be associated to a ""Jump-Out"" of the centre surface.
This instability is characterized by the non-buckling of the supported diagonal, consequently the shape of the forced diagonal is altered by the "Belt-Effect" imposed by the supported diagonal. *Thus, the cold-warping of the aluminium plate follow the second instability regime.*

The first deformation mode can de approximated by a hyperbolic paraboloid shape before the instability occur. After the instability the deformation mode depends on the type of instability (first or second regime). The stress pattern is then specific for each mode of deformation.

By performing numerical tests, different aspects have been investigated. Firstly a design table, for a point-supported panel, have been construct taking into account $\delta_{instability}$, the maximum principal stress and the ripple amplitude. According to [19] and the design table, a linear relation links the $\delta_{instability}$ to the glass thickness for square and rectangular panel. That relation is different for each panel size and seems to be depending on L and the ratio L/B.

The effect of a pressure or an initial imperfection, such as the induce deformation is in the opposite direction to δ, has been investigated. The first instability regime occurs for a smaller $\delta_{instability}$. However, the thicker are the panel the smaller is the effect, that's to say the behaviour during the shaping process would be the same as for a perfectly flat plate.
Accordingly, small imperfection such as the deformation is in the same direction of δ implies the second instability regime ("Jump-Out"). Thus, precurved hot-bend panels could be used to avoid the ripples along the supported diagonal.

By investigating the instability phenomenon for IGU, it has been observed that usual spacer are not enough stiff to delay the instability. However, by stiffening the plate's borders the instability mode change to the second mode one, the same effect as for curtain wall is then reported.

Finally, numerical investigations on curtain wall have highlighted the importance of a stiff frame in combination with a good silicone (a small width is mandatory) to delay the instability displacement.
Furthermore, investigation on two-side supported panel has highlighted real advantage. The stress acting on the panel as well as the reaction forces RF3 are smaller and $\delta_{instability}$ is larger.

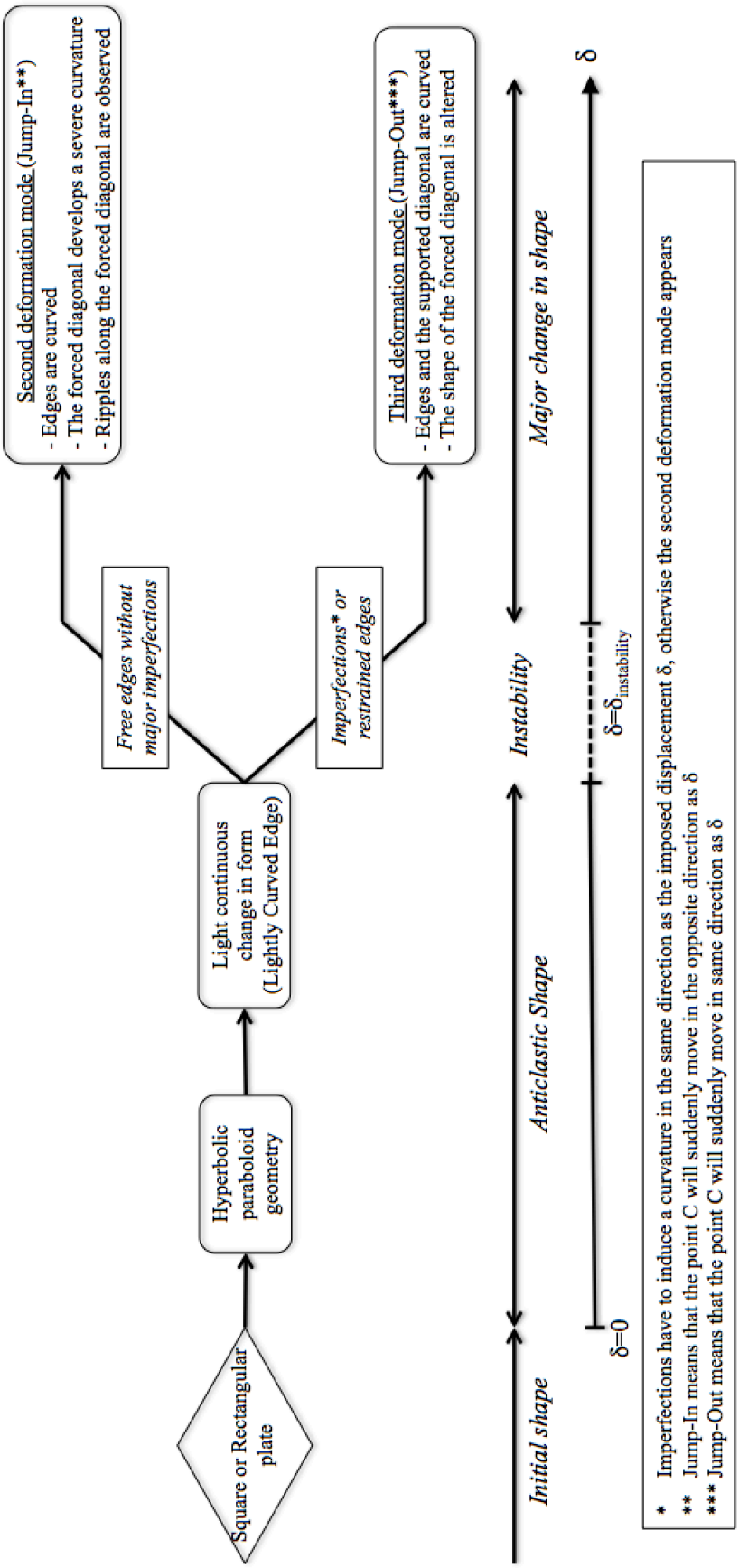

Figure 82 Behaviour of a cold-warped panel during the shaping progress; an out-of-plane displacement δ is applied on one corner while the other three are restrained

7. Recommendations for further study

7.1. Practical suggestions

The choice of the panel in size and thickness is fundamental. The experimental tests made at the EPFL have suffered from the flexibility of the panel. Indeed the LVDT weren't adapted for the too thin used panel, since the LVDT's springs were initially deforming the plate. Moreover, a vertical setup was mandatory to avoid the deflections due to the selfweight of the glass.
Nonetheless the small thickness of the panels was useful to performed test on HSG and the relative small reaction forces were also an advantage for the test setup. Moreover, $\delta_{instability}$ wasn't too high; consequently the tests weren't too long.

Thus, compromises have to be choosing between the panel size and the thickness. $\delta_{instability,}$ Smax and RF3 should be taking into account by the use of Appendix VIII, moreover, depending on the measurement system, special attention should be paid to the panel flexibility. The use of laser seems the more adapted to solve this problem. The use of LVDT with magnet end is not appropriate since for a too high curvature the magnet would slip.

Accordingly, for small panels the thickness of the panel should be thin enough to limit the amount of induce stresses. For large panel depending on the measurement system the thickness could be thin.

7.2. Further research

The behaviour of the two-side supported panel should be more deeply investigated. Additional numerical tests as well as experimental tests have to be done, since this kind of elements could be a nice and relatively non-expensive solution for futures cold-warped façades.

Moreover, based on [19] and Table 1 Instability displacement U3 [mm] at Ld_Point, the relation, which is linking $\delta_{instability}$ to the thickness of the plate should be find. The final relation should look like at the following relation $\delta_{instability}=C*t$, with $C=f(L,L/B)$.

The time dependency of the viscoelastic material should be include in the next research. Cyclic tests have been performed at the EPFL without failure problem. However, the static fatigue of the cold-warped glass should be investigated to guaranty the feasibility of real project. As well as include the effect of the dynamic wind load.

8. References

8.1. Papers

[1] EUROCODE, PREN 16612 AND PREN 16613, GLASS IN BUILDING

[2] ABAQUS, ANALYSIS USER'S MANUAL V6.12

[3] B.MORONI; PRESTUDY COLD BENT GLASS STRUCTURE

[4] C.LOUTER, EPFL; GLASS STRUCTURES AND FAÇADES COURSES

[5] J. M. DE WIT; COMPUTATIONAL MODELLING OF COLD BENT GLASS PANELS

[6] S.TIMOSHENKO, S.WOINOWSKY-KRIEGER; THEORY OF PLATES AND SHELLS

[7] B.BEER, COMPLEX GEOMETRY FACADES-INTRODUCING A NEW DESIGN CONCEPT FOR COLD-BENT GLASS

[8] L.GALUPPI, S.MASSIMIANI, G.ROYER-CARFAGNI; BUCKLING PHENOMENA IN DOUBLE CURVED COLD-BENT GLASS

[9] HBM; INDUCTIVE DISPLACEMENT TRANSDUCER WA

[10] K.G. DATSIOU, M.OVEREND; BEHAVIOUR OF COLD BENT GLASS PLATES DRUGIN THE SHAPING PROCESS

[11] EN 12150-1:2000 GLASS IN BUILDING; THERMALLY TOUGHENED SODA LIME SILICATE SAFETY GLASS.

[12] FRANÇOIS FREY, TGC VOL.2; MÉCANIQUE DES STRUCTURES

[13] FRANÇOIS FREY, JAROSLAV JIROUSEK, TGC VOL.6; MÉTHODE DES ELÉMENTS FINIS

[14] THE INSTITUTION OF STRUCTURAL ENGINEERS, SECOND EDITION; STRUCTURAL USE OF GLASS IN BUILDINGS

[15] J. WURM; GLASS STRUCTURES

[16] L.ZELLER; LABORATORY PROJECT, COLD BENT GLASS STRUCTURES

[17] E. GHERA, D.STANEK, LABORATORY PROJECT; LES CONNEXIONS ADHÉSIVES POUR LES STRUCTURES EN VERRE

[18] M.SANTARSIERO, C.LOUTER, J-P. LEBET; PARAMETRIC NUMERICAL INVESTIGATION OF ADHESIVE LAMINATD POINT CONNECTIONS

[19] M.EEKHOUT, D.STAAKS, COLD DEFORMATION OF GLASS

8.2. Web

[a] WEB.MIT.EDU

[b] SADEV.COM

[c] OCTATUBE.COM

[d] SCIELO.BR

[e] SCIENCEDIRECT.COM

[f] GLASSFILES.COM

9. Appendices

Appendix I. Mesh Study

Convergence tests have been made to define the appropriate density of the mesh. Particular attention has been given to the stress concentration near the support and also the stress jump.

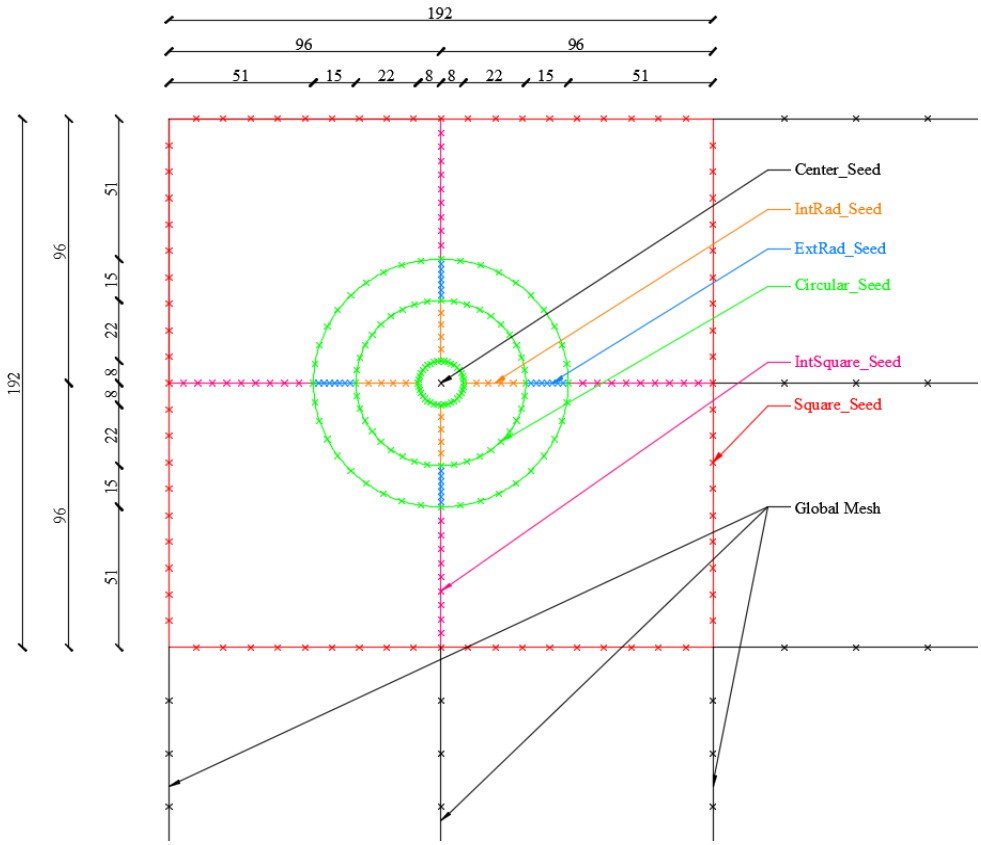

Figure 83 Mesh definition

The global mesh is defined by the element size; whereas the seed by number defines the mesh around the support.
A special refinement is done around the support. The mesh inside the support is less interesting as the stress peak concentration is outside the support area.

Table 9 Mesh study parameters and results

Parameters	*Mesh 0*	*Mesh 1*	*Mesh 2*	*Mesh 3*	*Mesh 4*	*Mesh 5*	***Chosen Mesh***
Global Mesh (size)	0.00	50	25	25	20	15	**25**
Circular_Seed (number)	0.00	5	6	8	10	12	**10**
ExtRad_Seed (number)	0.00	3	4	6	8	10	**8**
IntRad_Seed (number)	0.00	3	4	5	5	5	**5**
IntSquare_Seed (number)	0.00	5	6	8	10	12	**10**
Square_Seed (number)	0.00	5	6	8	10	12	**10**
Max Stress [MPa]	0.00	45.14	47.42	48.85	50.28	50.98	**50.30**
Computational Time [s]	0.00	90.00	180.00	248.00	391.00	652.00	**330.00**
Space [kB]	0.00	30'000.00	60'000.00	82'000.00	125'000.00	200'000.00	**105'000.00**

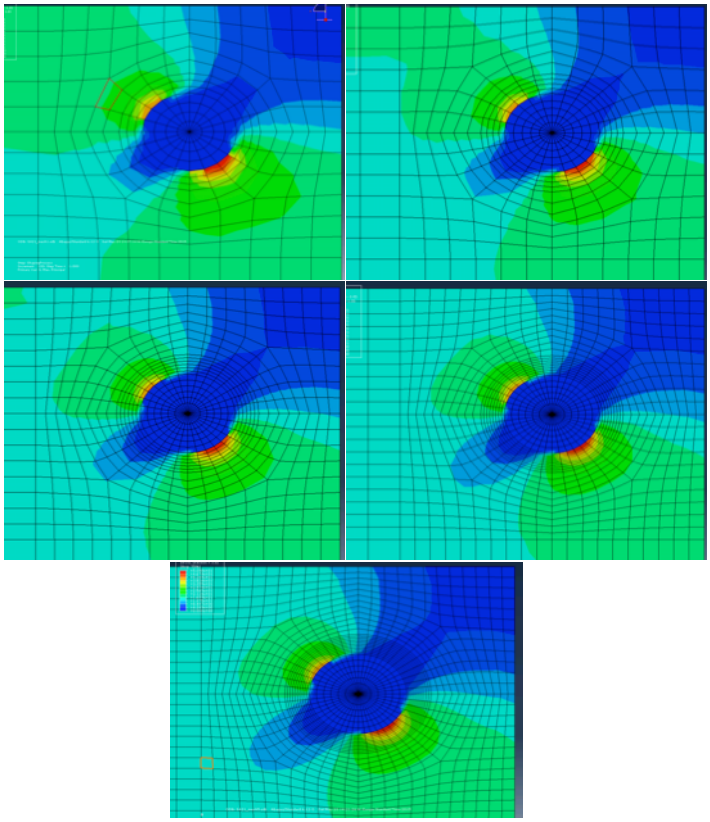

Figure 84 Meshes 1, 2, 3, 4, and 5

The mesh study is done with shell elements. The maximum principal stresses are then compared.

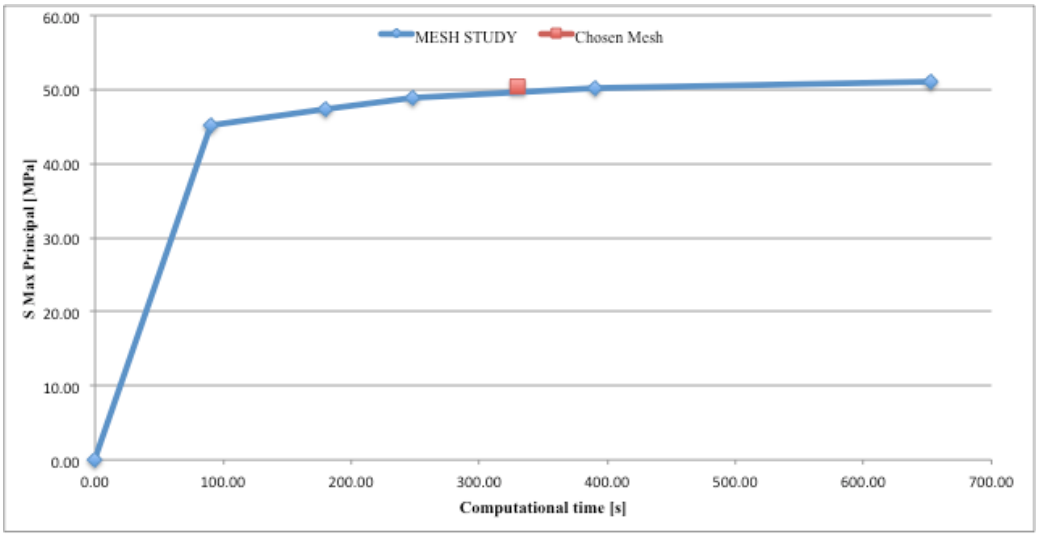

Chart 44 Mesh study

The chosen mesh is a compromise between the computational time and the stress convergence.

Appendix II. Shell/Solid comparison

The comparison takes place on a 4x1’000x2’000[mm] glass plate.

Shell elements are expected to be the best when computing plate problem. Indeed the time saving by the integration of the thickness represents a real advantage on solid model.
However, one may wonder if they actually give the same results. That’s the reason why both model are compared in this section.

o Models

S4R elements are used for the shell model; a tie coupling makes the link between the solid support and the shell plate.
C3D20R elements are used for the solid model; the link between the solid support and the shell plate is done as well by a tie coupling.

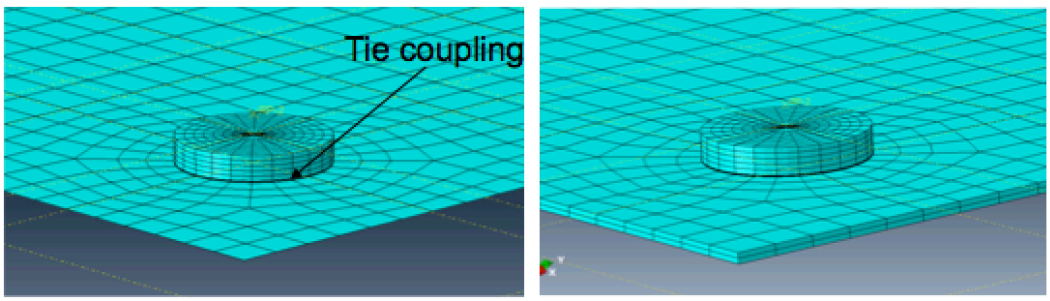

Figure 85 Shell model (left) and Solid model (right)

For both model the same mesh is used. The thickness of the glue is divided by four elements in each model.

o Deformation patterns during the shaping process

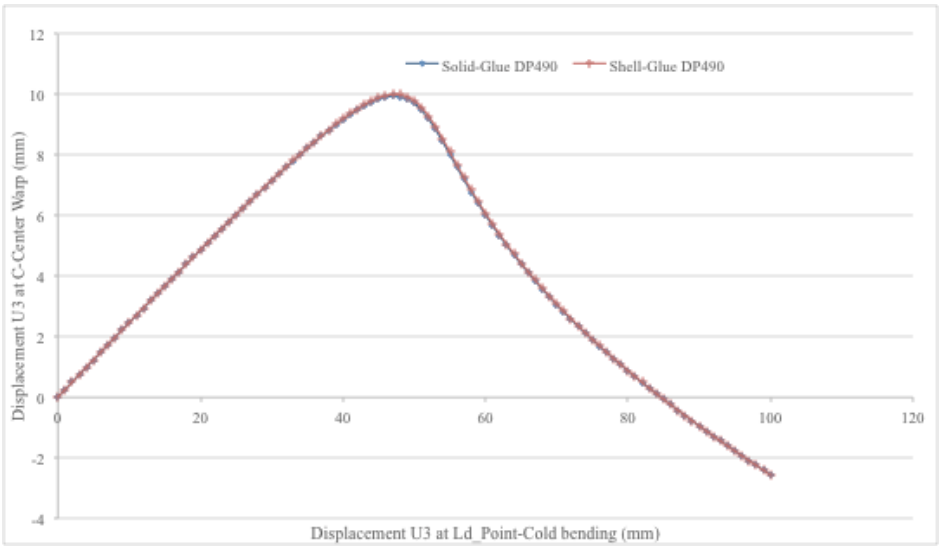

Chart 45 Instability comparison between a shell and a solid model

Concerning the deformation behaviour of the panel during the shaping-process, there are any differences between both models. The curves overlap perfectly.

Thus, the used of shell element is totally justified when studying the deformation of a cold-warped panel during the shaping process.

- Stress variation during the shaping process

The stress variation is also investigated. To compare the difference between each model, a screenshot of the stress pattern (maximum principal stress) around the support is taken for each model for δ=100[mm].

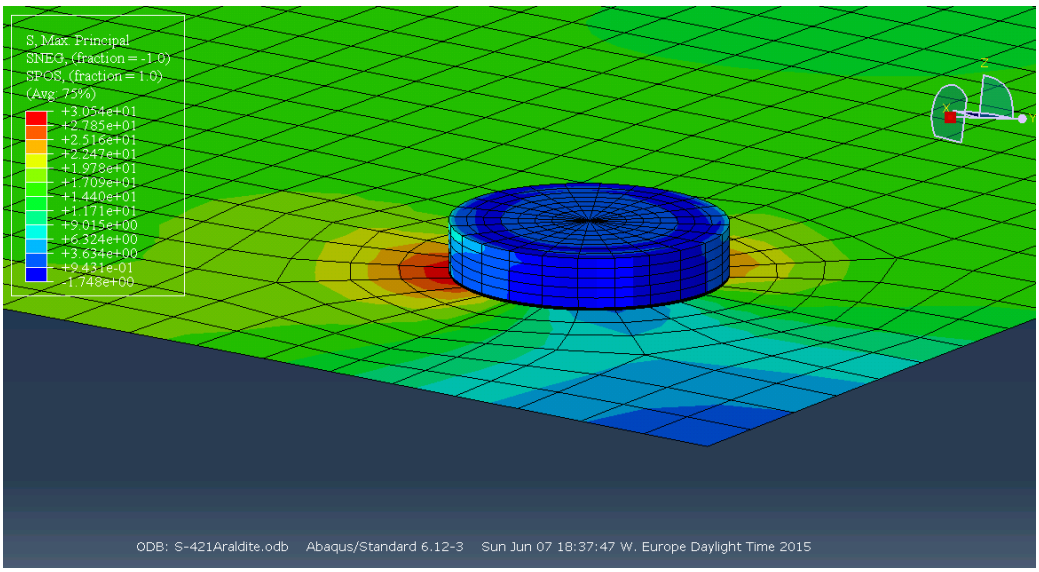

Figure 86 Maximum principal stresses, Shell Model δ=100[mm]

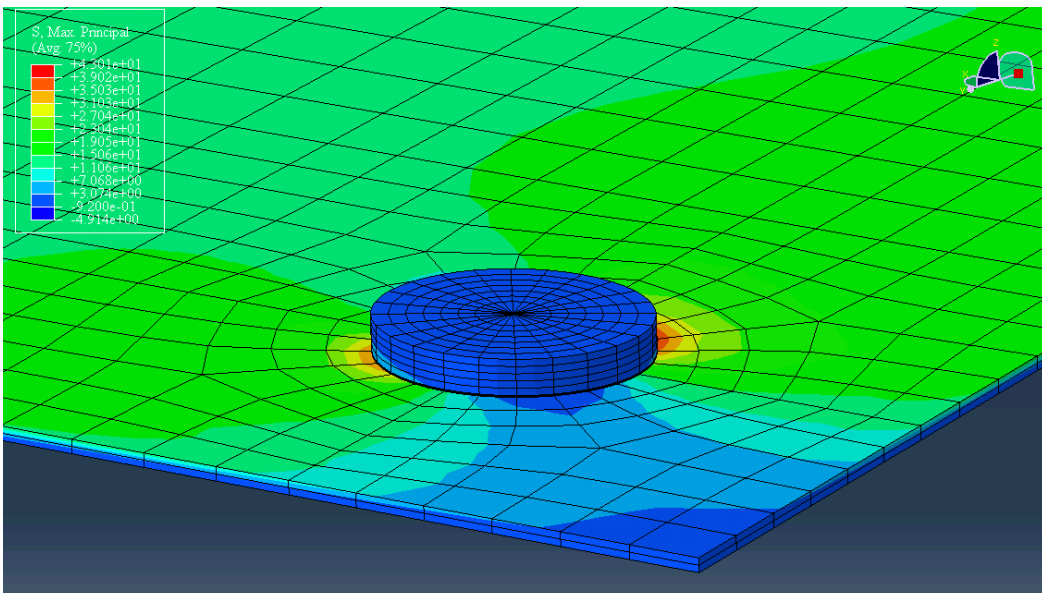

Figure 87 Maximum principal stresses, Solid Model δ=100[mm]

Even if, both stress patterns are very close, the magnitude is different. Indeed a maximum stress of 30.54[MPa] is observed for the shell plate whereas a value of 43.01[MPa] is funded for the solid model. An increasing of 40% is observed in the solid model. Thus, it seems that using shell element is not a on the safe side of the design.

In conclusion, shell elements work well when only deformations are requested. Stress results have to be taken with caution since values differ severely compare to the solid model. Hence, solid model are required for stress analysis (Stress comparison (§2.4.2) between experimental and numerical model has highlighted that the solid results were closer to the reality).

Appendix III. Influences of the glue's rigidity

One would wonder if the rigidity of the glue had an influence on the buckling behaviour. Indeed, if the glue's rigidity doesn't affect the buckling behaviour, then the plate modelling could be simplified.

The influences of the glue, on the buckling behaviour, are funded by computing the classic Ld_Point/C plot and the reaction forces for different types of glue.

Three different glues (different elastic properties) have been tested.

Parameters	E [Mpa]	ν [-]
Glue DP490	10200	0.35
Soft Glue	1	0.48
Super Rigid Glue	∞	0.33

The "Super Rigid Glue" is in fact the effect of the multipoint constraint with the slave surface corresponding to the glass surface.

The viscoelasticity of the material is not taken into account for this analysis.

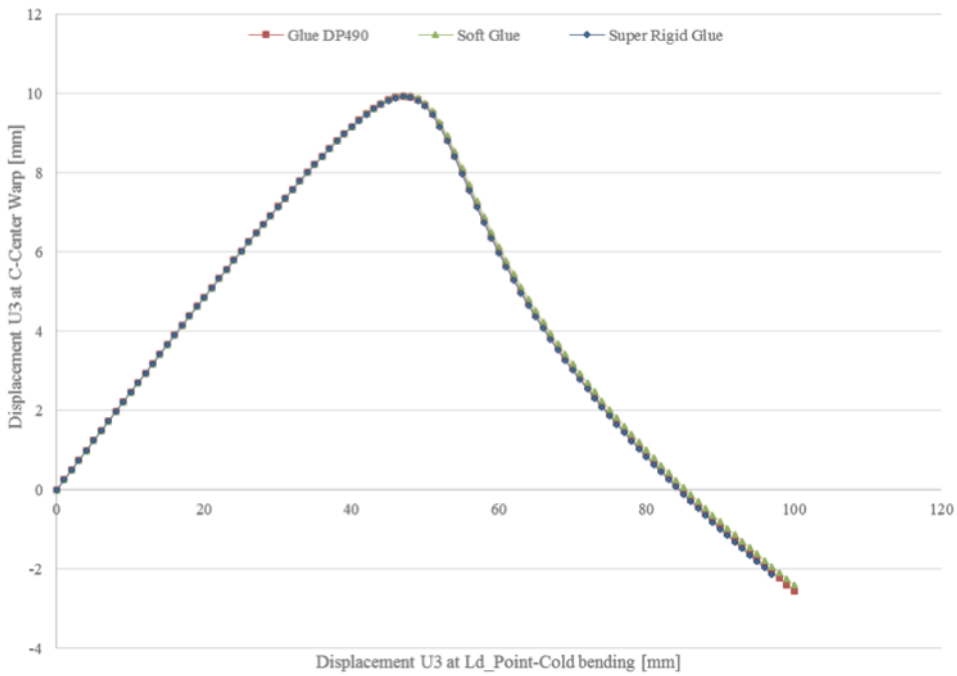

Chart 46 Influence of the elastic property of the glue on the instability behaviour, deformation U3

There are any differences between the three types of glass. In regard to this the influence of the glue rigidity can be neglected, for the deformation analysis.

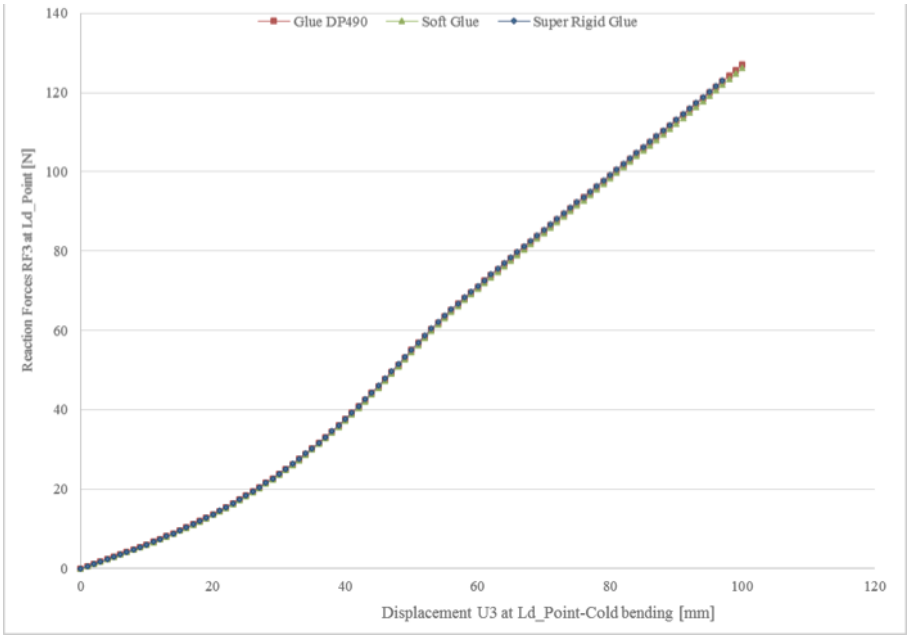

Chart 47 Influence of the elastic property of the glue on the instability behaviour, reaction forces RF3

Results are really close for each type of glue. Then, the “Super Rigid Glue” could be used to catch the instability and deformation behaviour of the panel.

The same study has been done for shell model. The results are the same as the solid one. The rigidity of the glue didn’t influence the deformation behaviour of the plate.

The same comparison has been done with influence on the stress in the plate. Indeed, as the peak stress is around the support, the influence of the glue may influence the concentration.

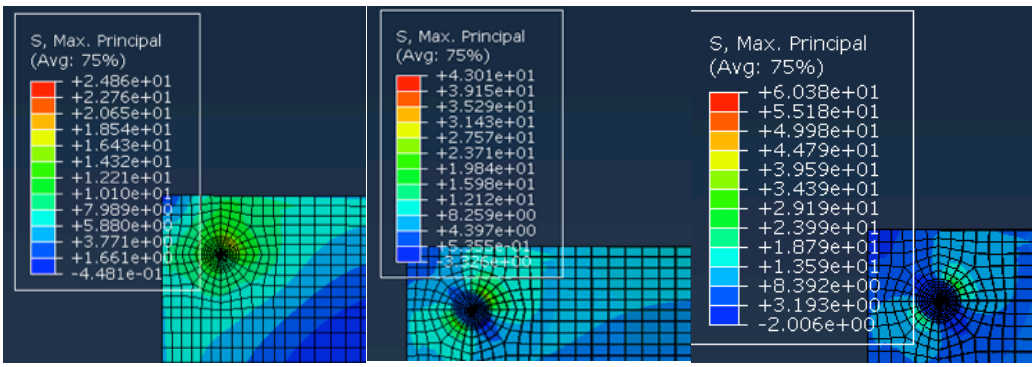

Figure 88 Stress Variation from the Soft Glue to the Super Rigid Glue model

An important stress variation is noticed between the different solid models. Thus, using the multipoint constraint is the better way to get the right deformation behaviour and a conservative design stress. Particularly when it’s used with shell element panel.

Moreover, one could notice that the glue’s rigidity have a huge impact on the stress peak near the support.

Appendix IV. First- and Second-order Analysis

As already said, a second-order analysis gives better results for bending problem. One would be interested to measure the difference between the first- and second-order in term of results.

Identical models were constructed one with solid C3D20R elements and the other with C3D8R elements. Additionally to that the experimental result is plotted.

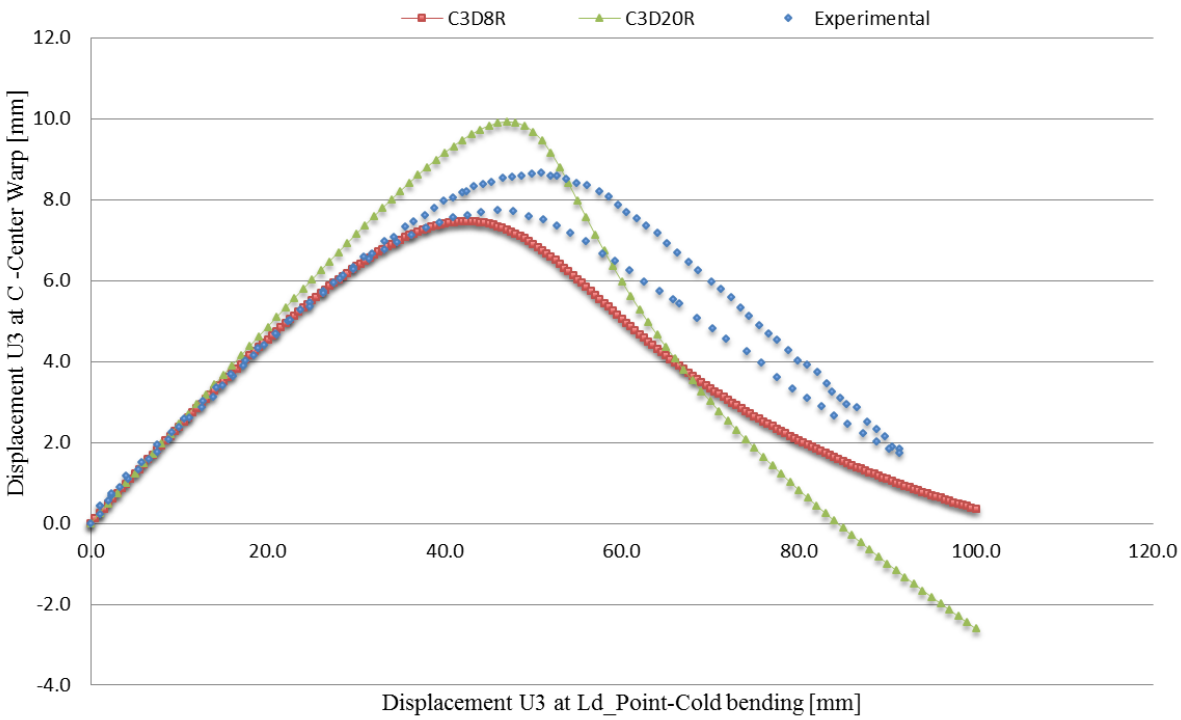

Chart 48 First- and second-order comparison

Both models detected the instability. However, the instability doesn't occur for the same out-of-plane displacement. The instability occurs in a smoother way for the first-order.

The C3D8R model is closer to the reality in the first part. However, the behaviour after the instability is clearly better for the second-order model (parallels curved). Moreover, the maximal displacement at C is closer for the second-order model, even if the shape of the C3D20R model is not really convincing.

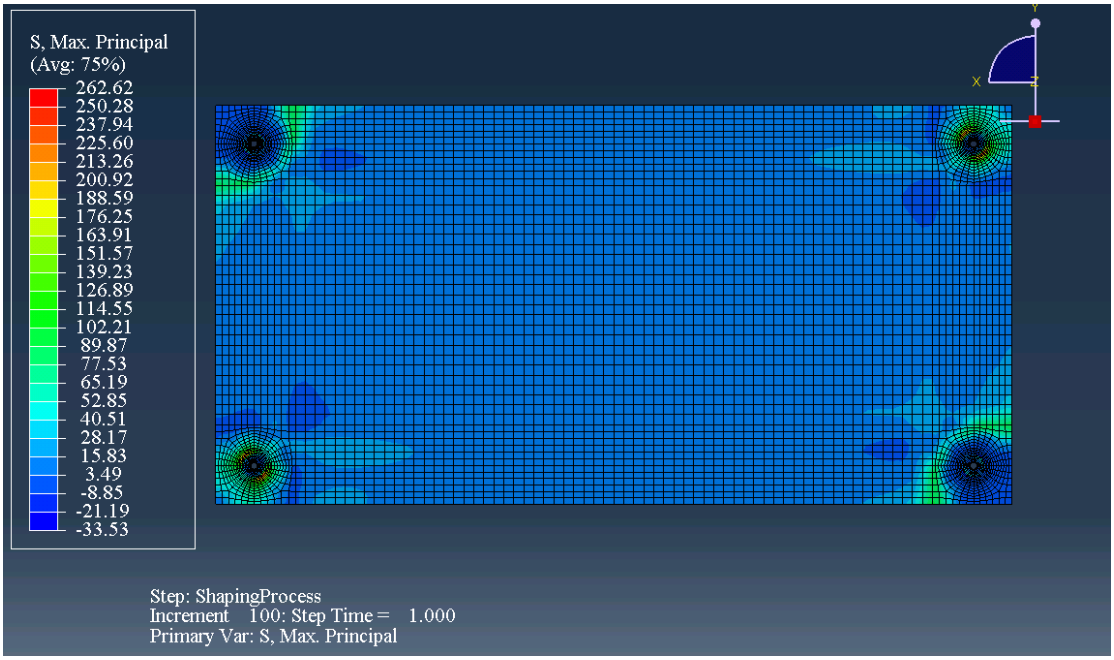

Figure 89 Maximum in plane principal stresses of the deformed plate for $\delta_{applied}$=100 [mm]

In term of stress, the first order gives inappropriate results. The stress explodes literally near the support area. Moreover, the stress pattern is different from the second order modelling. As the experimental and the second-order analysis gives close results for the stress, the first-order seems not appropriate for this kind of analysis.

In conclusion, there are clearly some differences between first- and second-order analyses. However, both analyses give different results from the experimental one.

The first-order can be used with caution for a good first (conservative) estimate of the panel behaviour.

Appendix V. Influence of the LVDT

The experimental part has highlighted the influence of the LVDT on the 4x1’000x2’000[mm] glass plate during the shaping process. Indeed, differences have been reported, during experimental test, on the deformation results when LVDT were applied or not.

Chart 49 plots the C Vs. δ relation, for one curve all the LVDT are applied and for the other only one on C is applied.

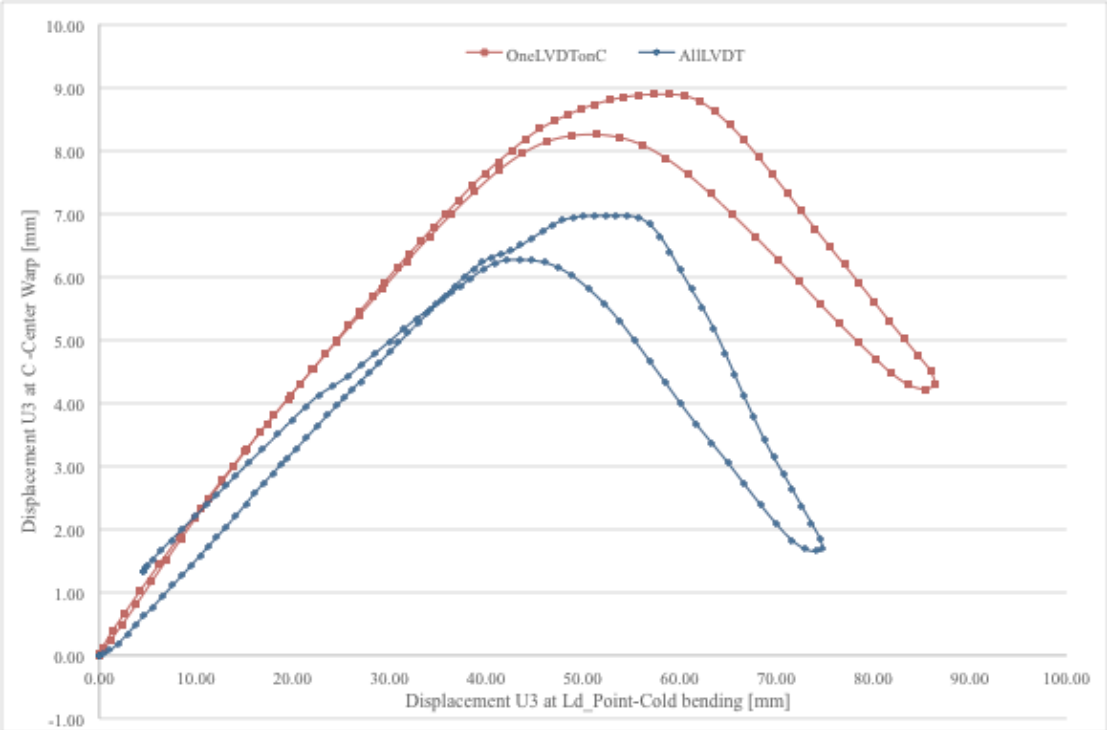

Chart 49 LVDT influence on the deformations results

The influence of the LVDT is huge. The LVDT’s spring applied a small pressure to the plate, but enough high to deform it. Indeed, the observed difference (2[mm]) concerning the displacement of C at the instability point is equal to the initial displacement induces by all the LVDT. Moreover, the forces act against the jump-down caused by the instability. When δ reaches the instability point the plate is globally highly unstable, the stability is then very sensitive, and depends on the external condition. Here the resistance to the buckling offered by the springs create a plateau (the plate reach a really unstable state) until the instability takes place.

A numerical model has been done with the forces of the LVDT’s spring. As the forces are function of the out-of-plane displacement (F = K.U3) it’s difficult to put the exact output of the spring forces (non-linear change of U3 during the shaping-process). Moreover, it’s difficult to know the exact initial pressing-in of the LVDT. That’s the reason why the replacement forces are constant approximation.

However, the LVDT used can only develop maximal forces of 8.2 [N] [9]. The global difference between the reality and the replacement is then small and negligible.

The results from this numerical model have not been retained. Indeed, has shown in §4.3.2, for really small imperfection the numerical solution may converge to a wrong unstable configuration. The rate of convergence is very poor and the results are not accurate. Therefore, the small deflection implies by the LVDT leads the numerical model to a bad outcome.

Due to the undesirable effect of the LVDT on the slender panel, only the results from the digital image correlation system when there are none LVDT are used. Those values are pretty accurate, according to a LVDT vs. Digital image correlation comparison (see Chart 50).

Appendix VI. Correlation between LVDT and the digital image correlation system

LVDT are perturbing the cold-warped results. For this reasons only the digital image correlation system is used. Then, a comparison between the results from the LVDT and the digital image correlation system is done.

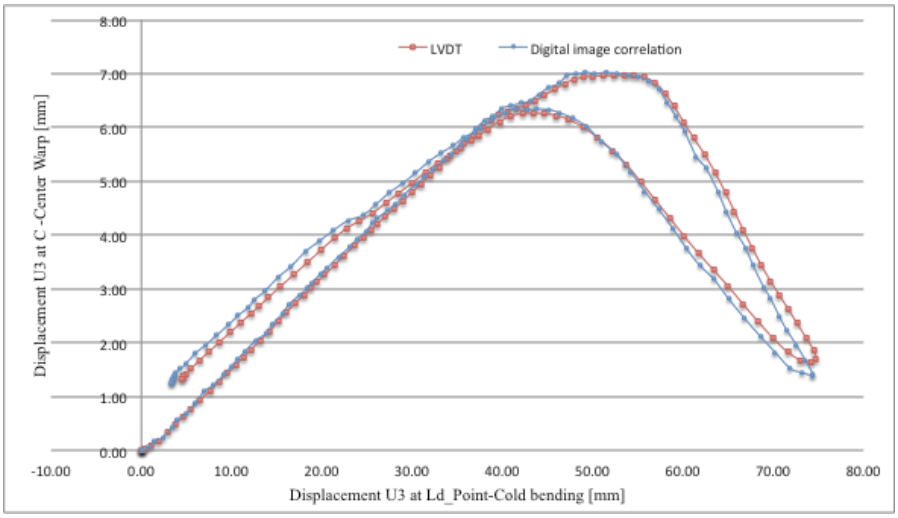

Chart 50 LVDT vs. digital image correlation system, results

The results are closed under the 5% of difference. The different performed tests move in this direction Chart 51

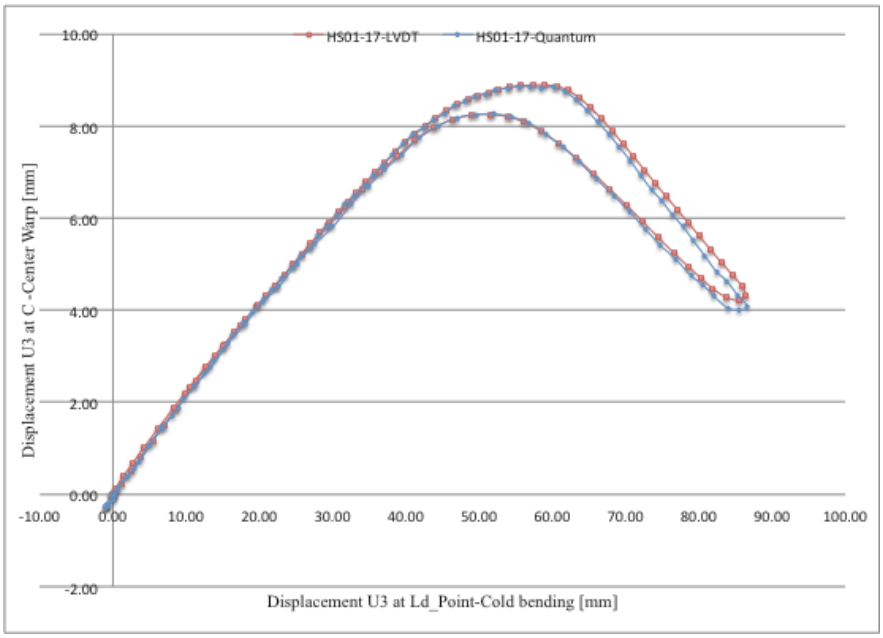

Chart 51 Correlation between LVDT and digital image correlation

The digital image correlation system can be used without accuracy problems.

Appendix VII. Curtain Wall Shell modelling

A first shell curtain wall model has been built. However the results weren't pertinent in particularly concerning the stress.

Peak stress and a non-symmetrical stress pattern have been reported. The applied load and the frame-support should involve distributed stress. Moreover, the reaction forces should induce a symmetrical pattern of the stress.

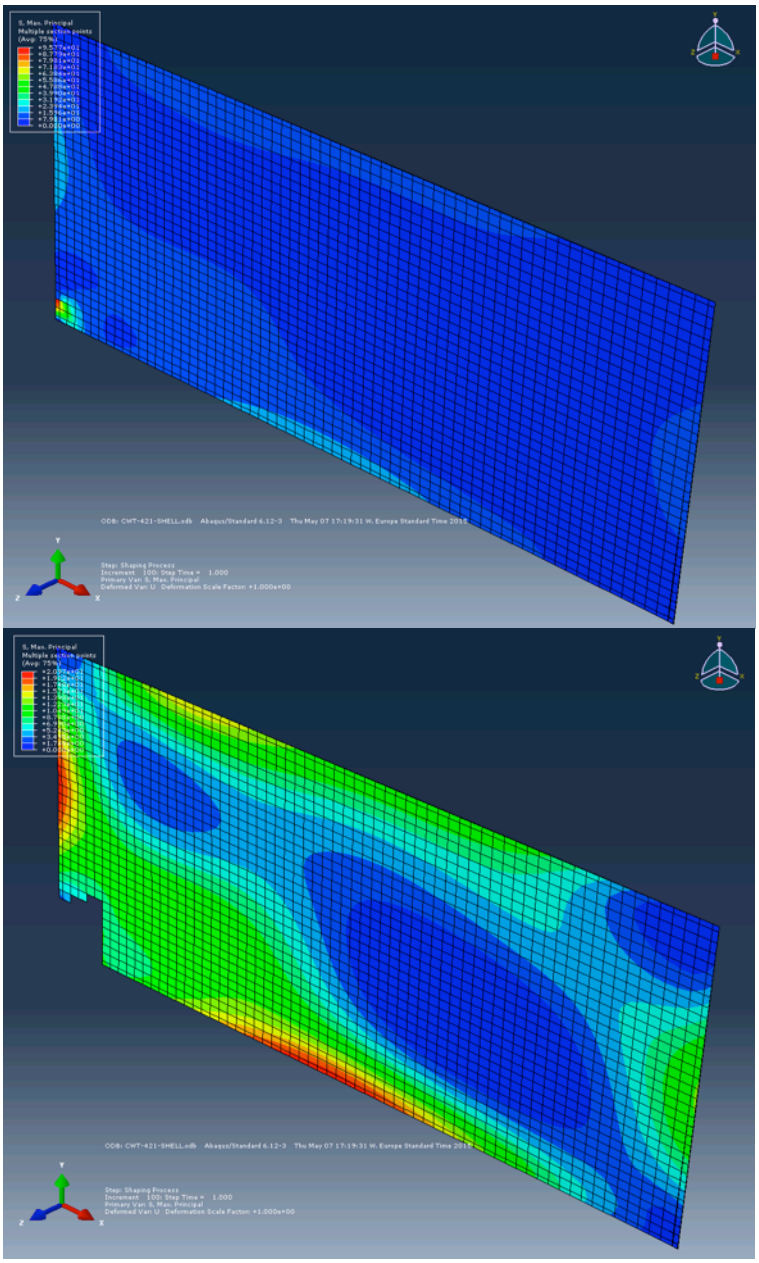

Figure 90 maximum principal stresses for curtain wall element using shell elements

The numerical results of the shell model are then inappropriate.

Appendix VIII. Design table of the four point-supported panel

From the results of §4.1.3, the following design table has been built.

Table 10 Design table for a four point-supported panel

Maximal U3 [mm] at Ld_Point f(buckling,Smax<50[MPa])						
Thickness	L/B					
[mm]	1'000/1'000	1'500/1'500	2'500/2'500	2'000/1'000	3'000/1'500	4'500/1'500
4.00	33.00	38.00	41.00	48.00	46.00	26.00
8.00	30.00	80.00	92.00	70.00	110.00	120.00
12.00	25.00	70.00	144.00	60.00	135.00	180.00
15.00	20.00	60.00	160.00	50.00	120.00	167.00
19.00	17.00	50.00	150.00	45.00	105.00	160.00
25.00	15.00	40.00	125.00	35.00	90.00	145.00
33.00	12.00	35.00	110.00	30.00	75.00	110.00

Limiting parameter:
Buckling
Smax> 50[Mpa]

Maximal U3 [mm] at Ld_Point f(buckling,Smax<100[MPa])						
Thickness	L/B					
[mm]	1'000/1'000	1'500/1'500	2'500/2'500	2'000/1'000	3'000/1'500	4'500/1'500
4.00	33.00	38.00	41.00	48.00	46.00	26.00
8.00	60.00	82.00	92.00	100.00	110.00	120.00
12.00	45.00	120.00	144.00	100.00	174.00	210.00
15.00	40.00	100.00	180.00	90.00	200.00	270.00
19.00	35.00	90.00	230.00	80.00	180.00	275.00
25.00	30.00	80.00	220.00	70.00	165.00	250.00
33.00	25.00	65.00	200.00	55.00	150.00	220.00

Limiting parameter:
Buckling
Smax> 100[Mpa]

Maximal U3 [mm] at Ld_Point f(ripple amplitude <0.5 [mm],Smax<50[MPa])						
Thickness	L/B					
[mm]	1'000/1'000	1'500/1'500	2'500/2'500	2'000/1'000	3'000/1'500	4'500/1'500
4.00	45.00	80.00	80.00	80.00	80.00	-
8.00	30.00	80.00	180.00	70.00	155.00	180.00
12.00	25.00	70.00	170.00	60.00	135.00	180.00
15.00	20.00	60.00	160.00	50.00	120.00	167.00
19.00	17.00	50.00	150.00	45.00	105.00	160.00
25.00	15.00	40.00	125.00	35.00	90.00	145.00
33.00	12.00	35.00	110.00	30.00	75.00	110.00

Limiting parameter:
Smax> 50[Mpa]
Ripple

Maximal U3 [mm] at Ld_Point f(ripple amplitude <0.5 [mm],Smax<100[MPa])						
Thickness	L/B					
[mm]	1'000/1'000	1'500/1'500	2'500/2'500	2'000/1'000	3'000/1'500	4'500/1'500
4.00	85.00	80.00	80.00	80.00	80.00	0.00
8.00	60.00	140.00	180.00	120.00	180.00	180.00
12.00	45.00	120.00	240.00	100.00	215.00	300.00
15.00	40.00	100.00	265.00	90.00	200.00	300.00
19.00	35.00	90.00	240.00	80.00	180.00	275.00
25.00	30.00	80.00	220.00	70.00	165.00	250.00
33.00	25.00	65.00	200.00	55.00	150.00	220.00

Limiting parameter:
Smax> 100[Mpa]
Ripple

Appendix IX. Experimental test on the glue

Several tests have been performed on the Araldite2000 and the DP-490. In order to have consistent model, the elastic properties of the epoxy was necessary. Moreover, supports of the supported diagonal are under tension, it was then necessary to verify the tensile resistance of the assembly.

As the shear resistance is small (only due to the selfweight of the panel) it was then not necessary to verify it.

o Tension test on assembly

➢ Specimen definition and test setup

Tension test on assembly have been performed on FTG 19[mm] thick glass plate. A circular stainless steel connexion is glue to the glass plate. The thickness of the resin is 0.5[mm].

Figure 91 Epoxy Resin Applications

Several tries have been necessary to manage the resin application.

By means of a thick steel plate and a circular aluminium ring (around the circular stainless steel connexion), the glass plate is fixed to the support. The aluminium is used in order to avoid premature failure due to the hard contact of the steel plate.
Then, the hydraulic machine pulls out the connection, by a M10 or M16 bolt depending on the thread rod. Initially all the connections were drilled with a M10 thread. Due to the yielding of the bar, first tests have shown that a M16 was more appropriate for the DP490.

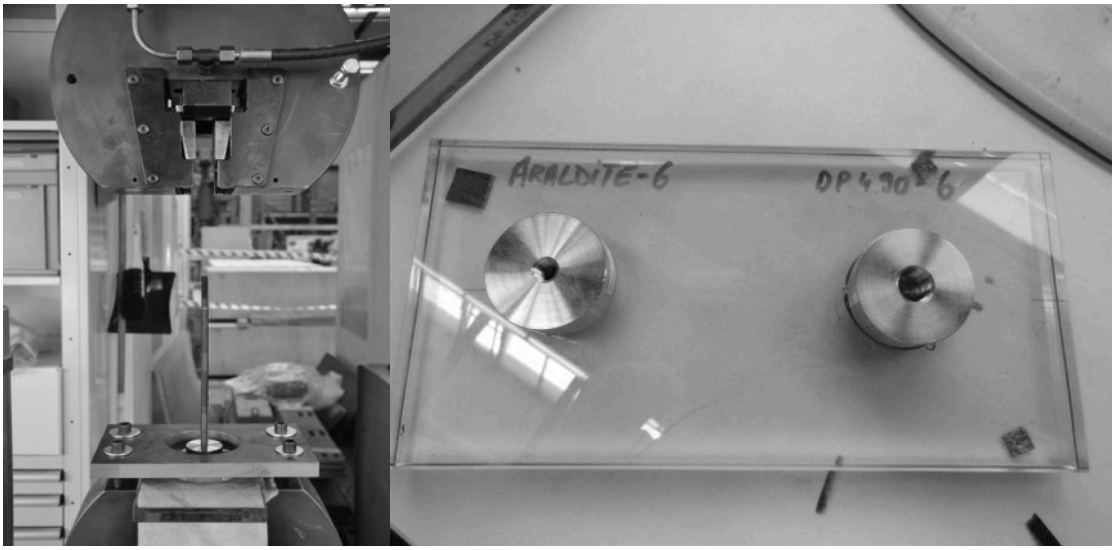

Figure 92 Picture of the test setup and the specimens

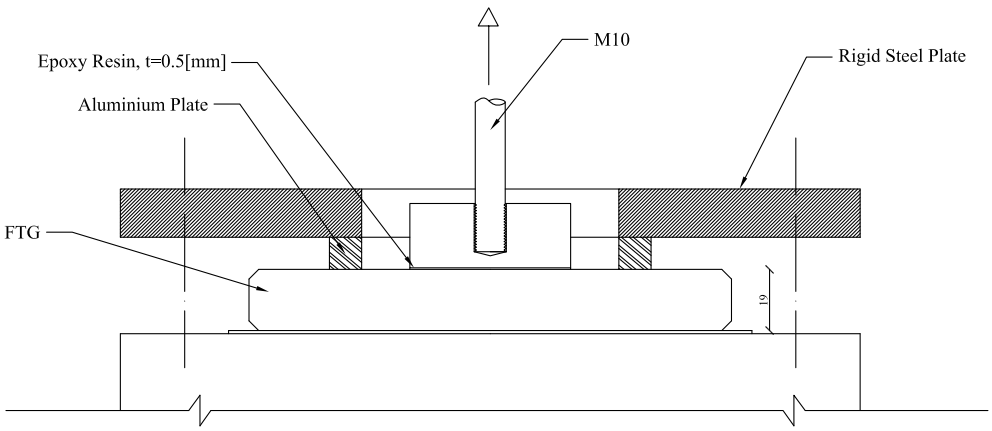

Figure 93 Tension test setup with a M10 bolt

- Results

The results have highlighted the difference between the two adhesives. Indeed apart from the colour, the gap between the strength is large. Results from the tests are exposed on the two tables below.

Test	*Failure Mode*	*Fmax [kN]*	*σnom [MPa]*	*αmax*	*σmax [MPa]*	
Araldite-1	Failure of the Epoxy Resin	8.89	5.85	4.00	23.39	Minimun
Araldite-2	Failure of the Epoxy Resin	**9.75**	**5.62**	**4.00**	**22.48**	
Araldite-3	Failure of the Epoxy Resin	14.34	7.30	4.00	29.21	Maximun
Araldite-4	Failure of the Epoxy Resin	**8.98**	**4.57**	**4.00**	**18.29**	
Araldite-5	Failure of the Epoxy Resin	**9.59**	**4.88**	**4.00**	**19.54**	
Araldite-6	Failure of the Epoxy Resin	**9.65**	**4.91**	**4.00**	**19.66**	
	Average Value	*9.49*	*5.00*	-	*19.99*	

Test	*Failure Mode*	*Exposed Sample*	*Fmax [kN]*	*σnom [Mpa]*	*αmax*	*σmax [MPa]*	
DP490-1	Yielding of the bar	No	41.67	21.90	4.00	87.62	☒
DP490-3	Failure of the glass	No	39.32	20.03	4.00	80.10	☒
DP490-4	Failure of the Epoxy Resin	**No**	**51.83**	**26.40**	**4.00**	**105.59**	☑
DPP490-6	Failure of the Epoxy Resin	**No**	**55.26**	**25.72**	**4.00**	**102.88**	☑
DP490-CO2	Failure of the glass	No	52.81	26.90	4.00	107.58	☒
DP490-CO3	Failure of the Epoxy Resin	**No**	**58.80**	**29.95**	**4.00**	**119.79**	☑
DP490-CO7	Failure of the Epoxy Resin	**Yes**	**35.56**	**18.11**	**4.00**	**72.44**	☑
DP490-CO8	Failure of the Epoxy Resin	**Yes**	**32.91**	**16.76**	**4.00**	**67.04**	☑
	Average Value	No	55.30	27.35	-	109.42	
		Yes	34.24	17.44	-	69.74	

According to [18], a factor $\alpha_{max} = 4$ is applied to get σ_{max} (average value between thickness, diameter, E and ν). That value is maybe protective but gives a good lower bound limit.

The strength of the assembly bound by the DP490 is 5.5 times bigger than the Araldite one!
The failure of the assembly bound with Araldite is linked to the debounding of the Araldite, whereas the failure of the resin is the cause of the failure of the assembly bound with DP490.

DP490 seems to be better stick to the glass, then the failure surface is larger and higher load is required to tear out the connection off the glass. The resin mechanical properties are well used.

Araldite seems to suffer from the interaction with the glass. Since the bounding to the glass is the weak point, the mechanical properties of the Araldite are not used in a good manner.

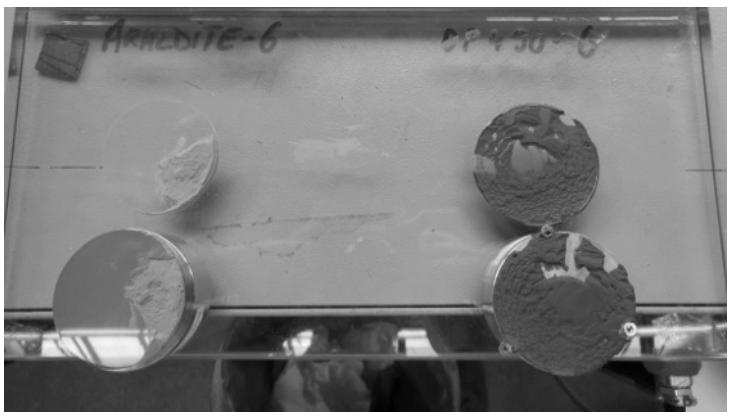

Figure 94 Failures surfaces for Araldite (grey) and DP490 (black)

Nonetheless, both resins can be used for glued point-fitted connection depending on the reaction forces.

Some samples of DP490 were already exposed to shear stress and severe climatic condition. As a result of that, the strength of the resins has almost decreased in half. Attention should to be paid to that kind of assembly, especially when they are exposed to a severe environment. The viscoelasticity of the material should not be neglected!

o Uniaxial tension test

The elastic properties of the Araldite (E and ν) have been defined by doing uniaxial tension test. DP490's properties were already defined by D.Stanek and E.Ghera in [17], for this reason only the Araldite 2000 have been tested.

➢ Specimen definition

Small samples have been made according to [17]. The production of the samples has been useful for the gluing of the assemblies, since I took advantage from that, of a better master in the resin application.

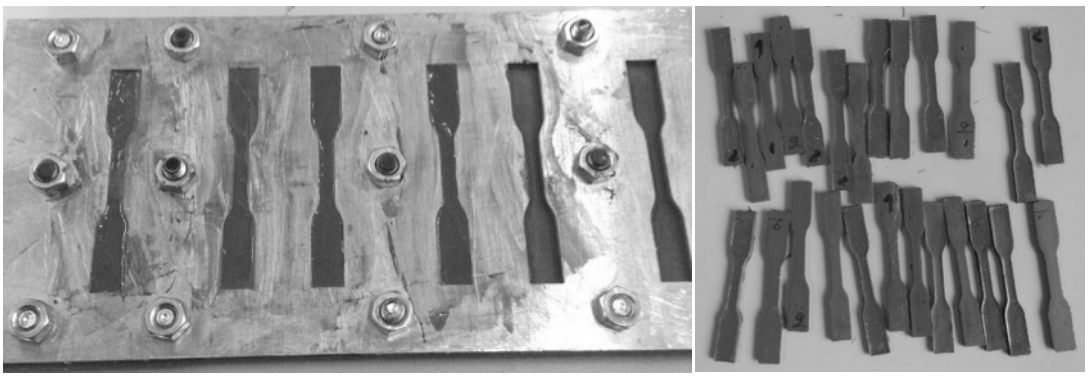

Figure 95 Mould for the glue sample and glue sample

Digital image correlation systems in parallel with LVDT have been used to record the deformation during the tests. The experiments and the results are resumed in [16].

In conclusion, the tests have shown that ν=0.4 and E=141[MPa] were applicable.

Appendix X. Change in the global rigidity and in shape during the shaping-process.

The change in form due to the instability implies a change of the global rigidity of the panel. This change can be observed by plotting the reaction forces RF3 during the shaping process.

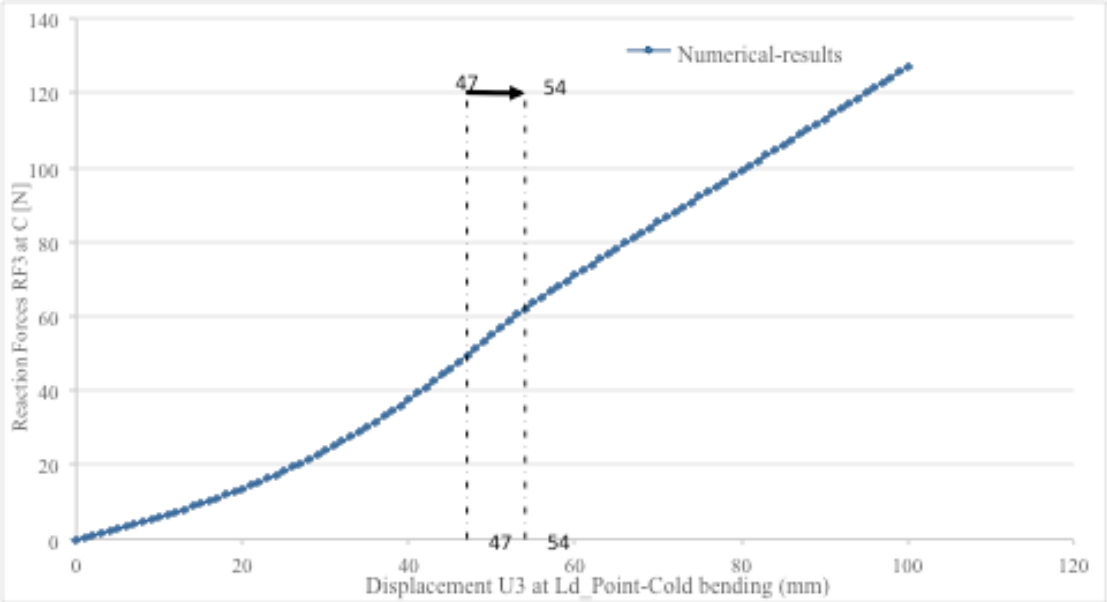

Chart 52 Reaction force RF3 in relation with δ

Before the instability RF3 changes from a linear shape to a curved one. That change of shape is the evidence that the perfect hyperbolic paraboloid shape (for small δ) changes before the instability (Kirchhoff-Love theory is not valid anymore). That's why on Chart 9, the forced long edge is not straight anymore just before the instability. That continuous change in geometry stiffens the global rigidity of the plate.

It's observed that right after the instability ($\delta_{instability}$=47[mm]) the new geometry of the plate is not fixed, since the curve is not linear immediately. Then, the imposed displacement have to reach the value δ=54[mm] to see the global rigidity of the panel unchanged. That's means that after the instability the geometry of the panel is not totally fixed, a higher displacement is needed to fix the second configuration mode.